DEVELOPMENT OF FORWARD FLIGHT TRIM AND LONGITUDINAL DYNAMIC STABILITY CODES AND THEIR APPLICATION TO A UH-60 HELICOPTER

A THESIS SUBMITTED TO
THE GRADUATE SCHOOL OF NATURAL AND APPLIED SCIENCES
OF
MIDDLE EAST TECHNICAL UNIVERSITY

BY

SEVİNÇ ÇALIŞKAN

IN PARTIAL FULFILLMENT OF THE REQUIREMENTS
FOR
THE DEGREE OF MASTER OF SCIENCE
IN
AEROSPACE ENGINEERING

FEBRUARY 2009

Approval of the thesis:

DEVELOPMENT OF FORWARD FLIGHT TRIM AND LONGITUDINAL DYNAMIC STABILITY CODES AND THEIR APPLICATION TO A UH-60 HELICOPTER

submitted by **SEVİNÇ ÇALIŞKAN** in partial fulfillment of the requirements for the degree of **Master of Science in Aerospace Engineering Department, Middle East Technical University** by,

Prof. Dr. Canan Özgen _____
Dean, Graduate School of **Natural and Applied Sciences**

Prof. Dr. İ. Hakkı Tuncer _____
Head of Department, **Aerospace Engineering**

Prof. Dr. Yusuf Özyörük _____
Supervisor, **Aerospace Engineering Dept., METU**

Examining Committee Members:

Prof. Dr. Nafiz Alemdaroğlu _____
Aerospace Engineering Dept., METU

Prof. Dr. Yusuf Özyörük _____
Aerospace Engineering Dept., METU

Assoc. Prof. Dr. Serkan Özgen _____
Aerospace Engineering Dept., METU

Prof. Dr. Ozan Tekinalp _____
Aerospace Engineering Dept., METU

Vahit ÖZVEREN, M.Sc. _____
Senior Expert Engineer, ASELSAN

Date: 02.02.2009

I hereby declare that all information in this document has been obtained and presented in accordance with academic rules and ethical conduct. I also declare that, as required by these rules and conduct, I have fully cited and referenced all material and results that are not original to this work.

Name, Surname: Sevinç ÇALIŞKAN

Signature:

ABSTRACT

DEVELOPMENT OF FORWARD FLIGHT TRIM AND LONGITUDINAL DYNAMIC STABILITY CODES AND THEIR APPLICATION TO A UH-60 HELICOPTER

Çalışkan, Sevinç
M. Sc., Department of Aerospace Engineering
Supervisor : Prof. Dr. Yusuf Özyörük
Co-Supervisor : Assoc. Prof. Dr. Serkan Özgen

February 2009, 141 pages

This thesis describes the development of a series of codes for trim and longitudinal stability analysis of a helicopter in forward flight. In general, particular use of these codes can be made for parametric investigation of the effects of the external and internal systems integrated to UH-60 helicopters. However, in this thesis the trim analysis results are obtained for a clean UH-60 configuration and the results are compared with the flight test data that were acquired by ASELSAN, Inc.

The first of the developed trim codes, called TRIM-CF, is based on closed-form equations which give the opportunity of having quick results. The second code stems from the trim code of Prouty. That code is modified and improved during the course of this study based on the theories outlined in [3], and the resultant code is named TRIM-BE. These two trim codes are verified by solving the trim conditions of the example helicopter of [3]. Since it is simpler and requires fewer input parameters, it is more often more

convenient to use the TRIM-CF code. This code is also verified by analyzing the Bo105 helicopter with the specifications given in [2]. The results are compared with the Helisim results and flight test data given in this reference. The trim analysis results of UH-60 helicopter are obtained by the TRIM-CF code and compared with flight test data.

A forward flight longitudinal dynamic stability code, called DYNA-STAB, is also developed in the thesis. This code also uses the methods presented in [3]. It solves the longitudinal part of the whole coupled matrix of equations of motion of a helicopter in forward flight. The coupling is eliminated by linearization. The trim analysis results are used as inputs to the dynamic stability code and the dynamic stability characteristics of a forward flight trim case of the example helicopter [3] are analyzed. The forward flight stability code is applied to UH-60 helicopter.

The codes are easily applicable to a helicopter equipped with external stores. The application procedures are also explained in this thesis.

Keywords: Helicopter, UH-60, Bo105, forward flight, hover, longitudinal, trim, dynamic stability, short period mode, phugoid mode, flight test, disturbance, data logging, onboard, flight certified data acquisition system, closed form equation, external store.

ÖZ

DÜZ UÇUŞ DURUMU İÇİN BİR DENGE VE DİNAMİK KARARLILIK KODU GELİŞTİRİLMESİ VE UH-60 HELİKOPTERİ ÜZERİNDE UYGULANMASI

Çalışkan, Sevinç

Yüksek Lisans, Havacılık ve Uzay Mühendisliği Bölümü

Tez Yöneticisi : Prof. Dr. Yusuf Özyörük

Ortak Tez Yöneticisi : Doç. Dr. Serkan Özgen

Şubat 2009, 141 sayfa

Bu rapor, bir helikopterin düz uçuştaki performansını, denge durumunu ve dinamik kararlılığını analiz eden bir dizi yazılımın geliştirilmesi çalışmalarını sunmaktadır. Bu kodların özel bir kullanımı, UH-60 helikopterlerine entegre edilen çeşitli sistemlerin etkilerinin parametrik araştırması için gerçekleştirilebilmektedir. Temiz bir UH-60 helikopteri konfigürasyonu için denge analizi sonuçları, ASELSAN, A.Ş. tarafından gerçekleştirilen uçuş testleri sonuçları ile karşılaştırılmaktadır.

Geliştirilen ilk yazılım, [3] referansında verilen kapalı-form denklemleri kullanmaktadır. TRIM-CF adını alan bu kodun en kullanışlı özelliği, parametrelerin çok hızlı hesaplanmasına olanak vermesidir. İkinci kod, Prouty tarafından geliştirilen denge yazılımını temel almaktadır. Yazılım, bu tez çalışması sırasında, [3] referans kitabında anlatılan teoriler esas alınarak değiştirilmiş ve iyileştirilmiştir. Elde edilen koda TRIM-BE adı verilmiştir. Her iki denge yazılımı, [3]'te verilen örnek helikopter üzerinde doğrulanmıştır. Daha basit olması ve daha az girdi gerektirmesi sebebiyle,

TRIM-CF yazılımını kullanmak sıklıkla daha elverişlidir. Bu kod, [2] referans kitabında verilen Bo105 helikopteri analiz edilerek de doğrulanmıştır. Analiz sonuçları, referans kitapta verilen Helisim yazılımı sonuçları ve uçuş test sonuçları ile karşılaştırılmıştır. UH-60 helikopterinin denge analizi TRIM-CF yazılımı kullanılarak gerçekleştirilmiştir ve uçuş test sonuçları ile karşılaştırılmıştır.

Tez kapsamında, [3] referans kitabında yer alan yöntemleri kullanan DYNA-STAB adlı bir düz uçuş boylamsal kararlılık analiz yazılımı geliştirilmiştir. Yazılım, bağımlı-birleşik olan düz uçuş hareket denklemleri matrisinin boylamsal kısmını çözümlemektedir. Bağımlı-birleşik denklem çözümü doğrusallaştırma yöntemi ile gerçekleştirilmektedir. Denge yazılımlarının çıktıları, kararlılık yazılımına girdi olarak kullanılmaktadır. Yazılım ile, [3] fererans kitabında yer alan örnek helikopterin, belirli bir ileri hızdaki kararlılık karakteristikleri incelenmiştir. Düz uçuş boylamsal kararlılık analiz yazılımı kullanılarak UH-60 helikopteri üzerinde inceleme gerçekleştirilmiş ve sonuçlar bu raporda sunulmuştur.

Yazılımlar, harici yük taşıyan helikopterlerin incelenmesine de olanak sağlamaktadır. Bu raporda, yazılımların bu helikopterlere uyarlanması konusuna da değinilmektedir.

Anahtar kelimeler: Helikopter, UH-60, Bo105, düz uçuş, hover, boylamsal, denge, dinamik kararlılık, short-period modu, phugoid modu, uçuş testi, bozanetken, veri kaydı, uçuş sertifikalı veri toplama sistemi, kapalı form denklem, harici yük.

To my close friends,
to my family and
to my love,

ACKNOWLEDGEMENTS

The author wishes to express her gratitude to Drs. Yusuf ÖZYÖRÜK and Serkan ÖZGEN for guiding this work. Thanks to Dr. Yusuf ÖZYÖRÜK for his sincere supervision and continuous patience.

Special thanks go to my colleague and close friend Vahit ÖZVEREN for his leadership, encouragement, considerable patience and friendship. This thesis would not be possible without his support.

Thanks to my family and my close friends, who showed great understanding and encouragement.

Special thanks to my darling for his magnificent love and understanding.

This study was supported by ASELSAN.

TABLE OF CONTENTS

LIST OF TABLES

TABLES

LIST OF FIGURES

FIGURES

LIST OF SYMBOLS

A	Area
A_1	1st harmonic lateral cyclic angle
$A.R.$	Aspect ratio
B	Tip loss factor
B_1	1st harmonic longitudinal cyclic angle
D	Fuselage drag
$D.L.$	Disc loading
H	H-force
HP	Power (hp)
I	Inertia
L	Lift
M	Mach number / Pitch moment
Q	Torque
R	Radius
T	Thrust
U	Local velocity component
V	Forward velocity
X	Force on X-direction
Y	Force on Y-direction
Z	Force on Z-direction
a	Lift curve slope / Speed of sound
a_0	Coning angle
a_1	Longitudinal flapping wrt the plane of no-feathering
a_{1S}	1st harmonic longitudinal flapping angle
b_1	Lateral flapping wrt the plane of no-feathering
b_{1S}	1st harmonic lateral flapping angle
c	Chord
c	Coefficient

e	Efficiency factor
f	Flat plate drag area
g	Gravitational acceleration
h	Height wrt cg
i	Incidence
l	Moment arm
m	Mass
q	Dynamic pressure / Pitch rate
υ_1	Induced velocity
υ_L	Local induced velocity
x	Displacement in X-direction
x_o	Cut out
z	Displacement in Z-direction
Θ	Pitch angle of fuselage
Ω	Revolution speed
α	Local angle of attack
α_S	Shaft angle of attack
α_{TPP}	Tip path plane angle of attack
β	Angle of sideslip
δ_3	Delta-three angle
ε	Downwash angle
γ	Lock number / Climb angle
σ	Solidity
θ_0	Collective angle
θ_1	Twist angle
λ	Inflow ratio wrt the shaft plane
λ'	Inflow ratio wrt TPP
μ	Advance ratio
ρ	Air density
θ	Pitch angle
θ_O	Collective angle
θ_1	Twist angle

ψ	Azimuth angle
υ	Local induced velocity
η	Sidewash angle

Subscripts:

T	Tail rotor / Thrust / Tangential
F	Fuselage
Q	Torque
H	H-force / Horizontal stabilizer
P	Perpendicular
R	Radial
N	Normal
M	Pitching moment
R	Rolling moment
V	Vertical stabilizer
W	Wing / Weight
b	Blade
$comp$	Compressible
eff	Effective
ind	Induced
int	Interference
l	Lift
d	Drag
f	Frictional
$para$	Parasite
pro	Profile
tot	Total

Other parameters are clearly defined wherever applicable.

CHAPTER 1

INTRODUCTION

1.1 BACKGROUND

A helicopter is an aircraft that uses rotating wings to provide lift, control, and forward, backward and sideward propulsion. Because of the rotating parts, it has much more capability of maneuvering, while having restrictions on high speeds and high altitudes. Unlike aircraft, the helicopter has the possibilities of vertical landing and takeoff, low speed flight, hover and safe autorotation. For these reasons, helicopters are used in low-altitude; small range combat and search-and-rescue purposes as well as pleasure travels.

For several years ASELSAN, Inc. has been conducting avionics systems integration projects on helicopters. Such integration work requires certification flight tests before entry of the modified aircraft into the service. However, prior to the certification phase, extensive investigations are needed to determine the effects of particularly the external stores on the aerodynamics, performance and stability characteristics of the aircraft, and to identify probability of any risks and consequently propose design or integration changes. Although there are some commercial computational fluid dynamics (CFD) programs which may readily be used for helicopter aerodynamic analyses, there are not many off-the-shelf programs for analyzing trim and dynamic stability characteristics of rotorcraft. Therefore, ASELSAN Inc. has developed several codes to analyze the trim characteristics as well as the dynamic stability characteristics of helicopters. Many of these codes interface with each other. One really much needed and extensively used feature that can be benefited from such codes during an aerodynamic analysis phase is the ability to link to some routines through

which the trim parameters such as the main rotor tip path plane (TPP) angle, collective angle, longitudinal and lateral cyclic angles, etc. can be acquired and placed very conveniently in hundreds of input files read in by the aerodynamic analysis codes, such as VSAERO and USAERO.

ASELSAN has also been performing certification flight tests after integration of a system cleared by aerodynamic, trim, performance and stability analyses. These tests aim to analyze the effects of the external stores and the systems integrated on the performance of the air vehicle. Flight data are recorded using a comprehensive data acquisition system and then analyzed. Helicopter handling qualities are also evaluated by using the Cooper-Harper Rating Scale.

Trim of a helicopter is the situation in which all the forces, inertial and gravitational, as well as the overall moment vectors are in balance in the three mutually perpendicular axes. Stability is the tendency of a trimmed aircraft to return to the trim condition after a disturbance is applied. Static stability analyzes the initial tendency, while the dynamic stability considers the subsequent motion in time. The aircraft is said to be stable if it returns to equilibrium, and unstable if diverges. The case in which the aircraft has no change in motion is called neutral stability. The motion can be oscillatory or non-oscillatory.

Trim and dynamic stability analysis combination composes a full dynamic helicopter flight model. In order to develop such a model, the five modules listed below should be completed and interfaced with each other:

1. Aircraft input parameters module,
2. Full trim module,
3. Static stability module,

4. Longitudinal and lateral dynamic stability module, including the coupling effects,
5. Control module

All modules are applicable to a continuous velocity range, from hover to maximum velocity.

Although a full model should be used if a comprehensive helicopter dynamic stability analysis is to be performed, it is possible to look at a partial analysis using engineering judgments. Longitudinal and lateral dynamic stability can be differentiated. Also, since the transition from hover to a low-speed forward flight (e.g. 30 knots) is continuous, the hover and forward flight cases can be analyzed separately.

1.2 UH-60 HELICOPTER

The primary mission of the UH-60 Black Hawk helicopter is as a troop carrier and logistical support aircraft, but in addition the helicopter can be configured to carry out medical evacuation, command-and-control, search-and-rescue, armed escort, electronic warfare and executive transport missions. The helicopter is flown by a crew of three, the pilot and the copilot at the flight deck and one crew member in the cabin. The cabin provides accommodation for 11 fully equipped troops. UH-60 is equipped with two General Electric turboshaft engines.

Figure 1-1: UH-60 Helicopter.

The UH-60 helicopter has Stability Augmentation System (SAS) and Flight Path Stabilization System (FPS). Those systems perform complex algorithms which aid in stabilizing the helicopter in flight and in hover. They reduce pilot workload by improving basic aircraft control harmony and decreasing (damping) disturbances.

The primary flight control system consists of the lateral control subsystem, the longitudinal control subsystem, the collective pitch control subsystem, and the directional control subsystem. Control inputs are transferred from the cockpit to the rotor blades by mechanical linkages and hydraulic servos. Pilot control is assisted by stability augmentation system (SAS), flight path stabilization (FPS), boost servos, and pitch, roll, and yaw trim. Dual cockpit controls consist of the cyclic stick, collective stick, and pedals. The pilot and copilot controls are routed separately to a combining linkage for each control axis. Outputs from the cockpit controls are carried by mechanical linkage through the pilot-assist servos to the mixing unit. The mixing unit combines, sums, and couples the cyclic, collective, and yaw inputs. It provides proportional output signals, through mechanical linkages, to the main and tail rotor controls.

The Automated Flight Computer System (AFCS) enhances the stability and handling qualities of the helicopter. It is comprised of four basic subsystems: stabilator, SAS, trim systems, and FPS. The stabilator system improves flying qualities by positioning the stabilator by means of electromechanical actuators in response to collective, airspeed, pitch rate, and lateral acceleration inputs. The SAS provides short term rate damping in the pitch, roll, and yaw axes. Trim/FPS system provides control positioning and force gradient functions as well as basic autopilot functions with FPS engaged.

The helicopter has a variable angle of incidence stabilator to enhance handling qualities. The automatic mode of operation positions the stabilator to the best angle of attack for the existing flight conditions. After the pilot engages the automatic mode, no further pilot action is required for stabilator operation. Two stabilator amplifiers receive airspeed, collective stick position, pitch rate, and lateral acceleration information to program the stabilator through the dual electric actuators (taken from Aircraft Flight Manual). There also exists a table at the Aircraft Flight Manual, which relates the horizontal stabilator incidence with the forward flight speed. Within this thesis work, the incidence is calculated from this chart, seen in Figure 1-2.

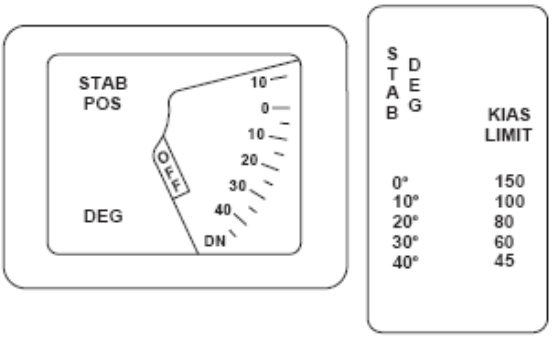

Figure 1-2: Stabilator pozition vs. airspeed.

1.3 OBJECTIVE OF THE THESIS

In summary, one of the goals of this thesis is to develop a series of codes that can be linked together and used for helicopter trim and dynamic stability analyses practically by industrial companies working on helicopter production and modifications. The mathematical development behind all these codes includes many simplifications and assumptions, which are explained in Chapter 2. Therefore, it should be remarked that the codes are applicable only to preliminary-design process and the analysis should be verified with extensive flight testing. The trim modules shall provide basic rotor parameters, such as flapping, to existing CFD codes and to the dynamic stability module.

Another goal of the thesis is to verify the developed codes by solving some example helicopter cases, then to apply the codes to a UH-60 helicopter and compare with flight test data.

1.4 SCOPE OF THE THESIS

In the first chapter of the thesis, some background information on the present problem is given, besides stating the scope and the objectives of the thesis. The second chapter is devoted to explain the basic theories behind the developed codes and their validation studies. These studies are performed on two examples but realistic helicopter configurations given in Prouty [3] and Padfield [2], respectively. Chapter 3 presents the trim solutions obtained for the UH-60 helicopter. This chapter also presents the flight test results for this helicopter in comparison with the trim analysis results. The fourth chapter involves the dynamic stability analysis for forward flight. The last chapter gives some future work plans and the main

conclusions drawn from this thesis work. Finally, some appendices are included at the end of the thesis giving some detailed formulations used in the development of the aforementioned codes.

The codes developed within the scope of this thesis involve

1) a general input module
2) two trim codes for forward flight, TRIM-CF and TRIM-BE, and
3) a longitudinal dynamic stability code for forward flight, DYNA-STAB

The relation among the codes can be seen in Figure 1-3. The input module which is numbered as the 1st module, contains general aerodynamic properties of the aircraft, such as the revolution speed of the rotors, the gross weight of the helicopter and the incidence of the stabilizers. Either the 2nd or the 3rd module can be used in order to calculate the required trim parameters at a given forward flight case. Those trim parameters, including the thrust of the main rotor, the drag on each of the helicopter components, the lift the components produce, the angle of attack values, etc., are used as inputs to the 4th module, DYNA-STAB. DYNA-STAB calculates the stability characteristics of the aircraft corresponding to the given forward flight velocity at the given weight and helicopter configuration.

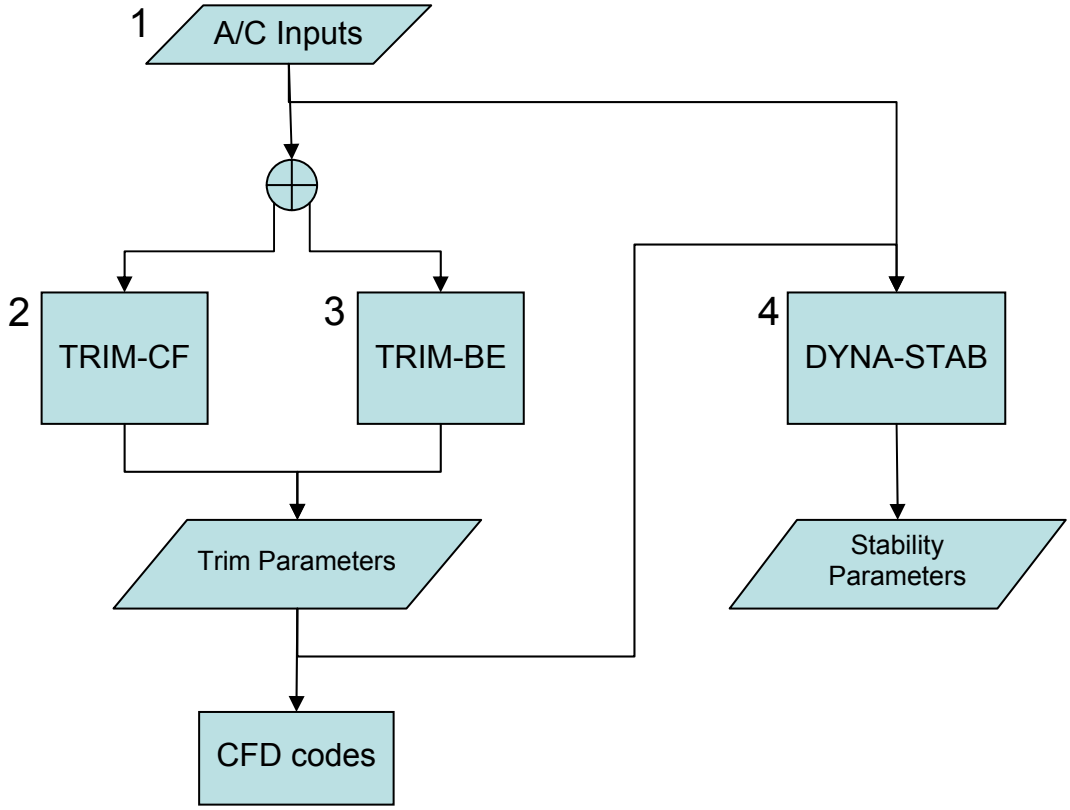

Figure 1-3: Interfaces of the codes.

A trim analysis code can be as simple as a program composed of -let's say- 10 simple equations, while it can be as complicated as a program having 10 interpenetrated and/or related loops. If a simple code is enough to satisfy the requirements, there are so many experimental and theoretical formulas available which can be used to approximate the aerodynamic parameters. And if accuracy is much more important and a complex program is intended to be used, there are several books and academic works which infer different approaches of solving a trim problem with integration of parameters along the rotors and with interpenetrated loops for converging some of the main trim parameters.

This thesis includes a semi-simple code and a complex code for trim analysis. The simple one, TRIM-CF, is based on approximated closed form equations which are used to linearize and solve the equations of motion, and the trim parameters are obtained straight forwardly with many simplifications. The complex code, TRIM-BE, also uses some simplifications however it has a 3-loop structure looking for convergence of three trim parameters and it calculates the main rotor parameters with an integration method, while the tail rotor, fuselage and empennage parameters are again calculated using closed form equations. TRIM-BE is originally written by R.W. Prouty and is called Forward. Since it was rather poor on catching the correct trim parameter values, many modifications are implied and the code was modified according to the methods given in [3] during this thesis work and TRIM-BE was obtained. The codes are explained in detail in Chapter 2 of this thesis. Since TRIM-CF code requires less parameters and gives almost the same accuracy faster, it was decided to use TRIM-CF for the dynamic stability analysis. TRIM-CF, is verified by the example helicopter given in [3] and one of the example helicopters (Bo105) given in [2]. There are flight test data for Bo105 helicopter presented in the reference book, and the analysis results are compared with flight test data also. The trim analysis results of UH-60 helicopter obtained by TRIM-CF code are presented and compared with flight test data within this report.

Forward flight longitudinal dynamic stability code named DYNA-STAB and developed in this thesis uses the methods and formulas presented in [3] and it solves the longitudinal part of the whole coupled matrix of equations of motion of a helicopter in forward flight. The coupling is eliminated by linearization. The trim analysis parameters are used as inputs to the dynamic stability code and the Short Period and Phugoid modes of a forward flight trim case of the example helicopter [3] were analyzed. The forward flight stability code is applied on UH-60 helicopter and the results are presented.

The codes are easily applicable to a helicopter equipped with external stores.

The codes were developed on MATLAB® environment.

The flight test data given for the UH-60 helicopter were logged with an advanced flight certified data acquisition system which includes proprietary software for logging, displaying the data onboard and analyzing.

CHAPTER 2

TRIM AND STABILITY CODE DEVELOPMENT

2.1 FORCES AND MOMENTS ACTING ON A HELICOPTER IN FLIGHT

The helicopters come in many sizes and shapes, but most share the same major components. The main rotor is the main airfoil surface that produces lift. The main rotor is the main control mechanism. A helicopter can have a single main rotor, two rotors can be mounted coaxially or they can be in tandem configuration. The main rotor provides the speed and maneuvering controls, as well as the lift needed for the helicopter to fly. The tail rotor is required from the torque effect produced by spinning the main rotor. There are some helicopters which does not have a tail rotor but have a “fan-in-tail” design (Fenestron) (like in Eurocopter EC 135 T2) or use an air blowing system (NOTAR) (like in MD 520N) in order to supply the anti-torque. The rotors are driven through a transmission system by one or two engines, generally being gas turbine engines. The horizontal stabilator serves as a wing which produces lift and helps stabilizing the helicopter in forward direction. The vertical stabilizer generally has a wing-like geometry which produces side force and helps stabilizing the helicopter in lateral directions. Some helicopters have wings too. The wings are mostly used for carrying weapons, as well as their lifting surface effect.

In Figure 2-1, the forces and moments acting on a helicopter in trim position are shown. In the figure, the vertical stabilizer side force is given as Y_V, in ideal case it is not directed straight to the side and has an angle, but for simplicity purposes it is shown as directed to (-)Y-axis. It is assumed that

the tail rotor has no incidence and its thrust vector is given as T_T. The drag forces on all of the components of the helicopter are shown as one vector D, which is directed to (–)X-direction for simplicity purposes again. The lift and pitching moment vectors L and M, stand for the lift and pitching moment produced by the fuselage and the horizontal stabilizer, as well as the wings if exist. Gross weight is shown as W. The torque vector produced by the main rotor which is rotating counter-clockwise is shown in order to state the anti-torque effect of the tail rotor.

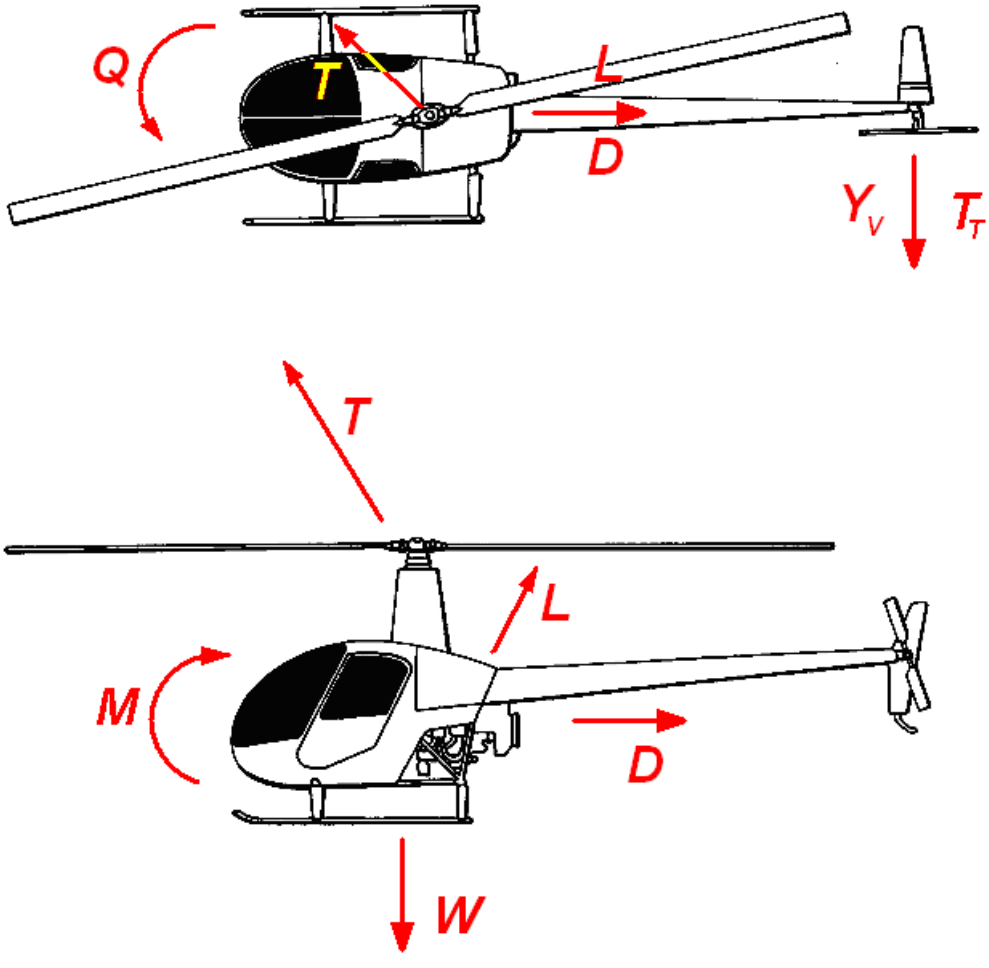

Figure 2-1: Forces and moments acting on a helicopter.

2.2 HELICOPTER ROTOR SYSTEM

There are four primary types of rotor systems: articulated, teetering, semi-rigid and hingeless. The articulated rotor system first appeared on the autogyros of the 1920s and is the oldest and most widely used type of rotor system. The rotor blades in this type of system can move in three ways as it turns around the rotor hub and each blade can move independently of the others. They can move up and down (flapping), back and forth in the horizontal plane, and can change in the pitch angle (the tilt of the blade). UH-60 helicopters have fully-articulated main rotor configuration. In the semi-rigid rotor system, the blades are attached rigidly to the hub but the hub itself can tilt in any direction about the top of the mast. This system generally appears on helicopters with two rotor blades. The teetering rotor system resembles a seesaw, when one blade is pushed down, the opposite one rises. The hingeless rotor system functions much as the articulated system does, but uses elastomeric bearings and composite flextures to allow for flapping and lead-lag movements of the blades in place of conventional hinges. Its advantages are improved control response with less lag and substantial improvements in vibration control. It does not have the risk of ground-resonance associated with the articulated type, but it is considerably more expensive.

The use of hinges was first suggested by Renard in 1904 as a means of relieving the large bending stresses at the blade root and of eliminating the rolling moment which arises in forward flight, but the first successful practical application was due to Cierva in the early 1920s. The most important of these hinges is the flapping hinge which allows the blade to flap. A blade which is free to flap experiences large Coriolis moments in the plane of rotation and a further hinge – called the drag or lag hinge – is provided to relieve these moments. Lastly, the blade can be feathered about

a third axis, parallel to the blade span, to enable the blade pitch angle to be changed. The hinges are shown in Figure 2-2, where an articulated rotor is demonstrated.

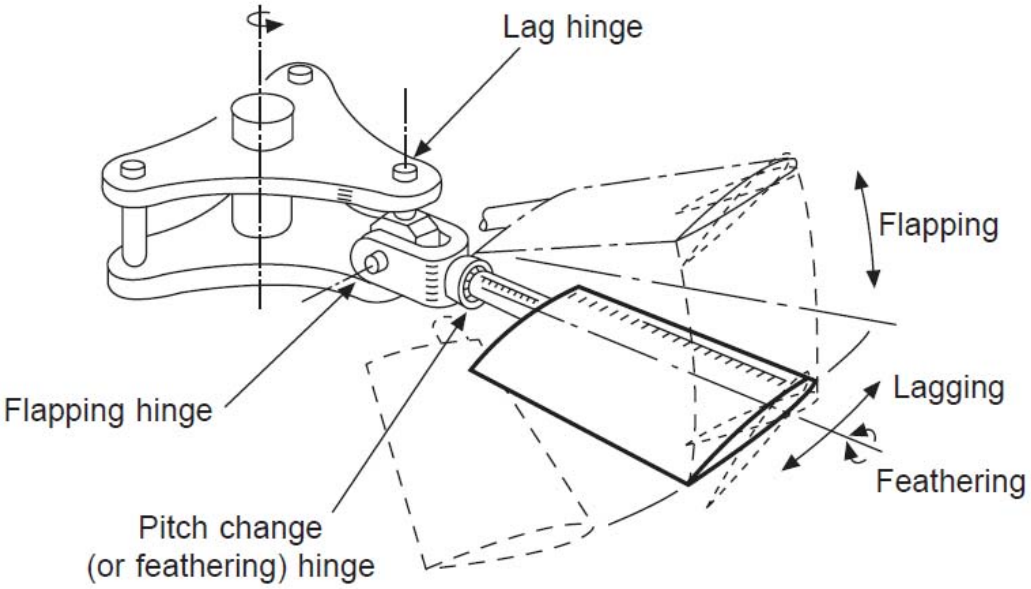

Figure 2-2: Hinges on an articulated rotor [22].

The blades of two-bladed rotors are usually mounted as a single unit on a ‘seesaw’ or ‘teetering’ hinge. No lag hinges are fitted. Figure 2-3 demonstrates a teetering rotor.

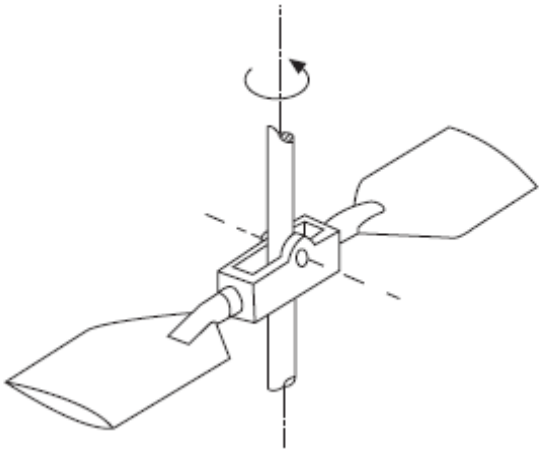

Figure 2-3: Teetering rotor [22].

The semi-rigid rotor resembles the teetering rotor, but now the hub itself also moves about the top of the mast. The hub is strictly attached to the blades.

Hingeless rotors does not have regular flapping and lagging hinges and have blades which are connected to the shaft in cantilever fashion but which have flexible elements near to the root, allowing the flapping and lagging freedoms. A hingeless rotor is shown in Figure 2-4.

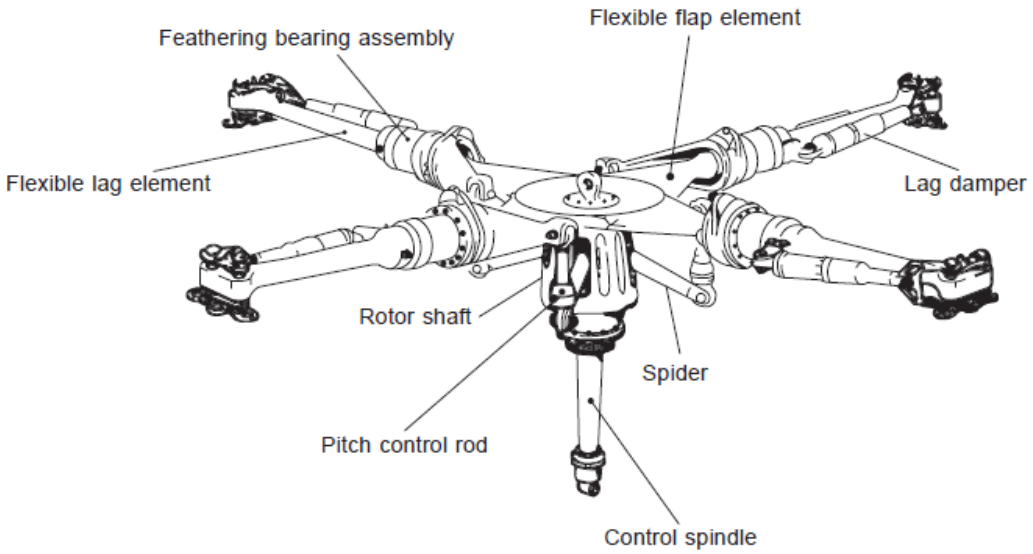

Figure 2-4: Hingeless rotor [22].

The collective changes the pitch angle of the rotor blades causing the helicopter to climb and descend. Through the swash plate, the cyclic controls the pitch angle distribution over the main rotor disc and by this way the disc is tilted sideways or backwards in order to turn, go backwards or change the speed of the helicopter. The anti-torque pedals control the helicopters tail rotor and are used to point the nose of the helicopter in the desired direction. The function of the throttle is to regulate the engine r.p.m.

2.3 HELICOPTER ROTOR AERODYNAMICS

There are two basic theoretical approaches to understand the generation of thrust from a rotor system: momentum theory and blade element theory. The momentum theory approximates the local forces and moments on the blades and assumes that the rotor is an ‘actuator’ disc which is uniformly loaded with an infinite number of blades so that there is no periodicity in the

wake. The theory solves the energy and momentum equations and relates the induced velocity parameter with the forward velocity.

The momentum theory makes certain additional assumptions, which limit the accuracy:

- The flow both upstream and downstream of the disk is uniform, occurs at constant energy and is contained within a streamtube.
- No rotation is imparted on the fluid by the action of the rotor.

In Figure 2-5, the stream tube used in the momentum theory is demonstrated. The actuator disc (rotor) which stands at the middle of the tube, shrinks the airflow and decreases its radius, increasing the velocity of the flow. The theory is also applicable to forward flight cases. The application and derivations are detailed in Appendix-A.

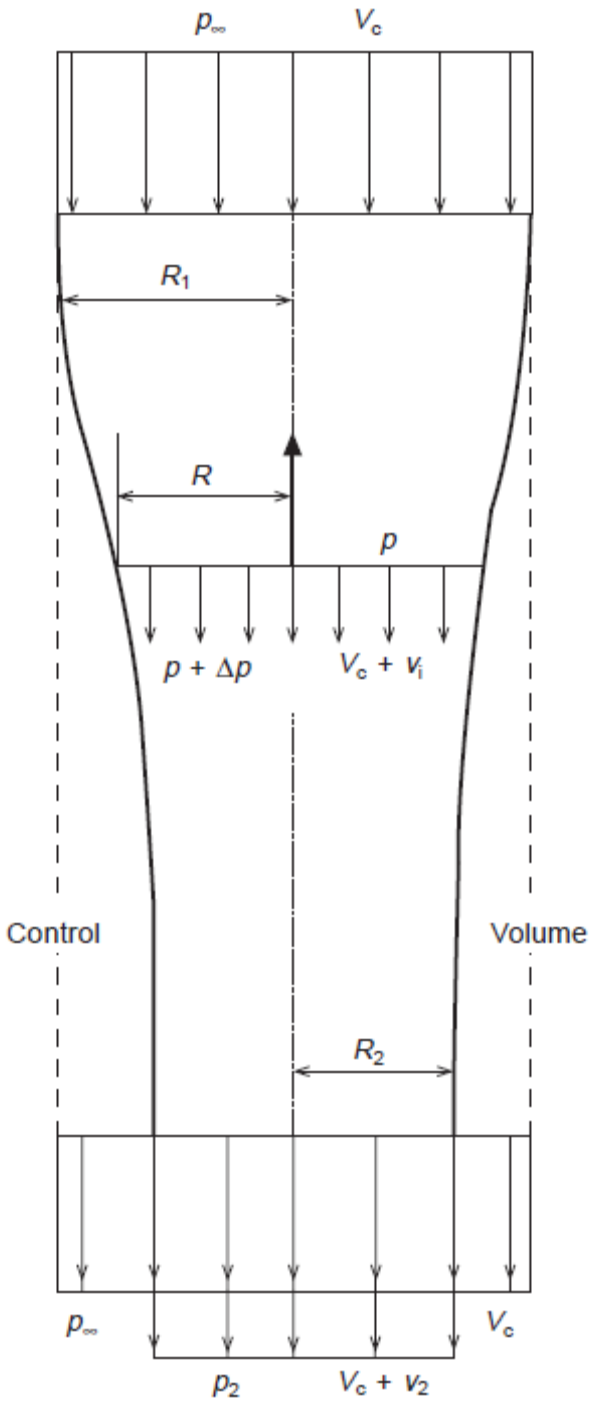

Figure 2-5: The streamtube in the momentum theory [22].

The blade element theory is based upon the idea that the rotor blades function as high aspect ratio wings constrained to rotate around a central mast as the rotor system advances through the air. It considers the local aerodynamic forces on the blade at radial and azimuthal sections, and integrates the forces to find the overall thrust and drag on the rotor. The momentum theory cannot be used to predict the magnitude of any losses associated with realistic flow around rotor blades, and the blade element theory overcomes some of the restrictions inherent in the momentum theory. The applications of the blade element theory on trim analysis are explained in detail in Appendix-A, on which the TRIM-BE module is based.

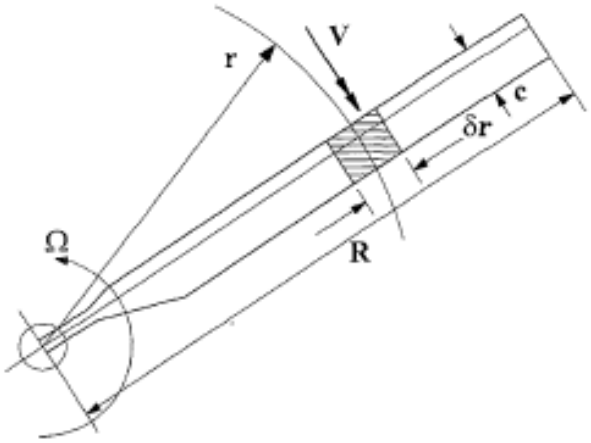

Figure 2-6: Blade element theory [22].

The finite number of blades leads to a rotor performance loss not accounted for by the actuator disk analysis. The lift at the blade tips decreases to zero over a finite radial distance, rather than extending all the way out to the edge of the disk. Thus, there will be a reduction in the thrust, or increase in the induced power of the rotor.

Forward flight is a more complex situation compared to the hover. Because of the forward velocity, the relative speed of the blade sections differ around the azimuth, and therefore, an imbalance of aerodynamic forces occur along the main rotor disc. The advancing blade has a velocity relative to the air higher than the rotational velocity, while the retreating blade has a lower velocity relative to the air. This lateral asymmetry has a major influence on the rotor and its analysis in forward flight.

One of the major characteristics of the forward flight aerodynamics is the reversed flow region. Depending on the forward speed, there occurs a region on the retreating side where the local velocity on the blade section becomes reversed (the velocity relative to the blade is directed from the trailing edge to the leading edge), and therefore the lift is dropped down. One other feature belonging to forward flight is the compressibility effect seen on the advancing side at the tips of the blades where the local speed is greatest and approaches almost the speed of sound. Since it increases the drag drastically, the blade tips are swept back to decrease its effects. Figure 2-7 and Figure 2-8 explain these phenomena.

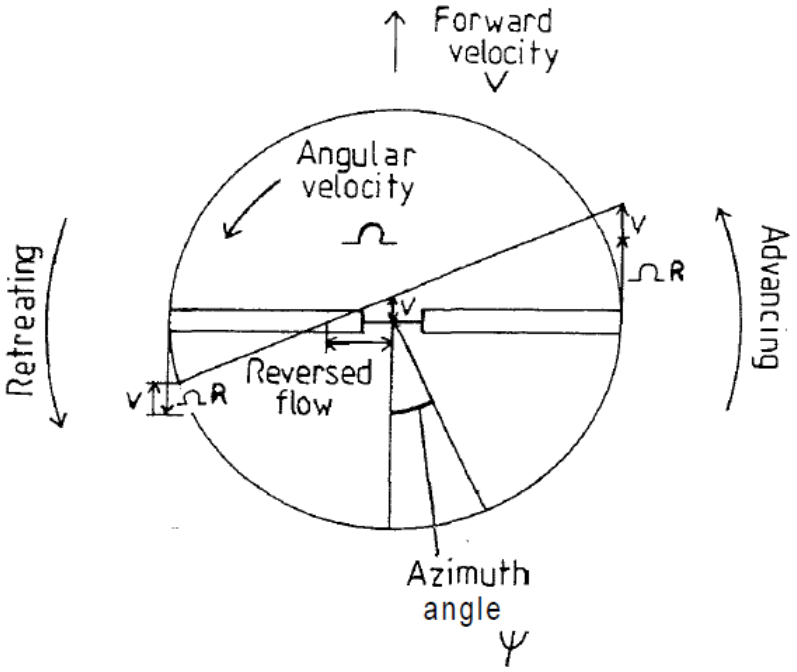

Figure 2-7: Local velocity sketch over the rotor [1].

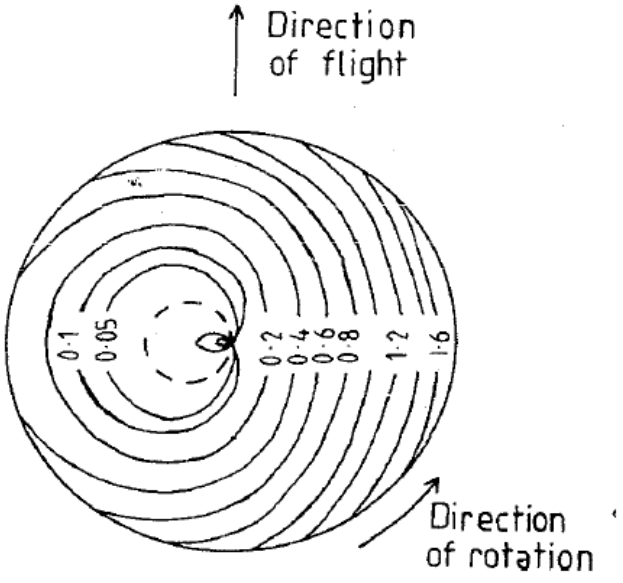

Figure 2-8: The pressure distribitution over the rotor [1].

The dynamic stall phenomenon is another effect coming with the forward flight situation. As blade incidence increases beyond the static stall point, flow reversals are observed in the upper surface boundary layer, but for a time these are not transmitted to the outside potential flow region. Consequently, the lift goes on increasing with incidence. Eventually, flow separation develops at the leading edge (it may be behind a recompression shock close to the leading edge), creating a transverse vortex which begins to travel downstream. As the vortex rolls back along the upper surface into the mid-chord region, lift continues to be generated but a large nose-down pitching moment develops owing to the redistribution of upper surface pressure. The passage of the vortex beyond the trailing edge results in a major breakdown of flow. Finally, when the incidence falls below the static stall angle as the blade approaches the rear of the disc, the flow reattaches at the leading edge and normal linear lift characteristics are re-established.

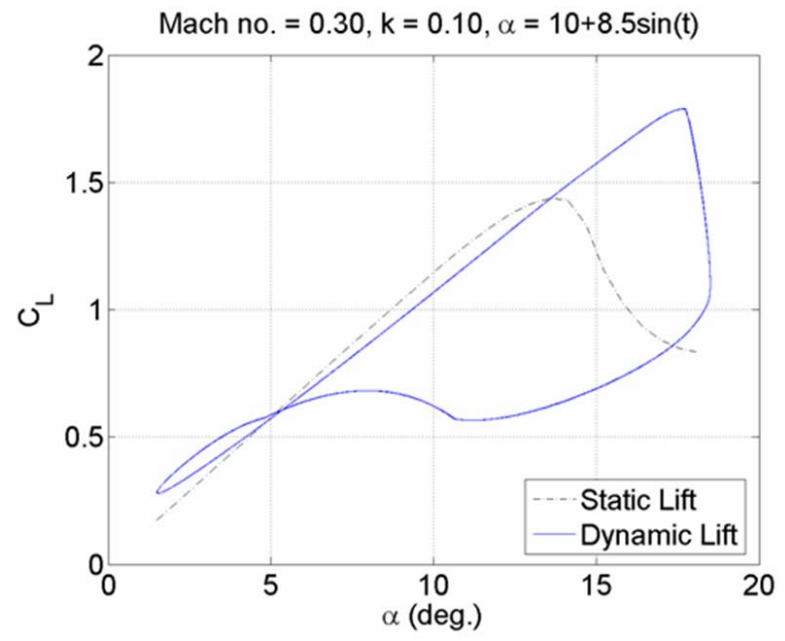

Figure 2-9: The dynamic stall effect on the lift.

The lift of an airfoil is affected by the rate of change of angle of attack and by the rate of plunge, both of which produce shed vorticity lying behind the trailing edge, which induces velocities at the front of the airfoil coming after. This phenomenon is called classical unsteady potential flow.

The proximity of the ground to the hovering rotor disk constrains the rotor wake and reduces the induced velocity at the rotor, which means a reduction in the power required for a given thrust; this behavior is called ground effect. The effect exists at low speed forward flight also. Equivalently, ground proximity increases the rotor thrust at a given power. Because of this phenomenon, a helicopter can hover in ground effect (IGE) at a higher gross weight or altitude than is possible out of ground effect (OGE).

2.4 TRIM AND STABILITY

When all of the forces and moments (i.e. the aerodynamic, inertial and gravitational) about three mutually perpendicular axes are equal, the aircraft is in a state of equilibrium. That equilibrium state is called trim. When propulsive force is greater than drag the aircraft will accelerate; when lift is greater than the weight the aircraft will climb.

Each of the blades has two primary degrees of freedom: flapping and lagging, which take place about either mechanical or virtual hinges near the blade root. A third degree of freedom allows cyclic pitch or feathering of the blade. Despite the fact that helicopter blades are relatively flexible, the basic physics of the blade dynamics can be explained by assuming them as rigid. In hovering flight the airloads do not vary with azimuth, and so the blades

flap up and lag back with respect to the hub and reach a steady equilibrium position under a simple balance of aerodynamic and centrifugal forces. However, in forward flight the fluctuating airloads cause continuous flapping motion and give rise to aerodynamic, inertial, and Coriolis forces on the blades that result in a dynamic response. The flapping hinge allows the effects of the cyclically varying airloads to reach an equilibrium with airloads produced by the blade flapping motion. The flapping motion is highly damped by the aerodynamic forces.

The part played by the rotor is highly complicated, because strictly each blade possesses its own degrees of freedom and makes an individual contribution to any disturbed motion. Fortunately, however, analysis can almost always be made satisfactorily by considering the behavior of the rotor as a whole.

Considering the flapping, feathering, lead-lag motion of the blades of both main rotor and the tail rotor, as well as the motion of the main rotor with respect to the fuselage, the swash plate mechanism and the moving horizontal stabilators in some of the helicopters, there are so many equations of motion that one should solve in order to analyze.

Because of the fact that a helicopter has so many degrees of freedom, it is much more difficult to analyze. The fuselage has 6 degrees of freedom, the main rotor has 4 DOF, 3 for rotor flapping and one for the rotation of the rotor (throttle), tail rotor has also 4 DOF, etc. However, with some feasible assumptions, the helicopter system can be reduced to 6 DOF like a fixed-wing aircraft, three for translation and three for rotation.

The static stability of an air vehicle is the tendency of the vehicle to return to its trimmed condition following a disturbance. Meanwhile, the dynamic stability considers the subsequent motion in time. If the aircraft tends to

return to its trimmed position then the aircraft is stable; if there exists no motion, then it is neutrally stable; and if the aircraft tends to diverge from its initial state, then the aircraft is unstable. The divergence or convergence motions can either be oscillatory or not. A statically unstable motion is also dynamically unstable but a statically stable motion may be either stable or unstable dynamically.

2.5 THEORY AND CODE DEVELOPMENT

A helicopter with a main rotor and a tail rotor, assuming it as having a rigid structure, has about 36 differential equations [19], which makes the problem really non-linear and very difficult to solve. The following general simplifications are implemented in order to make the problem easier:

- The helicopter structure is considered to be absolutely rigid;
- Longitudinal and lateral motions are uncoupled so they can be treated independently;
- No time lags are considered;
- One DOF coming from the throttle is eliminated and the rotor speed is set as constant;
- The blades are assumed as uniform and the lag bending, elastic twist, and axial deflections are disregarded, except the flapping motion;
- The blades do not bend or twist elastically;
- The blades have homogeneous mass distribution;
- Harmonics higher than 2nd order of flapping and cyclic angles are neglected;
- Empirical downwash, sidewash, L&D of empennage relaons are used;
- The codes are applicable only to helicopters with single main rotor and a tail rotor;
- Climb angle and sideslip angle are set as zero.

On the basis of these simplifications, the system describing the helicopter motion can be reduced to six equations. These equations are the total forces and moments on each of the coordinate axis:

$$\sum X = 0 \Leftrightarrow X_M + X_T + X_H + X_V + X_F = W.Sin\Theta$$
$$\sum Y = 0 \Leftrightarrow Y_M + Y_T + Y_V + Y_F = -W.Sin\Phi$$
$$\sum Z = 0 \Leftrightarrow Z_M + Z_T + Z_H + Z_V + Z_F = -W.Cos\Phi$$
$$\sum L = 0 \Leftrightarrow L_M + Y_M h_M + Z_M y_M + Y_T h_T + Y_V h_V + Y_F h_F + L_F = 0$$
$$\sum M = 0 \Leftrightarrow \begin{pmatrix} M_M - X_M h_M + Z_M l_M + M_T - X_T h_T + Z_T l_T - X_H h_H \\ + Z_H l_H - X_V h_V + M_F + Z_F l_F - X_F h_F \end{pmatrix} = 0$$
$$\sum N = 0 \Leftrightarrow N_M - Y_M l_M - Y_T l_T - Y_V l_V + N_F - Y_F l_F = 0$$

The forces and moments with the moment arms are demonstrated in Figure 2-10. The details on the calculations of the forces are expressed in appendices A and B.

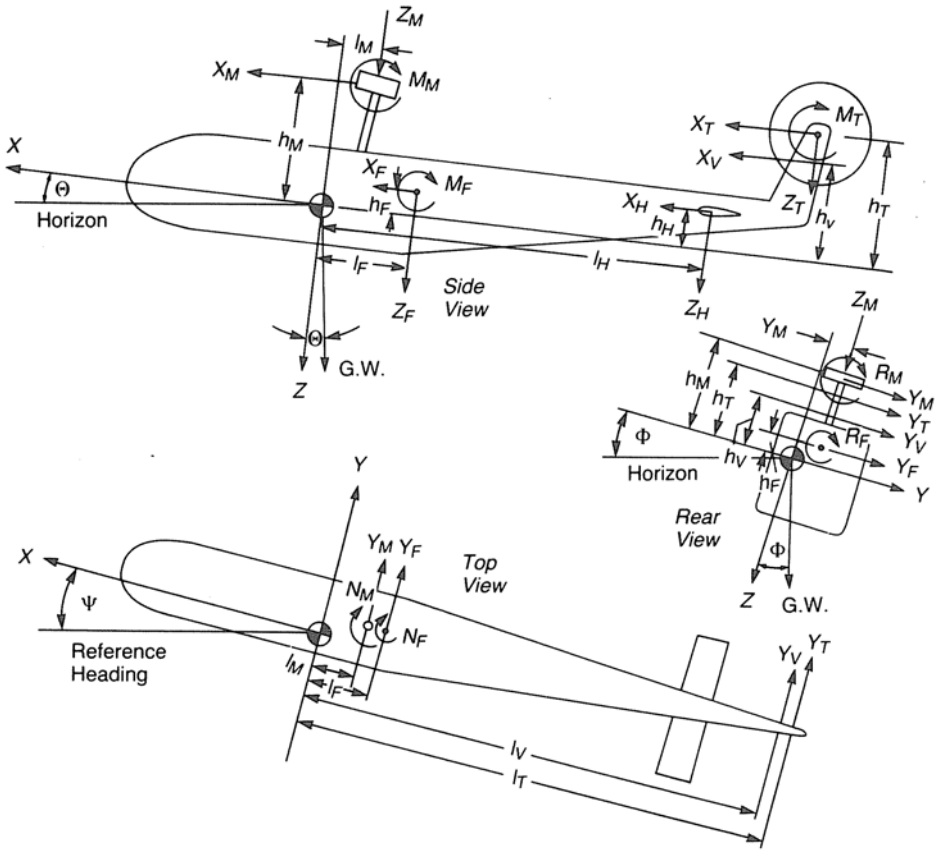

Figure 2-10: Forces and moments acting on a helicopter [3].

The set of forces and moments acting on the helicopter has been modeled as follows:

1. **Main rotor forces and moments:** For the main rotor thrust, in some parts of the codes it is assumed that the inflow is steady and uniform, and in some other parts a sinusoidal approximation is used. In TRIM-CF the thrust is computed using a momentum theory based iterative scheme, while in TRIM-BE it is computed using the blade element theory. As for the rotor moments, two contributions have been considered. The first contribution comes from the blade attachment to the rotor head, where the restraint forces can be approximated using a linear torsional spring with a constant stiffness. The second contribution comes from the tilting of the thrust vector.

Those two contributions can be explained in Figure 2-11, where the first one is designated with M_M and the second term is $T_M l_M Cos(a_{1s})$. Assuming that the thrust vector is perpendicular to the TPP (Tip Path Plane), the thrust vector will tilt proportionally to the rotor flapping angles.

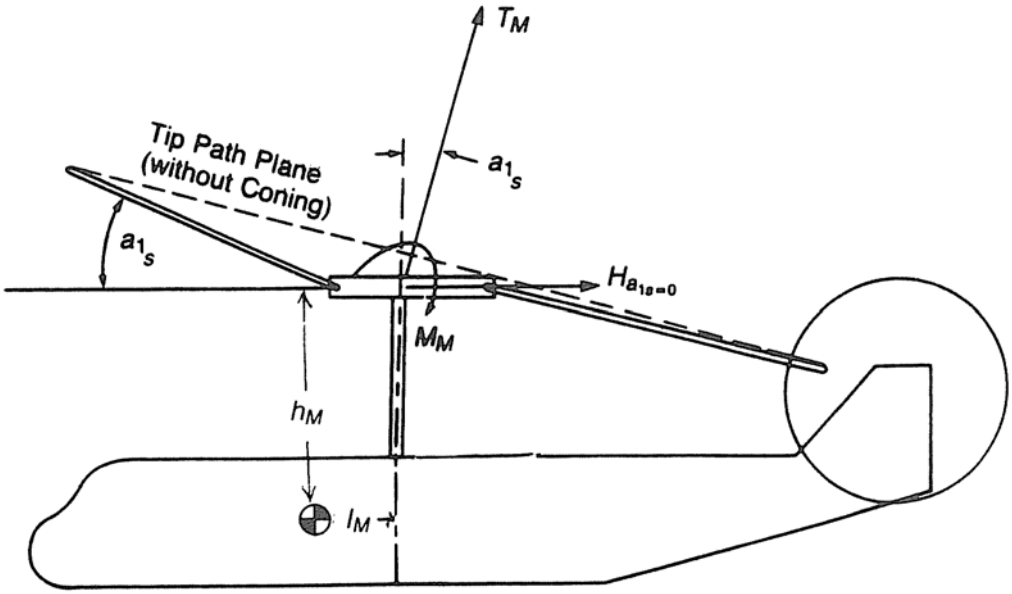

Figure 2-11: The thrust vector on main rotor [3].

2. **Fuselage forces:** The fuselage creates lift and drag. Main rotor downwash effects are also included.

3. **Tail rotor forces and moments**: The only control input is the collective pitch coming from the pedals, directly influencing induced velocity and therefore thrust.

4. **Empennage forces and moments**: The horizontal and vertical stabilizers produce lift and drag. The empennage forces take into account the effect of the main and tail rotor wake. The corresponding moments are computed as the forces multiplied by their distance from the helicopter center of gravity.

Atmosphere parameters are used for taking into account the altitude effect on air density, pressure and temperature. Climb angle γ_c is taken as zero and is not included in the equations within this report. Also the sideslip angle β is taken as zero. The helicopter is assumed to combine the six degrees of freedom rigid body equations of motion (in body axis) with the lateral & longitudinal flapping dynamics.

The codes are applicable only to helicopters with single main rotor and a tail rotor.

The effect of external stores on the trim and dynamic stability can be included in the analysis by taking into account of the fuselage force and moment calculations, as well as the total weight effect. Those parameters can be found using package CFD programs, wind tunnel measurements or with a very rough local drag calculations.

2.5.1 TRIM-BE CODE

The TRIM-BE code consists of four loops. The outermost loop provides trim parameters for the full velocity regime, increasing the velocity values incrementally from about 30 knots to the maximum obtainable velocity value. The maximum obtainable velocity for the example helicopter is 165 knots, while for UH-60 helicopter it is about 150 knots. The other rotorcraft parameters are accepted as the inputs to the code. The second and third loops going from outer side to the inner side make sure that the total longitudinal and vertical forces acting on the helicopter converge to zero within tolerable limits. The innermost loop makes sure that the roll and pitch moment coefficients of the main rotor converge to a value within tolerances. The loops are clearly demonstrated in Figure 2-12.

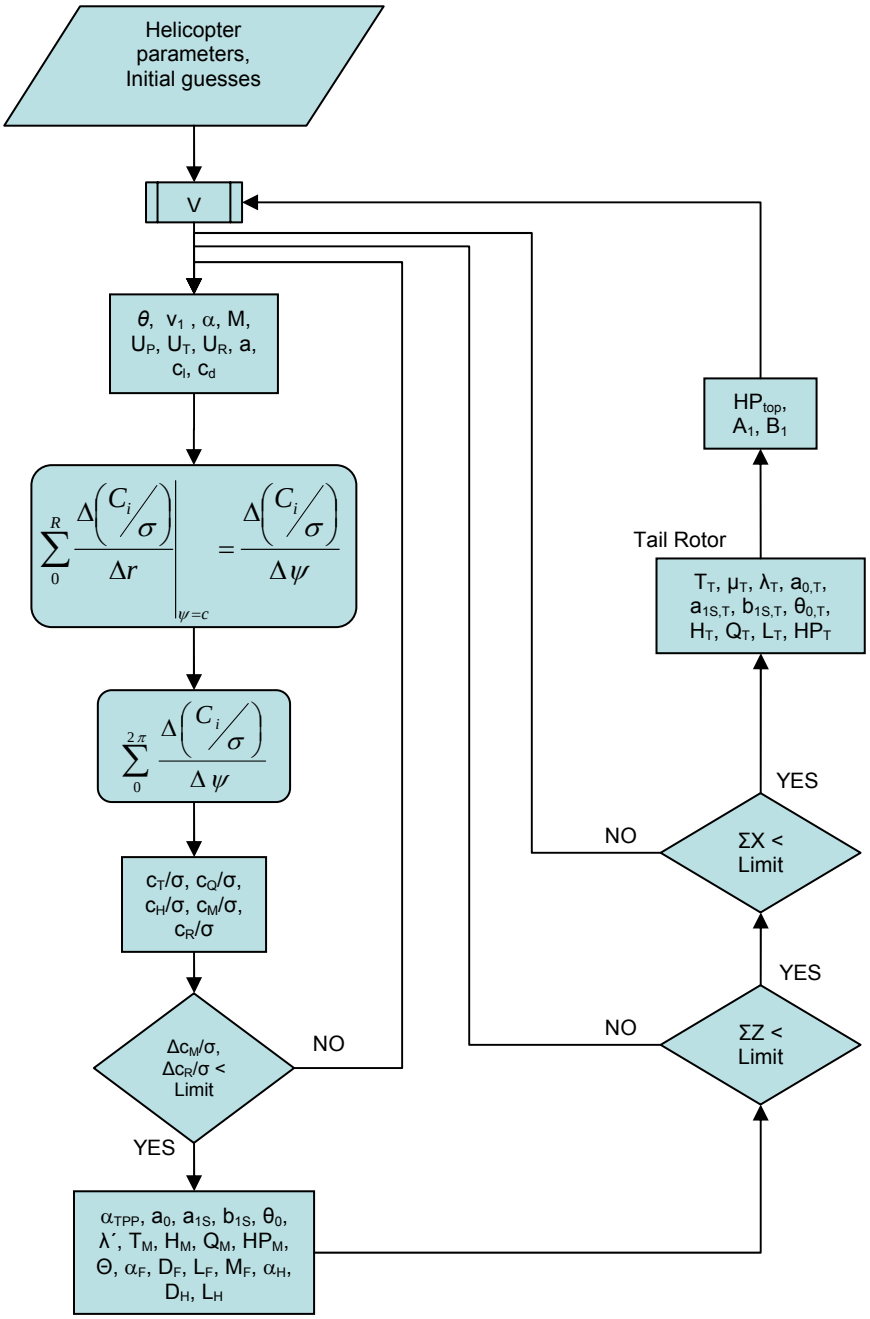

Figure 2-12: Flowchart of TRIM-BE code.

The assumptions used in the module are the general assumptions listed in the previous section, as well as the items given below:

- Among the blade characteristics, the twist is assumed as constant [15]; 20 degrees sweep on the tip region of the blade is ignored; the blade section from the cut-out section to the radial station of 0.1925R where SC1095 airfoil section is started is assumed as having an airfoil section SC1095; the chord increase in the swept region and the trim tab region (between 0.7316R and 0.8629R) are ignored; the cord difference between the two airfoil sections are ignored and an approximate cord is used; the zero lift angle of attack is taken as an approximate value, comparing to the -0.2 degrees for the SC1095 airfoil and -1.5 degrees for SC1094 R8 airfoil.
- Momentum theory used to find the average induced velocity. The induced velocity distribution is a sinusoidal function through the azimuth.
- Empirical A/F parameters aree used.

Within the core of the program, the local lift and drag coefficients of the main rotor blades' sections corresponding to the assigned azimuthal and radial stations are calculated using the experimental two-dimensional airfoil lift and drag coefficients. Lift and drag coefficients are used to calculate the three-dimensional force coefficients. The code accounts for the reverse flow, the compressibility effect occurring on the advancing side in high speeds, dynamic stall effect, root and tip losses, drag divergence effects and unsteady aerodynamics. The local lift and drag coefficients are used to calculate the local thrust, torque, H-force and moment coefficients, which are integrated to obtain the main rotor total force and moment values. Simpson's Rule is used as the integration method. The blades are divided into 10 radial sections and the disc is divided into 36 azimuthal angle sections. Although the code can be modified to solve for different increments of blade and azimuth angles, the present values are accepted

as giving satisfactory accuracy for a trim analysis. The integration method allows us to exclude the tip and root losses with simple subtractions.

One of the empirical approaches used in the code is relating the roll and pitch moment coefficients to the first harmonics of the blade feathering. The innermost loop of the code is completed after those related parameters are converged to tolerable values. Some other empirical approaches are relating the total longitudinal and vertical forces acting on the helicopter to the inflow ratio and to the collective angle. Those relations compose the criteria of the second and third loops.

The limitations and assumptions additional to the ones listed before are:

1. Obtaining performance and trim conditions is the primary objective, while still the first flapping harmonics are calculated.
2. Two dimensional main rotor airfoil and drag characteristics are available.
3. The blades do not bend or twist elastically
4. The induced velocity distribution is a sinusoidal function through the azimuth.

The tail rotor trim parameters are calculated using closed-form equations.

The power losses introduced by the power generators, hydraulic system and transmission system are also taken into account in the power calculations.

The code is able to calculate the effects of load carrying wings if there exist any.

The formulations and detailed theory used in the code are given in Appendix-A.

2.5.2 TRIM-CF CODE

The motion of a helicopter in trim is governed by 6 equations, three for total forces acting on the aircraft and three for the total moments on each coordinate of the body frame. One can separate the longitudinal and lateral equations and solve for the related parameters without much degradation on the accuracy. Therefore, the code solves for only three equations, which are the total forces on the longitudinal and vertical axes and the total moments on the lateral axis.

The code is composed of two modules, called CF and XZM. The first module supplies approximate trim parameters which are used as inputs to the second module. The second module, uses those input parameters in order to linearize the non-linear equations of motion and gives the exact trim parameters. The flowchart of the code is given in Figure 2-13.

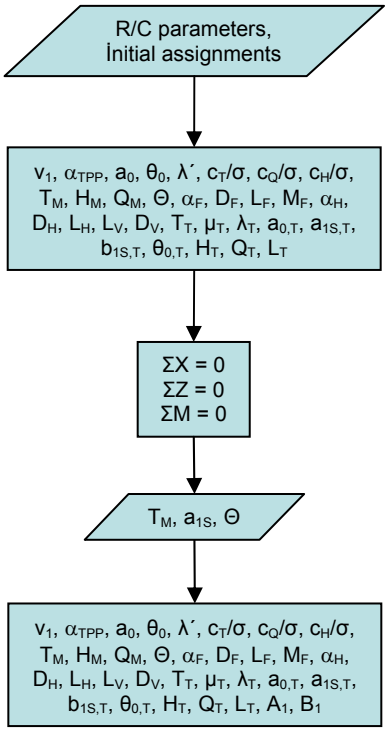

Figure 2-13: Flowchart of TRIM-CF code.

The additional assumptions, after the general assumptions given before are:

- Momentum theory is used to find the induced velocity
- Approximated rotor characteristics are used
- Flapping motion of individual blades replaced by the motion of the cone
- Actions of the MR and TR replaced by forces and moments applied to hubs

The equations used in the TRIM-CF code are closed form equations. The code is applicable to flight velocities higher than 30 knots. This is because the angle of attack over the empennage diverges to unreasonable values.

In the CF module the first harmonic flapping angles a_{1s} and b_{1s} are set to zero, i.e. the first order harmonics are also neglected. Those flapping angles are computed at the XZM module.

The first module is based on calculating the following two parameters, α_{TPP} and T_M, and modifying the other trim variables according to those parameters.

$$\alpha_{TPP} = \tan^{-1}\left(\frac{D_{F,em.on} + H_M + H_T}{W - L_{F,em.on}}\right) \quad (1)$$

$$T_M = \sqrt{\left(W - L_{F,em.on}\right)^2 + \left(D_{F,em.on} + H_M + H_T\right)^2} \quad (2)$$

Here $L_{F,em.on}$ and $D_{F,em.on}$ correspond to the lift and drag over the fuselage for the empennage on case.

The closed form equations include the tip losses, the compressibility effects and the reverse flow effects also. The fuselage lift, drag and pitching moment parameters are calculated using the wind-tunnel force measurement results of the helicopter.

The second module calculates the total forces and moments stated below:

$$\sum X = X_M + X_T + X_H + X_V + X_F - W\Theta = 0 \quad (3)$$

$$\sum Z = Z_M + Z_T + Z_H + Z_V + Z_F + W = 0 \quad (4)$$

$$\sum M = \begin{pmatrix} M_M + M_T + M_F - X_M h_M + Z_M l_M - X_T h_T \\ + Z_T l_T - X_H h_H + Z_H l_H - X_V h_V + Z_F l_F - X_F h_F \end{pmatrix} = 0 \quad (5)$$

Here the unknown parameters are the thrust of the main rotor, the pitch attitude and the first harmonic longitudinal flapping angle. In order to solve

those coupled equations, some of the variables are taken as constant, the values of which are calculated with the CF module.

The thrust of the tail rotor is found from the main rotor torque. To find the pedals angle, the precone angle of the tail rotor of the UH-60 helicopter is subtracted from the calculated a_{0_T} value. The 20 degrees inclination of the tail rotor is also included in the calculations.

2.5.3 DYNA-STAB CODE

Longitudinal stability of the helicopter in forward flight is analyzed in two modes: short period mode and phugoid mode. Those frequently oscillatory motions are observed just after a disturbance -like a vertical gust or a longitudinal cyclic step input- occurs. The short period response is based mainly on pitching motion and generally damps quickly. Almost no change occurs in altitude. The phugoid mode is based mainly on altitude change and is generally divergent, able to cause a drastic loss of control on the helicopter. The energy is converted to kinetic energy while descending and the velocity increases; increased velocity increases the thrust and the helicopter is forced to climb; then as the climbing occurs, the velocity is decreased again. The responses of the helicopter after a disturbance are shown in Figure 2-14.

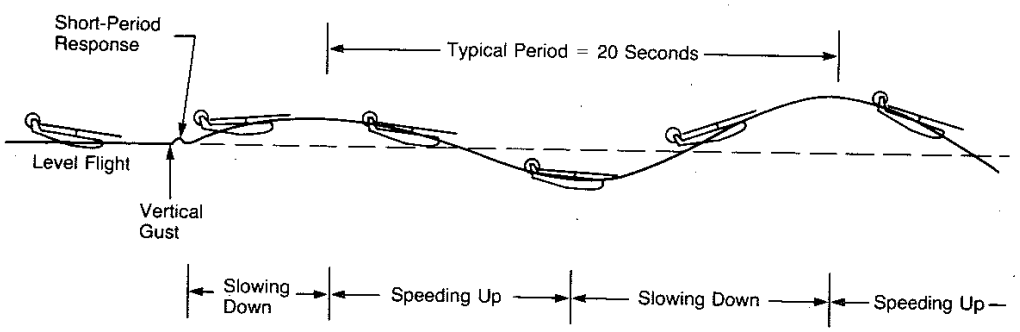

Figure 2-14: The Phugoid and Short Period Modes.

Ignoring the coupling between the lateral-directional and longitudinal motions, the equations of motion governing the longitudinal forward flight can be reduced to three, which are composed of total forces on x and z direction on body frame and pitching moments, with longitudinal cyclic and collective inputs:

$$\underbrace{\begin{bmatrix} -\frac{W}{g}s^2 + \frac{\partial X}{\partial \dot{x}}s & \frac{\partial X}{\partial \dot{z}}s & \left(\frac{\partial X}{\partial q} - \frac{W}{g}\overline{V\Theta}\right)s - W \\ \frac{\partial Z}{\partial \dot{x}}s & \left(\frac{\partial Z}{\partial \ddot{z}} - \frac{W}{g}\right)s^2 + \frac{\partial Z}{\partial \dot{z}}s & \left(\frac{\partial Z}{\partial q} + \frac{W}{g}\overline{V}\right)s \\ \frac{\partial M}{\partial \dot{x}}s & \frac{\partial M}{\partial \ddot{z}}s^2 + \frac{\partial M}{\partial \dot{z}}s & -I_{yy}s^2 + \frac{\partial M}{\partial q}s \end{bmatrix}}_{A} \begin{bmatrix} x(s) \\ z(s) \\ \Theta(s) \end{bmatrix} = \begin{bmatrix} -\frac{\partial X}{\partial \theta_{0_M}} & -\frac{\partial X}{\partial B_1} \\ -\frac{\partial Z}{\partial \theta_{0_M}} & -\frac{\partial Z}{\partial B_1} \\ -\frac{\partial M}{\partial \theta_{0_M}} & -\frac{\partial M}{\partial B_1} \end{bmatrix} \begin{bmatrix} \theta_{0_M} \\ B_1 \end{bmatrix} \tag{6}$$

Without solving the equations, the A matrix alone gives the stability characteristics of the helicopter. The characteristic equation is found and the roots are calculated. Because of the number of equations of motion, the characteristic equation is in a form:

$$As^4 + Bs^3 + Cs^2 + Ds + E = 0 \tag{7}$$

And the Routh's Discriminant (Routh's Test) is described as:

$$R.D.= BC - AD \tag{8}$$

A negative Routh Discriminant shows that the system is unstable, while a positive value indicates that no unstable oscillation occurs. Also, if all coefficients of the characteristic equation are positive, the system in that condition has no positive real root and therefore no pure divergence occurs. If the constant D is zero, there will be one zero root and one degree of freedom will have non-oscillatory neutral stability. If one of the coefficients is negative, then there will be either a pure divergence or an unstable oscillation.

The roots of the characteristic equation give the details of the oscillations, such as the frequency. If the real part of one root is negative, then that root introduces a convergent motion, and vice versa. If an imaginary part exists, two roots being complex conjugate, those two roots introduce an oscillatory motion, the convergence depending on the real part.

The period, frequency and the time-to-double parameters are calculated as described below:

The period of the oscillation:

$$T = \frac{2\pi}{|im(s)|}. \tag{9}$$

Here s is a complex root.

The time-to-double:

$$t_{double} = \frac{\ln(2)}{re(s)}. \tag{10}$$

And the neutral frequency of the oscillation is:

$$\omega_n = |im(s)| \tag{11}$$

The DYNA-STAB code calculates the required stability derivatives, the characteristic equation and the roots, and determines about the stability of the helicopter after a step disturbance given by the longitudinal cyclic, the collective or due to a vertical gust. The calculations of the stability derivatives are given in Appendix C.

Some of the inputs the DYNA-STAB code uses are the wind tunnel test results for the fuselage lift, drag and pitching moment as a function of angle of attack. Those parameters can also be calculated using package CFD programs.

2.6 VERIFICATION

2.6.1 PROUTY'S EXAMPLE HELICOPTER

The example helicopter described in [3] is used to verify the trim codes. The trim results at 115 knots are obtained and compared with the results given in the reference book [3]. The helicopter is very similar in geometry to the UH-60 helicopter as it can be seen in Figure 2-15. Therefore, it is expected that the results are also comparable. The input parameters are as listed in Table 2-1. Both TRIM-BE and TRIM-CF codes are used to compute the trim parameters of the example helicopter at 115 knots forward speed and the results are tabulated in Table 2-2.

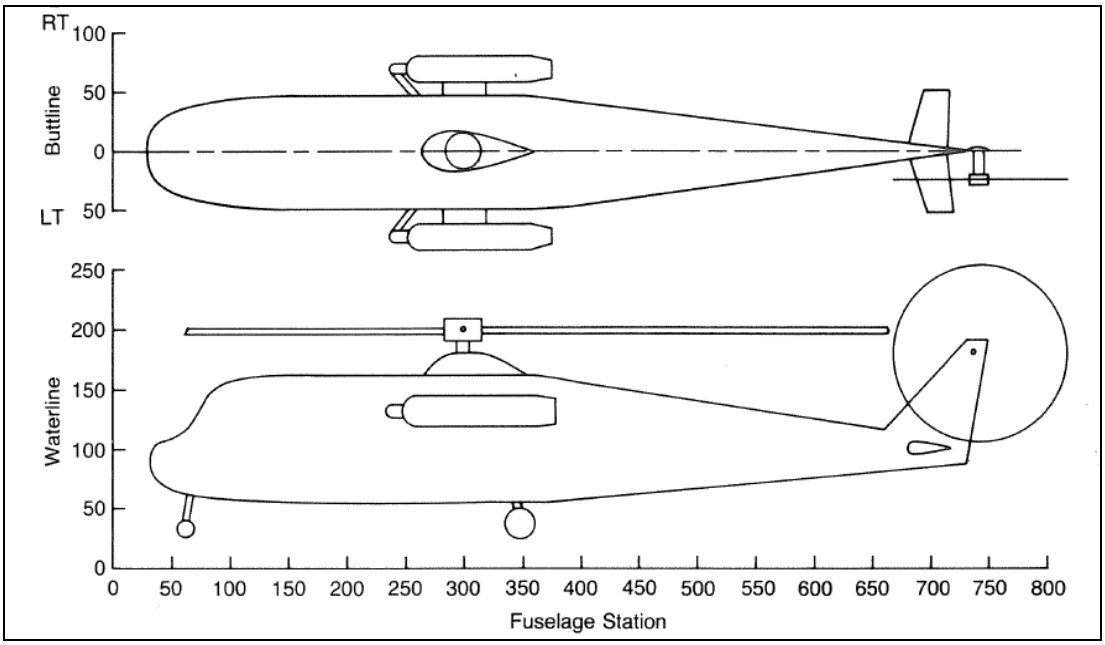

Figure 2-15: The example helicopter in [3].

Table 2-1: Example helicopter input parameters in [3].

Description	Algebraic Symbol	Value	Unit
Moment of inertia about y axis	I_{yy}	40000	slug.ft^2
Weight of the helicopter	GW	20000	lb
MAIN ROTOR			
Radius	R_M	30	ft
Chord	c_M	2	ft
Number of Blades	b	4	
Revolution Speed	Ω	21.667	rad/sec
Lift curve slope (NACA 0012)	a	5.73	per radian
Zero Lift Angle of Attack	$\alpha_{L=0}$	0	
Blade twist angle	θ_1	-10	degrees
Height of the rotor above C.G.	h_M	7.5	ft
Long. Distance to C.G.	l_M	-0.4839	ft
Hinge offset ratio	e	0.05	

Table 2-1 Continued: Example helicopter input parameters in [3]

Description	Algebraic Symbol	Value	Unit
Blade cut-out ratio	$\frac{x_o}{R}$	0.15	
Flapping inertia of one blade	I_b	2900	slug.ft^2
Polar moment of inertia	J_M	11600	slug.ft^2
Shaft incidence	i_M	0	degrees
TAIL ROTOR			
Radius	R_T	6.5	ft
Chord	c_T	1	ft
Number of Blades	b_T	4	
Revolution Speed	Ω_T	100	rad/sec
Lift curve slope	a_T	6	per radian
Blade twist angle	$\theta_{1,T}$	-5	degrees
Height of the rotor above C.G.	h_T	6	ft
Long. Distance to C.G.	l_T	37	ft
Shaft incidence	i_T	0	degrees
Delta3 angle	δ_3	-30	degrees
Flapping inertia of one blade	$I_{b,T}$	6.25	slug.ft^2
HORIZONTAL STABILIZER			
Span	b_H	9	ft
Area (incl. area inside tail boom)	A_H	18	ft^2
Zero Lift Angle of Attack	$\alpha_{L=0,H}$	0	rad
Moment arm (measured from its rotational axis)	l_H	33	ft
Height above C.G	h_H	-1.5	ft
Incidence	i_H	-3	degrees
VERTICAL STABILIZER			
Span	b_V	7.7	ft
Area (incl. area inside tail boom)	A_V	33	ft^2
Rudder deflection	$\delta_{r,V}$	10	degrees
Moment arm	l_V	35	ft

Table 2-1 Continued: Example helicopter input parameters in [3]

Description	Algebraic Symbol	Value	Unit
Height above C.G	h_V	3	ft
FUSELAGE	f_o $\frac{\partial f}{\partial(\alpha_F^2)}$	17.9 0.023	ft^2 ft^2/deg^2
Wetted area	S_{W_F}	680	ft^2
Moment arm	l_F	-0.5	ft
Lift - Empennage on	$\left(L_F/q\right)_{\alpha_F=0}$ $\frac{\partial\left(L_F/q\right)}{\partial\alpha_F}$	-5 111.8987	ft^2 ft^2/rad
Pitch Moment $M_F = q\left(\left(M_F/q\right)_{\alpha_F=0} + \frac{\partial\left(M_F/q\right)}{\partial\alpha_F}\alpha_F\right)$	$\left(M_F/q\right)_{\alpha_F=0}$ $\frac{\partial\left(M_F/q\right)}{\partial\alpha_F}$	-160 1789	ft^3 ft^3/rad
Drag divergence Mach #	M_{dd}	0.725	

Table 2-2: TRIM-BE and TRIM-CF results for the example helicopter [3]

Parameter	TRIM-CF Results	TRIM-BE Results	[3] Given Values	Unit
Main Rotor				
υ_1	7,87	7,91	7.8783	-
λ'_M	-0,0200	-0,0309	-	-
a_{0_M}	4,13	4,37	-	Degree
a_{1S_M}	-0,90	-1,31	-1.0886	Degree
$A_{1_M} - b_{1S_M}$	-1,58	-2,39	-	Degree
B_{1_M}	5,98	4,58	-	Degree
θ_{0_M}	15,48	13,38	-	Degree

Table 2-2 Continued: TRIM-BE and TRIM-CF results for the example helicopter [3]

Parameter	TRIM-CF Results	TRIM-BE Results	[3] Given Values	Unit
α_{TPP}	-1,51	-3,60	-	Degree
T_M	20544,29	20648,95	20586	lbf
H_M	-287,58	381,73	-145	lbf
Q_M	33512,22	35433,42	34573	lbf.ft
HP_M	1320,20	1395,86	-	hp
Tail Rotor				
λ_T	-0,0079	-0,0105	-	-
a_{0_T}	0,58	0,83	-	Degree
a_{1S_T}	1,43	0,42	-	Degree
b_{1S_T}	-0,17	-0,26	-0.3094	Degree
θ_{0_T}	6,28	6,01	-	Degree
Q_M / l_T	905,74	957,66	934.4	lbf
T_T	629,70	835,17	661	lbf
H_T	-19,55	29,77	40	lbf
Q_T	120,73	268,07	127	lbf.ft
Fuselage				
α_F	-2,94	-4,62	-3.6752	Degree
L_F (empennage on)	-480,66	-629,26	-556	lbf
D_F (empennage on)	871,86	884,66	867	lbf
L_F (empennage off)	-239,28	-338,74	-283	lbf
D_F (empennage off)	810,33	884,66	794	lbf
M_F	-11248,68	-13618,07	-11722	lbf.ft
Θ	-0,61	-2,29	-0.9454	Degree
Horizontal Stabilizer				
α_H	-7,92	-7,73	-8.0743	Degree
L_H	-267,46	-261,32	-273	lbf
D_H	14,30	14,06	15	lbf

Table 2-2 Continued: TRIM-BE and TRIM-CF results for the example helicopter [3]

Parameter	TRIM-CF Results	TRIM-BE Results	[3] Given Values	Unit
Vertical Stabilizer				
L_V	287,93	130,33	287	lbf
D_V	51,48	-14,06	58	Lbf

Considering the results given in Table 2-2, the TRIM-CF code gives more accurate results for the main rotor parameters than TRIM-BE. It also shows good agreement to the actual results for the tail rotor thrust and torque. Fuselage, horizontal stabilizer and vertical stabilizer parameters as well are closer to the values given in the reference book. Moreover, TRIM-CF code uses less input parameters and less computing time. Therefore, it is considered more feasible to use TRIM-CF code in UH-60 helicopter analysis.

There is a difference on the values for the H-force, however, it should be noted that H-force is a very difficult parameter to consider. It is composed of the horizontal component of the thrust vector and the drag over the rotor disc, therefore minor changes in the angle of attack, the thrust and drag cause major differences in the H-force.

2.6.2 PADFIELD'S EXAMPLE HELICOPTER

The example helicopter given in [2] is the twin engine, light weight Bo105 helicopter which is shown in Figure 2-16. The input parameters for the Bo-105 helicopter are tabulated in Table 2-3.

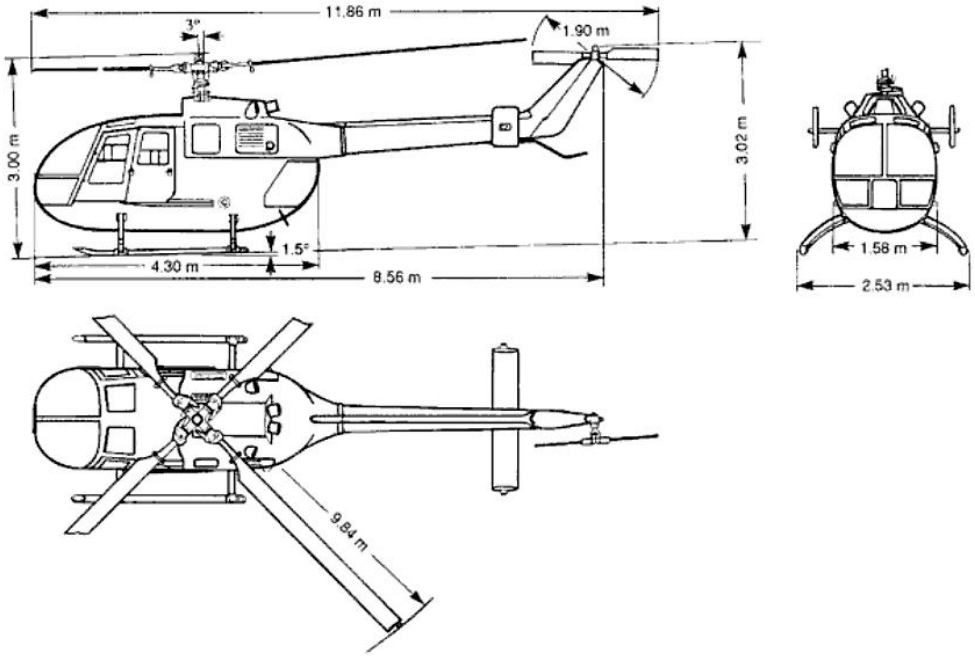

Figure 2-16: Bo105 helicopter [2].

Table 2-3: Example helicopter input parameters in [2].

Description	Algebraic Symbol	Value	Unit
Moment of inertia about y axis	I_{yy}	4973	kg.m^2
Weight of the helicopter	GW	2200	kg
MAIN ROTOR			
Radius	R_M	4.91	m
Chord	c_M	0.27	m
Number of Blades	b	4	
Solidity	σ	0.12	
Revolution Speed	Ω	44.4	rad/sec
Lift curve slope (NACA23012)	a	6.113	per radian
Drag coefficient $c_D = \delta_o + \delta_2 C_T^2$	$c_{D,o} = \delta_o$ δ_2	0.0074 38.66	
Blade twist angle	θ_1	-0.14	rad
Long. Distance to C.G.	l_M	-0.0163	m
Flapping inertia of one blade	I_b	231.7	kg.m^2
Lock No	γ_M	5.087	

Table 2-3 Continued: Example helicopter input parameters in [2]

Description	Algebraic Symbol	Value	Unit
Shaft incidence	i_M	-3	degrees
TAIL ROTOR			
Radius	R_T	0.95	m
Number of Blades	b_T	2	
Revolution Speed	Ω_T	233.1	rad/sec
Lift curve slope	a_T	5.7	per radian
Long. Distance to C.G.	l_T	6.0163	m
Shaft incidence	i_T	0	degrees
Delta3 angle	δ_3	-45	degrees
Drag coefficient $c_D = \delta_o + \delta_2 C_T^2$	$c_{D,o,T} = \delta_{o,T}$ $\delta_{2,T}$	0.008 9.5	
HORIZONTAL STABILIZER			
Area	A_H	0.803	m^2
Moment arm	l_H	4.5763	m
VERTICAL STABILIZER			
Area	A_V	0.805	m^2
Moment arm	l_V	5.4323	m

Drag, lift and pitch moment parameters of the fuselage are calculated as it is explained in the reference book pages 266-267 [2]. Those parameters belonging to the empennage-on case are illustrated in Figures 2-17 to 2-19. They are used as inputs to the trim code.

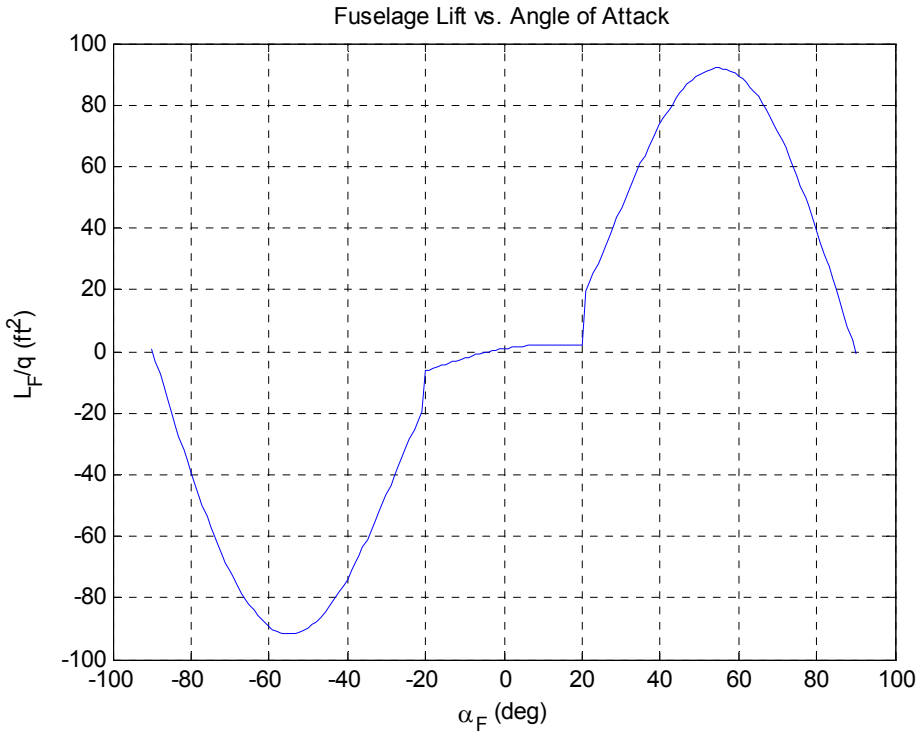

Figure 2-17: Lift per unit dynamic pressure obtained from the fuselage of Bo105 [2]

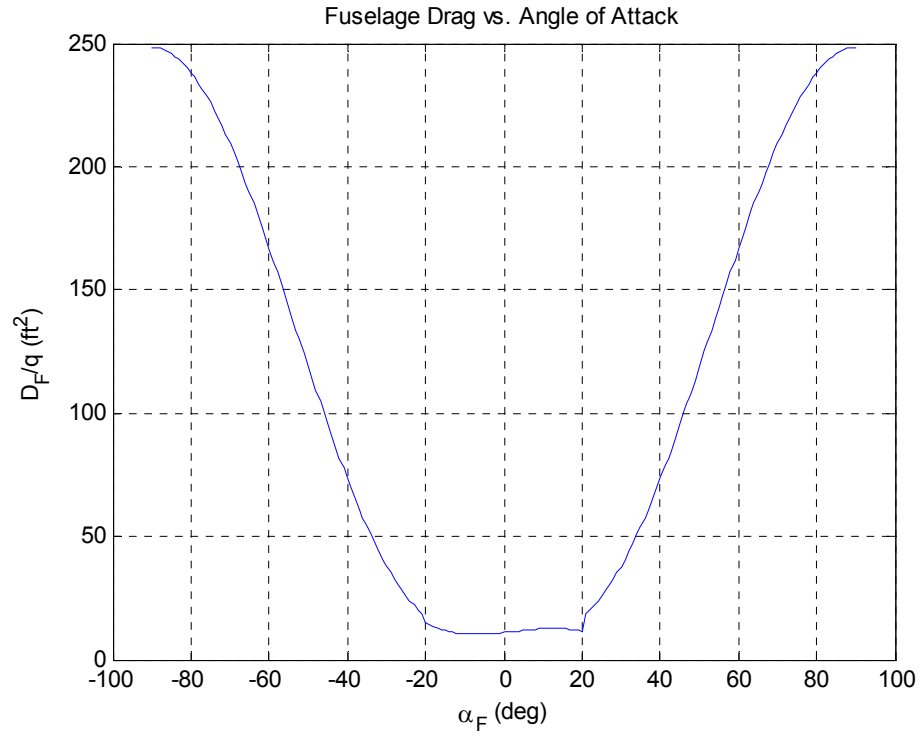

Figure 2-18:Drag per unit dynamic pressure obtained from the fuselage of Bo105 [2].

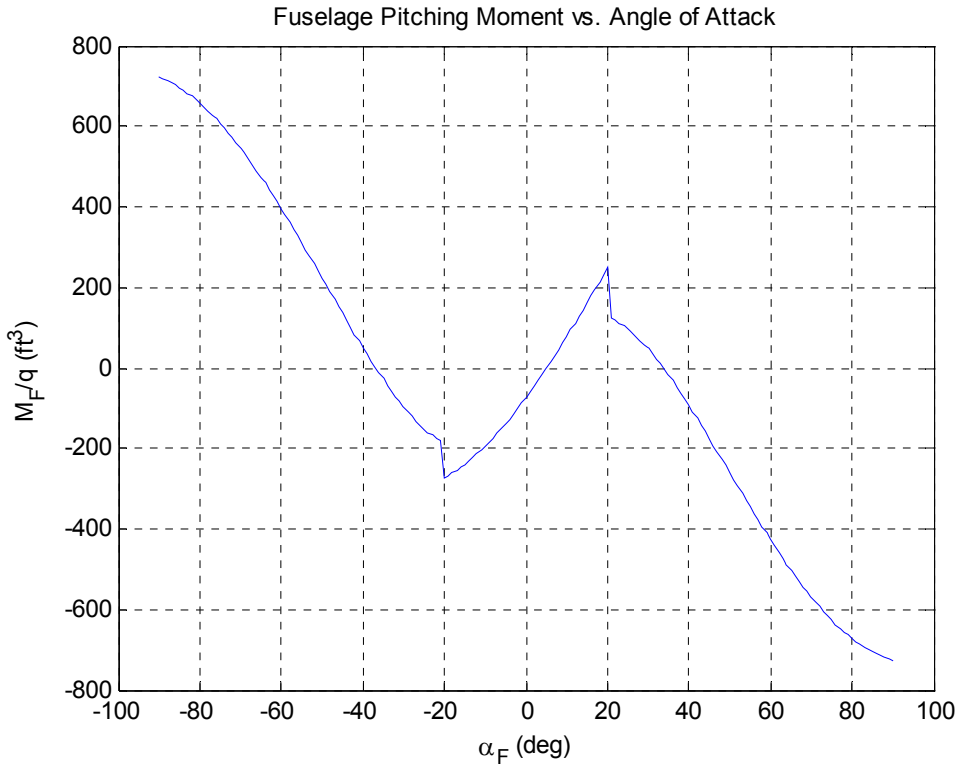

Figure 2-19: Pitching moment per unit dynamic pressure obtained from the fuselage of Bo105 [2].

The trim analysis results are shown with respect to the data given in the reference book [2]. The given data is composed of the main rotor torque, main rotor power, collective angle of the main and tail rotors, the pitching attitude of the fuselage and the longitudinal cyclic angle (1^{st} longitudinal harmonic of the flapping angle). The book gives both the flight test results of the helicopter and the analysis results obtained by a trim code called Helisim. The graphs below include both the given flight test data and the Helisim results, as well as the results obtained with the present TRIM-CF code.

Figure 2-20 shows the calculated torque and the data of Ref. [2] together. It is evident from the figure that the torque values lack a little bit from the accuracy compared to the flight test data. It is difficult to consider which

code, Helisim or TRIM-CF, gives closer results to the flight test data. The shift in the curves shall be analyzed, which is a deficiency in the TRIM-CF code. Figure 2-21 also shows the torque value associated only with the main rotor power.

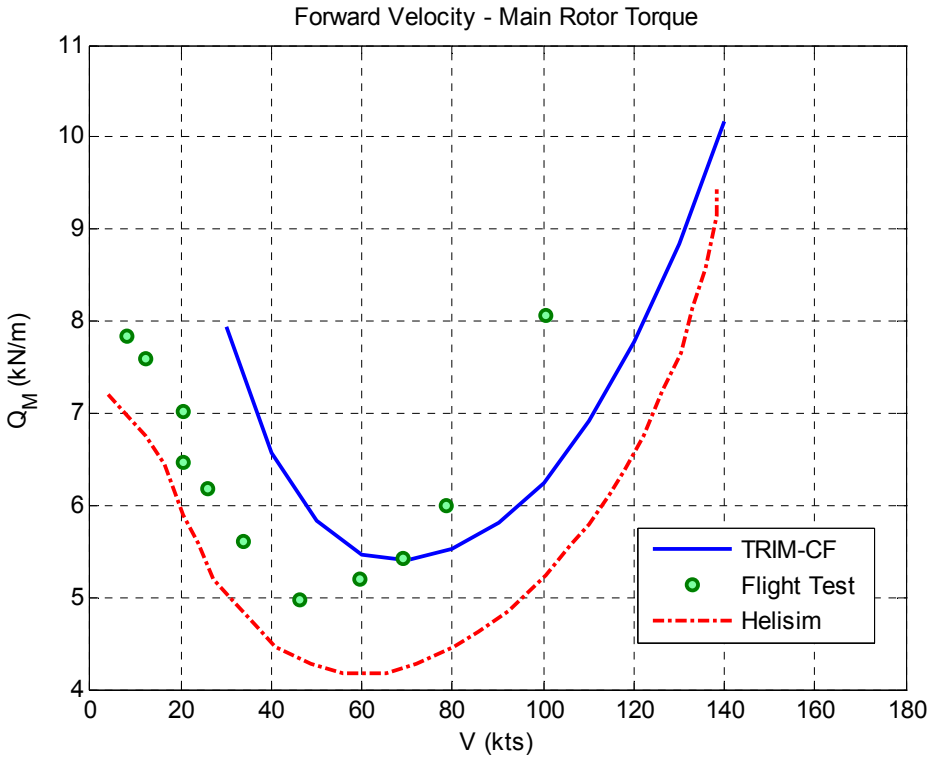

Figure 2-20: Main rotor torque compared with flight test data and Helisim results for Bo105 [2].

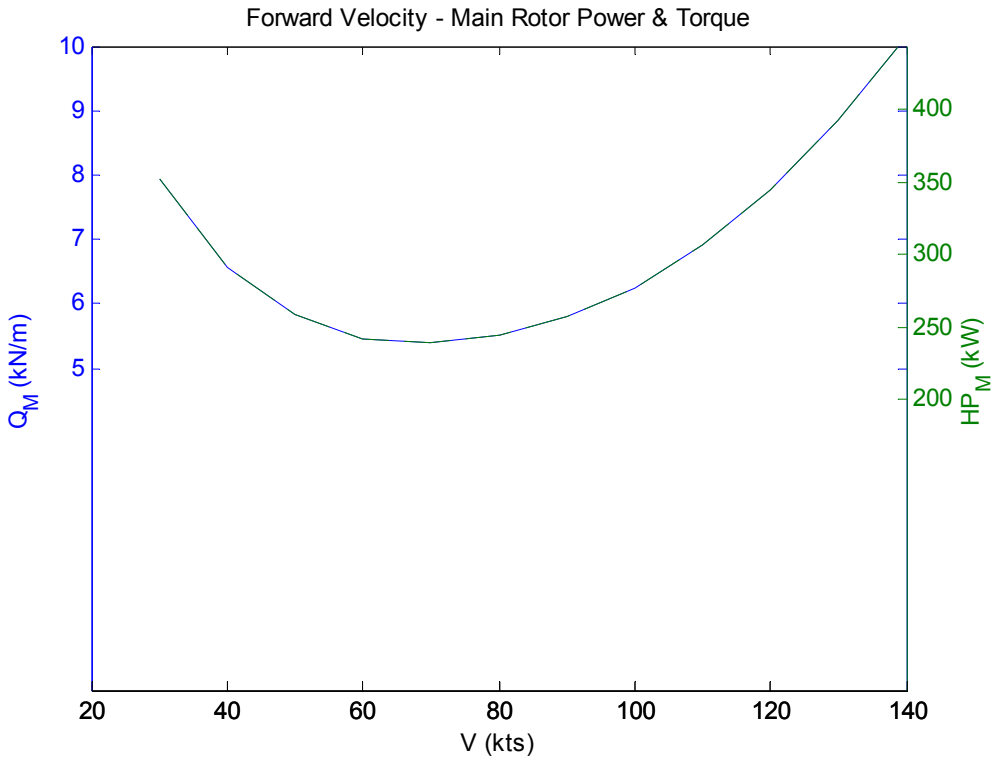

Figure 2-21: Main rotor torque and power for Bo105 [2].

The collective angle results shown in Figure 2-22 are very good compared to the ones obtained with the Helisim results of [2]. Especially for low flight velocities, the analysis results fit very well to the test data.

The longitudinal cyclic angle results in Figure 2-23 fit the attitude of the test data curve just like the Helisim code does, however, Helisim gives best results. There is about half a degree of difference between the test data and the TRIM-CF results.

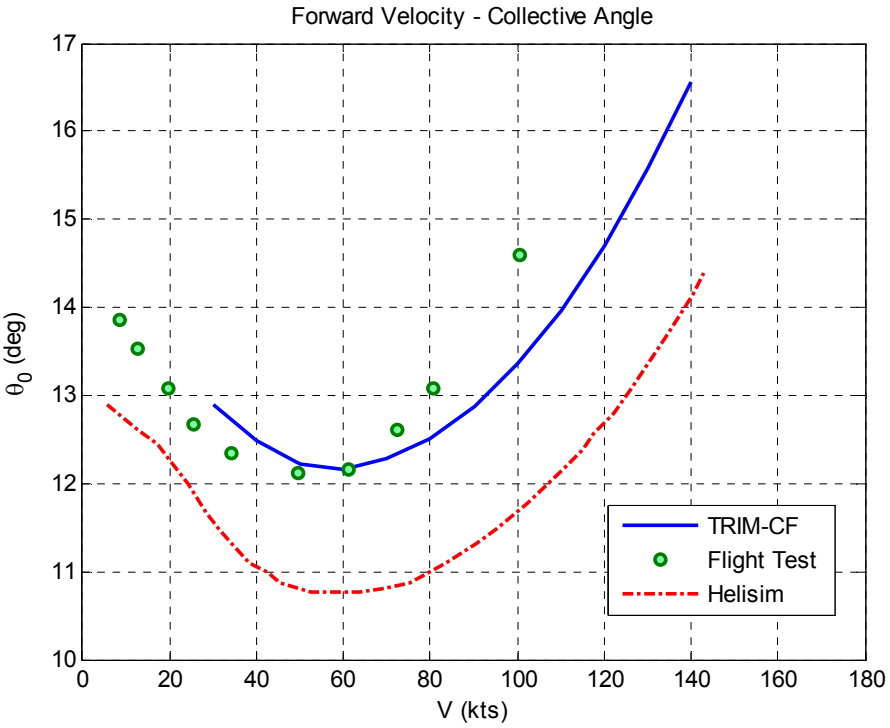

Figure 2-22: Collective angle compared with flight test data and Helisim results for Bo105 [2].

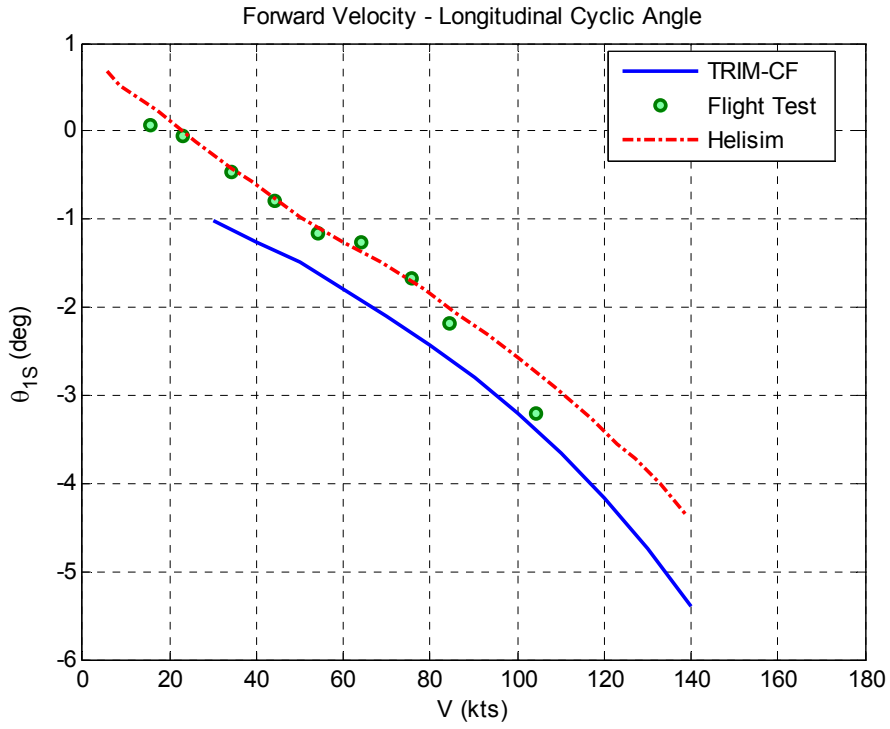

Figure 2-23: Longitudinal cyclic angle compared with flight test data and Helisim results for Bo105 [2].

The tail rotor parameters depend on greatly the main rotor torque. Since there is a shift on the torque curve in Figure 2-24, it is reasonable to have a similar shift on the tail rotor collective angle curve.

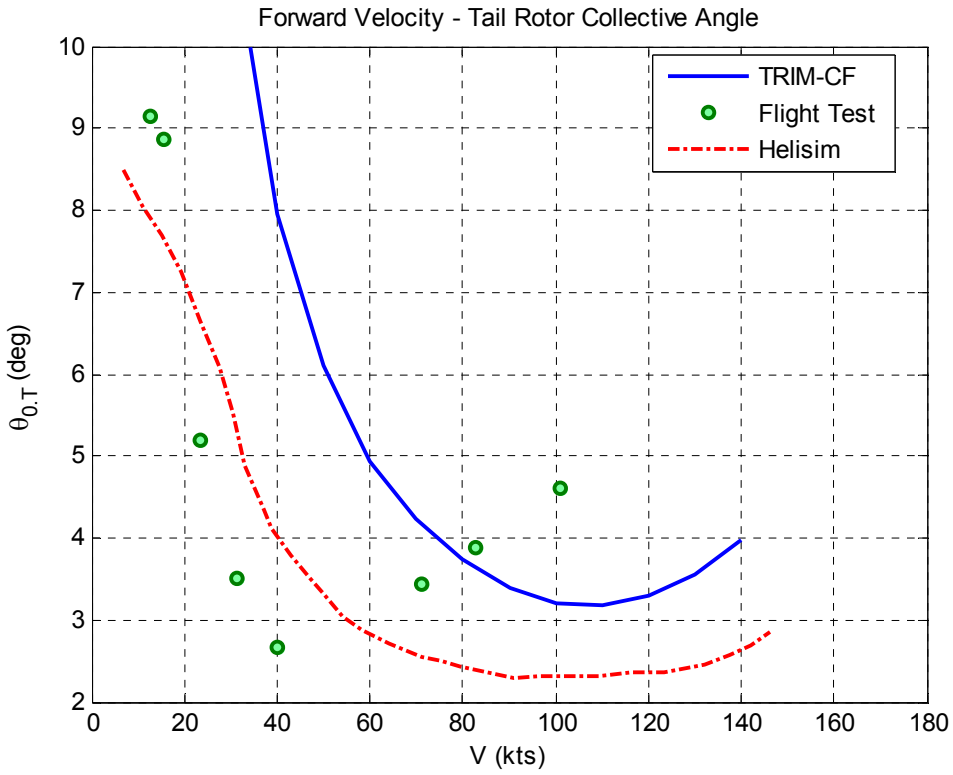

Figure 2-24: Tail rotor collective (pedals) angle compared with flight test data and Helisim results for Bo105 [2].

Pitch curve attitude is very similar to the test data, as seen in Figure 2-25. There is about a 2 degrees shift between the curves, which is not a very good result. Compared to the flight test data and the Helisim results, the present trim results obtained by the TRIM-CF code are acceptable, considering the accuracy expectations from the trim code.

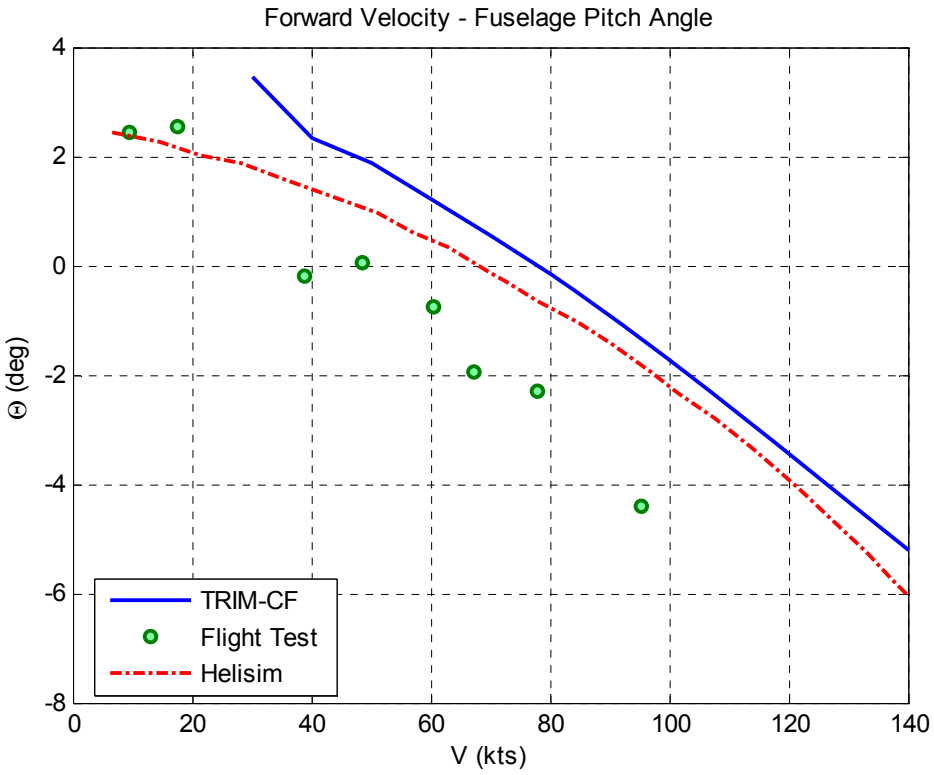

Figure 2-25: Fuselage pitch attitude compared with flight test data and Helisim results for Bo105 [2].

CHAPTER 3

TRIM ANALYSIS OF UH-60

In this chapter, the trim characteristics of a UH-60 helicopter are analyzed using TRIM-CF code and compared with the flight test data.

3.1 FLIGHT TESTS

Extensive flight tests were performed on the UH-60 helicopter by ASELSAN Inc. The flight profiles included forward flight at every 10 knots incremental forward velocities from maximum achievable forward flight speed, which is approximately 150 knots for the UH-60 helicopters, to 10 knots. The test instrumentation, data logging process and analysis steps are all explained in the following sub-chapters.

3.1.1 INSTRUMENTATION

The instrumentation was composed of mainly a data acquisition system, KAM-500, which is a flight certified modular data acquisition system produced in ACRA CONTROL, Inc. The DAS can be used to gather, store and analyze data coming from different sensors which produce voltage or current. It can also log analog or digital data; ethernet, GPS and data coming from ARINC, MIL-STD-1553, RS-232, RS-422 and RS-485 busses. The DAS combines high reliability with high performance in a compact modular system. Over 50 plug-in modules including advanced signal conditioning, avionics bus monitoring, video/audio compression, integrated data logging and multiple output formats are supported within a single unit or master/slave network distributed system. KAM-500 is designed for harsh airborne environments where space and power are limited.

For our flight test purposes, we used KAM-500 to gather data coming from the Multi-Functional Display (MFD) and EGI (Embedded INS & GPS). The synchronization was important, since flight test data are difficult to analyze. We tapped to the related connectors of the instruments to log the flight data. Pitch angle values are supplied from EGI; true airspeed (TAS) and barometric altitude values are supplied from MFD; and torque and fuel quantity values are supplied from their gauges.

3.1.2 DATA LOGGING

The data logged can be listed as:

1. TAS [knots]
2. Barometric altitude [ft]
3. Pitch [deg]
4. Total torque [%]
5. Fuel quantity [lb]

The raw data were logged online to the laptop PC. The acquisition interface of the software of the DAS allows the user to see the data in any format during the flight. The software is capable of logging high speed data and it offers an extensive analysis tool, which includes adding conversion factors, doing mathematical and logical operations, taking the average, finding the standard deviation, calculating the Fast Fourier Transformation etc. Figure 3-1 shows the interface of the software.

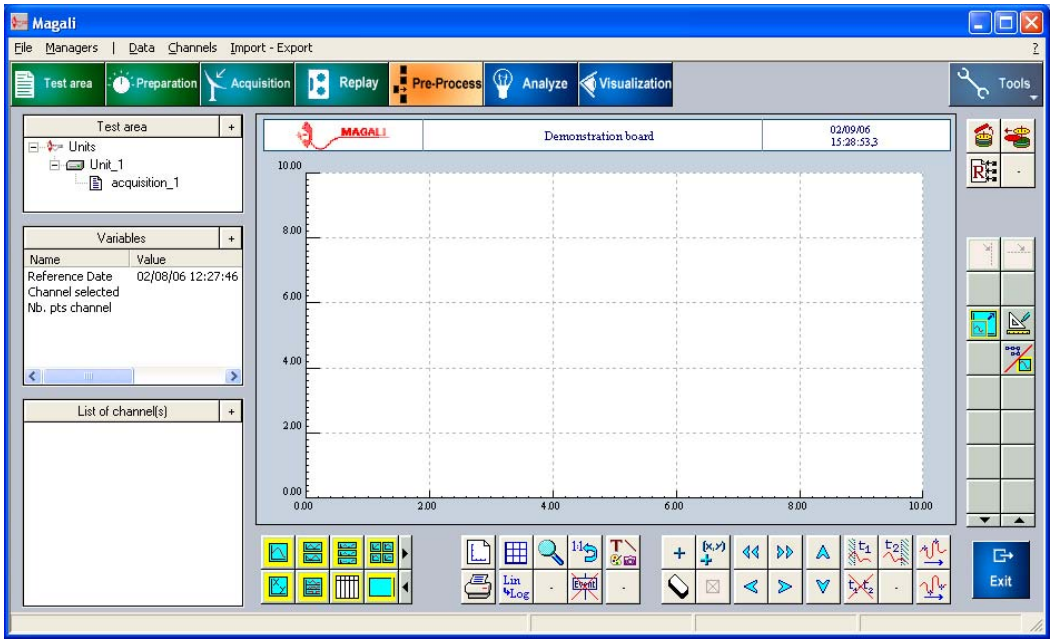

Figure 3-1: A snap-shot of the software.

3.1.3 DATA PROCESSING AND RESULTS

Most of the data logged were used to identify the trimmed forward flight time intervals where neither the altitude nor the attitude changes. Only pitch, TAS, torque and fuel quantity parameters are directly used in the analysis. Fuel quantity is used to calculate the exact gross weight. The full scale torque value corresponding to 100% torque is measured for one engine. It is obtained as a result of a test on the engine performed in an engine test bench.

The analysis is based on finding the torque and pitch attitude for a given gross weight and a given forward flight velocity in order to compare the values with the TRIM-CF results. The comparison part will be analyzed in section 3.2.1.

It should be noted that during the flight the gross weight decreases. As stated in section 3.2, the analysis is performed taking the weight change into account.

3.2 TRIM ANALYSIS OF UH-60 HELICOPTER

The test data were taken during a single flight. To account for the weight decrease during the flight as a result of fuel consumption, the forward velocity was decreased incrementally. In order to compare the test results of the UH-60 helicopter with the trim code results, the trim analysis is performed for the weights the flight data were taken at. The pitch attitude and torque values are compared with the test data. Parameters are nondimensionalized with some reference values.

Fuselage forces and moments are calculated using the force versus angle of attack curves given in [16], which are based on wind tunnel measurements.

The pitch attitude was predicted close to the flight test data, as seen in Figure 3-2. However, it should be reminded that the helicopter used in flight test has a Stability Augmentation System (SAS) and a Flight Path Stabilization System (FPS) which help the pilot with smooth flight. Therefore, it is not expected that the analysis results fit exactly the test results, but expected to be close enough. Looking at Figure 3-3, there is a drift between the total torque flight test data and the analysis results curves. The code does not seem to calculate the torque values very accurately. However, since the attitudes of the curves resemble each other, the results can be accepted as fairly good enough.

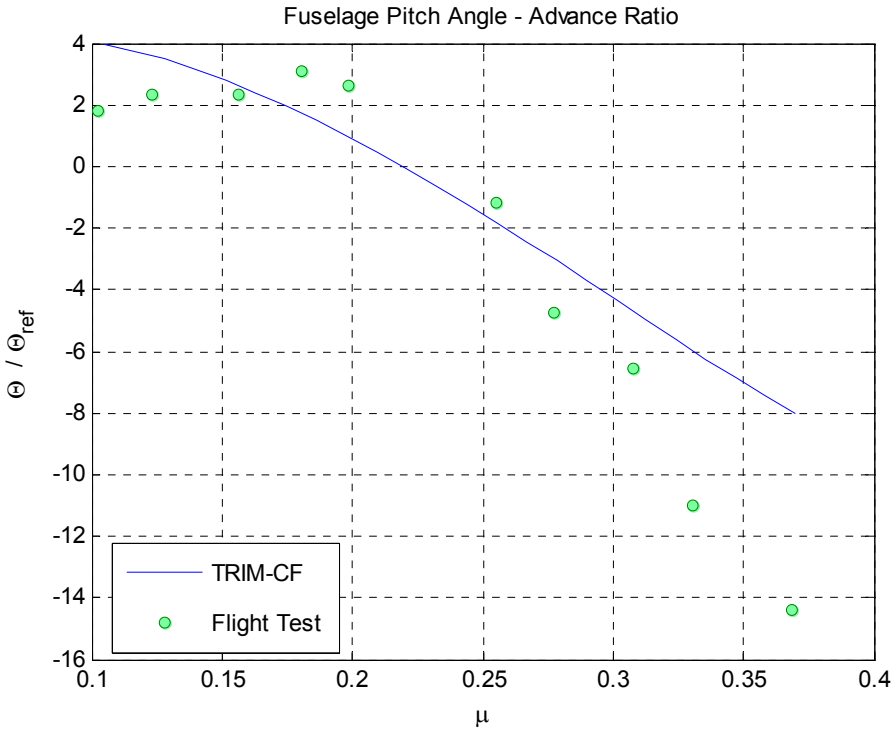

Figure 3-2: Fuselage pitch attitude vs. advance ratio.

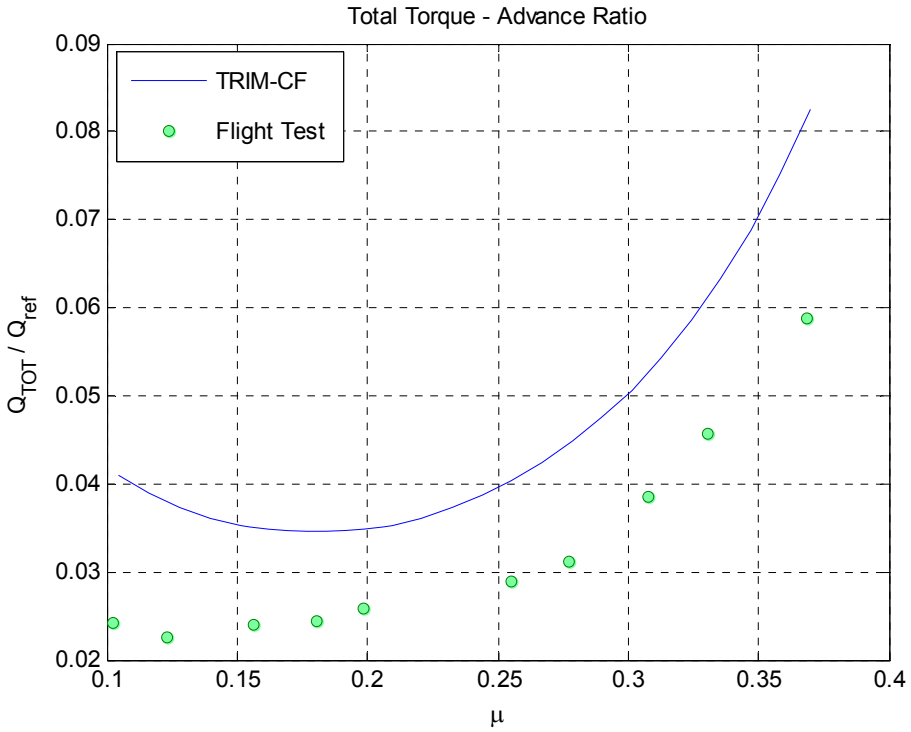

Figure 3-3: Total torque vs. advance ratio.

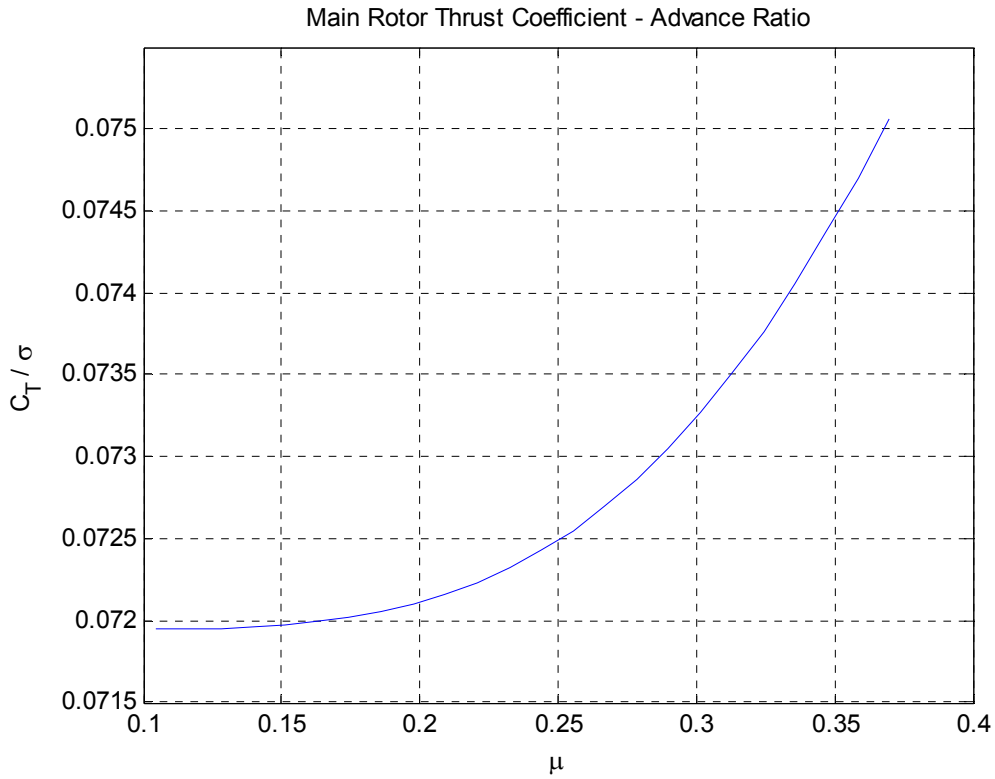

Figure 3-4: Main rotor thrust coefficient vs. advance ratio.

Figure 3-5 demonstrates the variation of the H-force. The H-force is composed of the drag over the blades of the rotor and the horizontal component of the thrust force. While the sign of the H-force is positive on the advancing side, it becomes negative on the retreating side. Therefore, the sign changes depending on which side of the rotor is dominant. The greatest effect comes from the induced drag due to the great dynamic pressure on the advancing side blade tips. The drop of the H-force after about $\mu = 0.25$ can be explained with the drop of the induced drag with the increasing velocity. The case is reverse for the retreating side.

One other phenomenon influencing the sign of the H-force is the local angle of attack. The local angle of attack is proportional to the local pitch angle and the local perpendicular velocity component on the blades. Figure 3-12

shows that beyond a forward flight speed, the collective angle starts to increase with the increasing velocity. Perpendicular component of the local velocity is a function of inflow ratio and the coning angle; therefore, we could say that after about $\mu = 0.17$ the perpendicular velocity component starts to increase with the increasing forward speed (See Figure 3-11 and Figure 3-13). Considering the collective angle as well, one could decide that the local angle of attack for the overall rotor disc is increasing as the forward flight increases. This is the reason why the H-force increases till $\mu = 0.25$ is reached. The horizontal component of the thrust vector increases with the increasing speed (See Figure 3-9); however, the induced drag is comparatively much greater so that the H-force increases. After that speed, the thrust force becomes dominant and the H-force decreases.

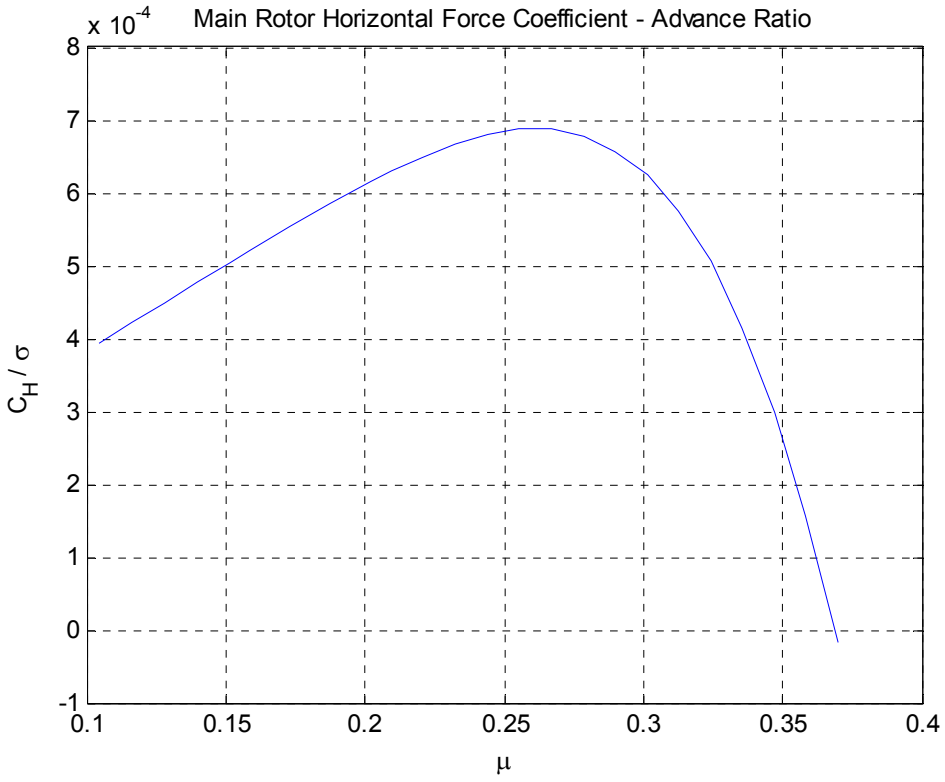

Figure 3-5: Main rotor H-force coefficient vs. advance ratio.

Figure 3-6 shows the induced, profile, parasite, compressibility and total main rotor power values. As expected, the induced power decreases with increasing speed. This is due to the decrease of the induced drag. The profile power is more or less constant, while the parasite drag increases drastically. It can be seen from the figure below that the power loss due to compressibility effect occurring at the blade tips starts to increase after about $\mu = 0.25$. This also shows that, although the drag increases drastically after that speed, the thrust vector increases even more so that it dominates on the H-force.

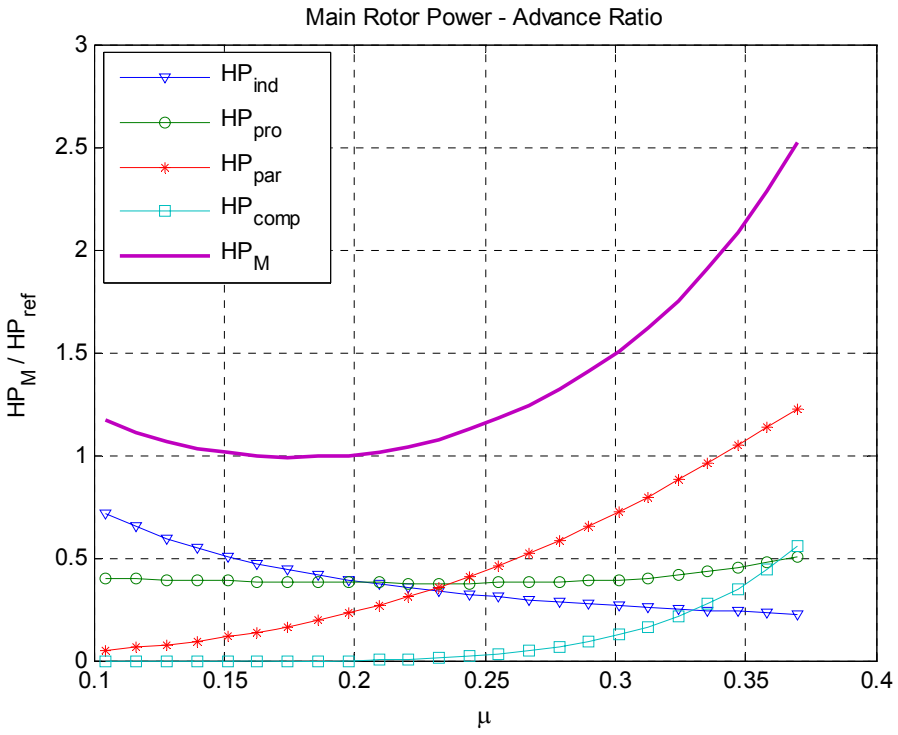

Figure 3-6: Main rotor power vs. advance ratio.

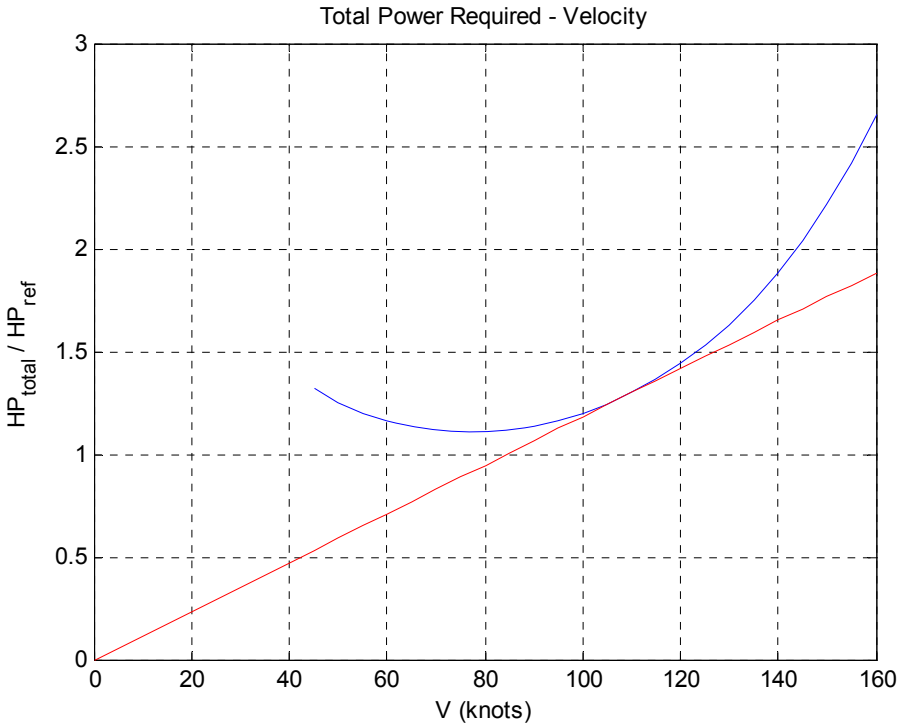

Figure 3-7: Total power required vs. forward velocity.

In Figure 3-7, the intersection point of the total power required graph with the tangent line passing through the origin gives the maximum range speed of the helicopter, which is found to be about 107 knots. This is the speed the helicopter has minimum drag and therefore the minimum fuel consumption rate is reached. The minimum value of the power bucket gives the maximum endurance velocity, which is found as about 77 knots.

Torque is directly related with the power required. Therefore, the same conclusions can be drawn for the torque. Like the H-force, torque is also a resultant force of the drag and horizontal component of the thrust vector. The second one increases continuously as the speed increases. But the first term differs much depending on which component of the drag is considered. Therefore, profile, parasite, induced and compressibility related torque curves directly point out the respective drag components. Seen on Figure

3-8 there is an additional torque component which comes from the effect of the H-force.

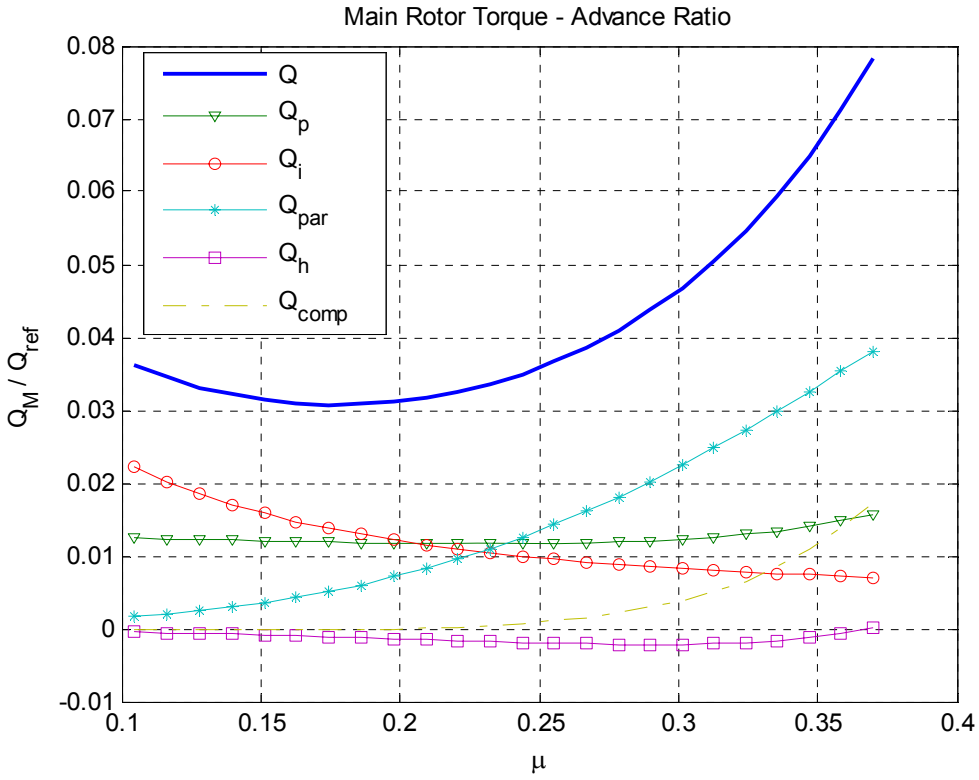

Figure 3-8: Main rotor torque vs. advance ratio.

The angle of attack of the tip path plane is positive if the main rotor disc aligns backward. Therefore, looking at Figure 3-9, the tip path plane seems to steadily lean forward down and therefore the thrust vector is continuously aligning forward with the increasing forward velocity.

The induced velocity is the indicator of how much the main rotor deflects the forward velocity downward. Since the thrust vector aligns forward down as the forward velocity increases, the induced velocity decreases, as seen in Figure 3-10.

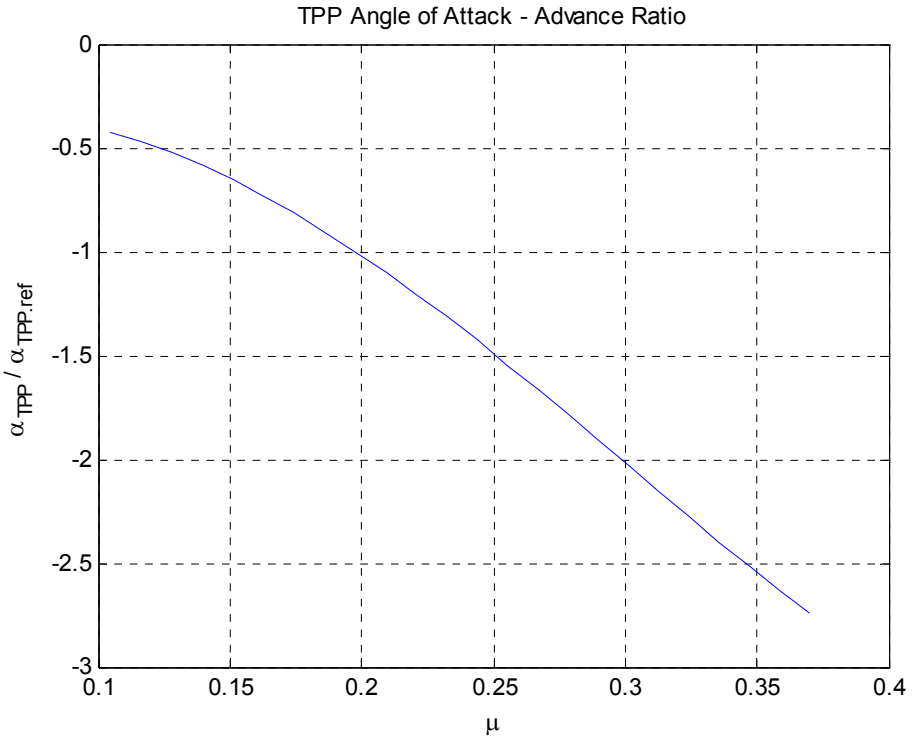

Figure 3-9: TPP angle of attack vs. advance ratio.

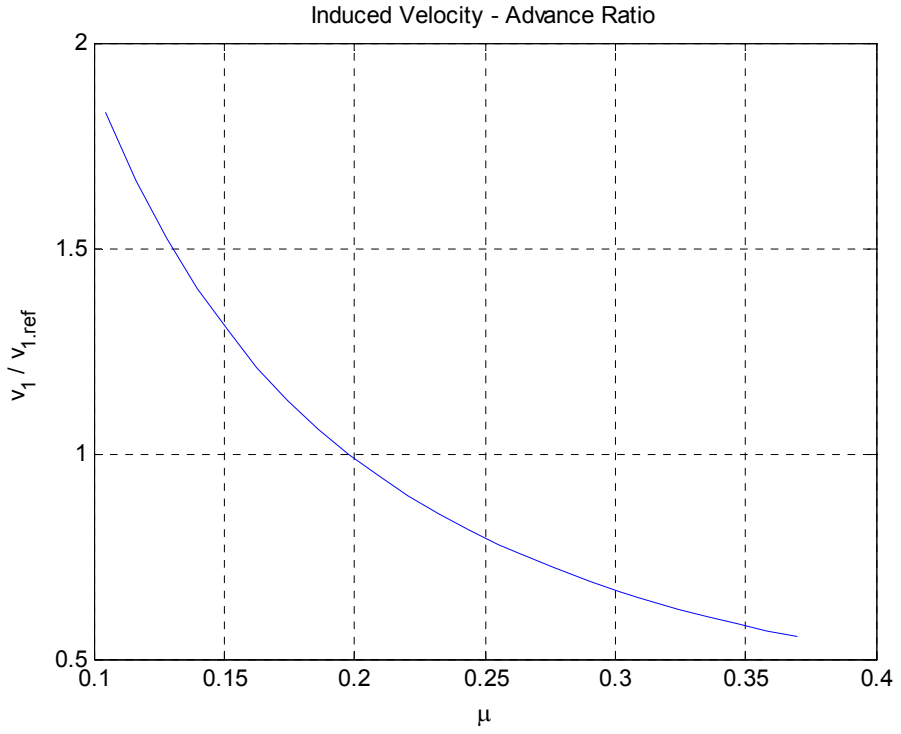

Figure 3-10: Induced velocity vs. advance ratio.

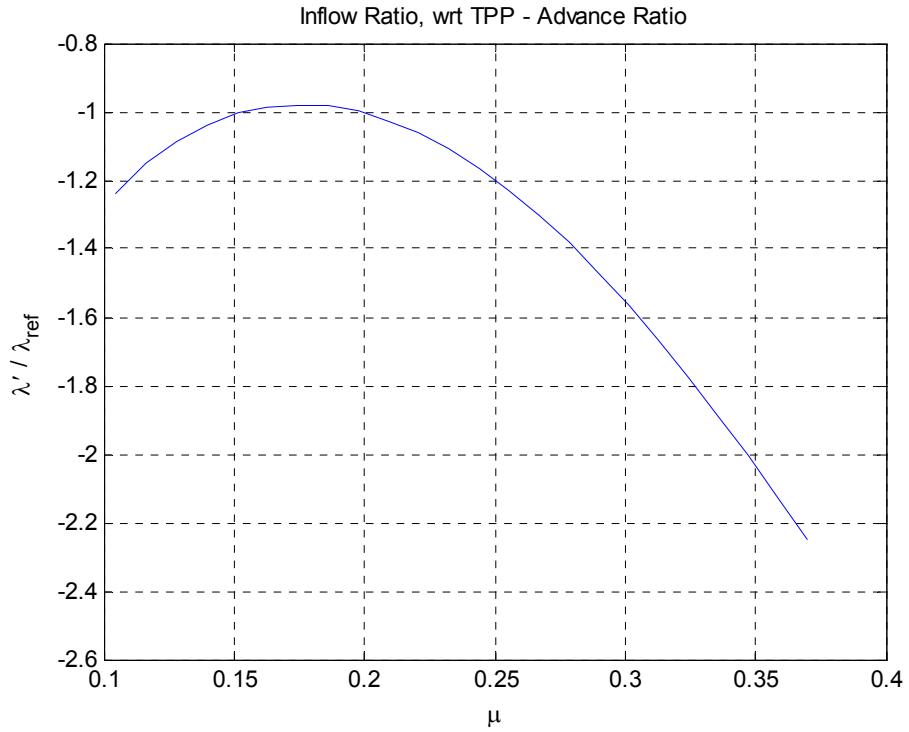

Figure 3-11: Inflow ratio vs. advance ratio.

The inflow ratio is a function of the forward speed, the tip path plane angle of attack and the induced velocity. There is a compromise between the induced velocity and the multiplication of the angle with the forward velocity. For low forward velocities, the first term is dominant and the inflow ratio increases; while for higher velocities the case is reversed. The attitude change is seen in Figure 3-11.

The collective angle is related with the local angle of attack, as explained above, and therefore, it is almost a direct measure of the thrust force. In Figure 3-12, it shows similar attitude with the thrust curve, that is it is increasing with the speed.

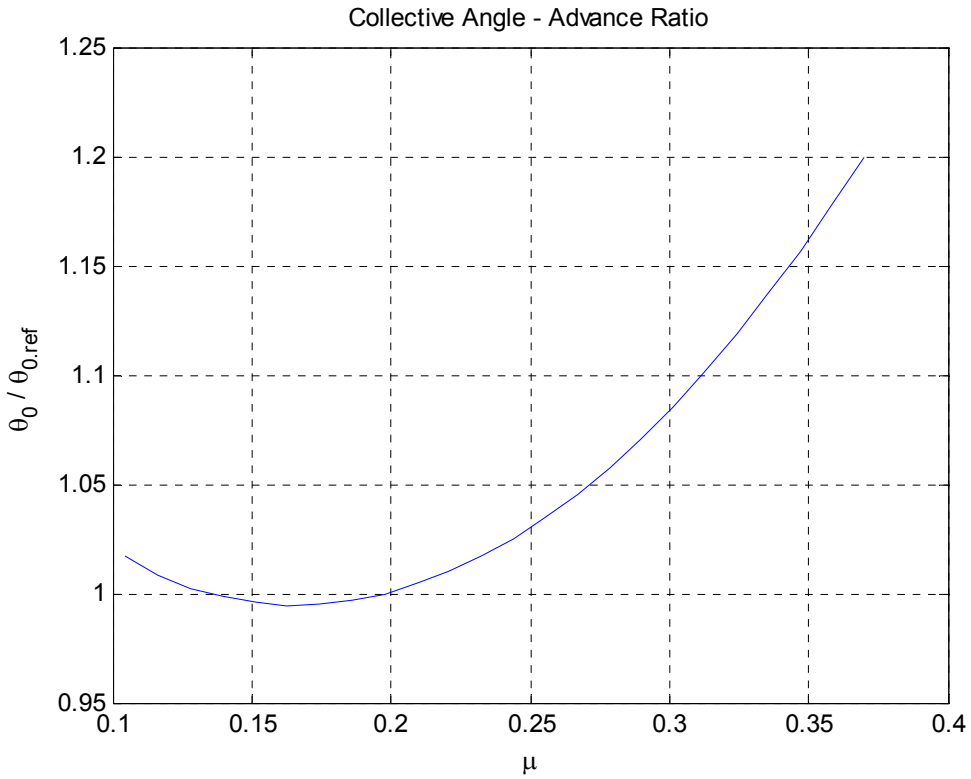

Figure 3-12: Collective angle vs. advance ratio.

The calculated coning angle is shown in Figure 3-13. The coning angle, like the first harmonic longitudinal and lateral flapping angles, is the output of the input motion given to the collective and the cyclic. It is the average value of the blades flapping, positive sign representing an upward motion. The collective greatly affects the coning angle, while the cyclic is dominant on the first harmonic flapping angles. Therefore, the coning angle is increasing as the collective is raised.

The longitudinal flapping angle is positive when the blade passing through 180 degrees azimuth flaps up. It represents the amplitude of the flapping oscillation at the nose azimuth. Looking at Figure 3-14, it is seen that the oscillation amplitude decreases as the forward flight speed increases.

The tail rotor thrust is the anti-torque force which controls the yawing motion. Since there is no yawing on the forward flight cases we are analyzing, the two curve should be matching with the main rotor torque curve. However, there is a shift between the tail rotor thrust curve shown in Figure 3-16 and the main rotor torque seen in Figure 3-8, which is the effect of the vertical stabilizer (See Figure 3-31). The sideward force produced by the vertical stabilizer helps the tail rotor so that the thrust produced is less.

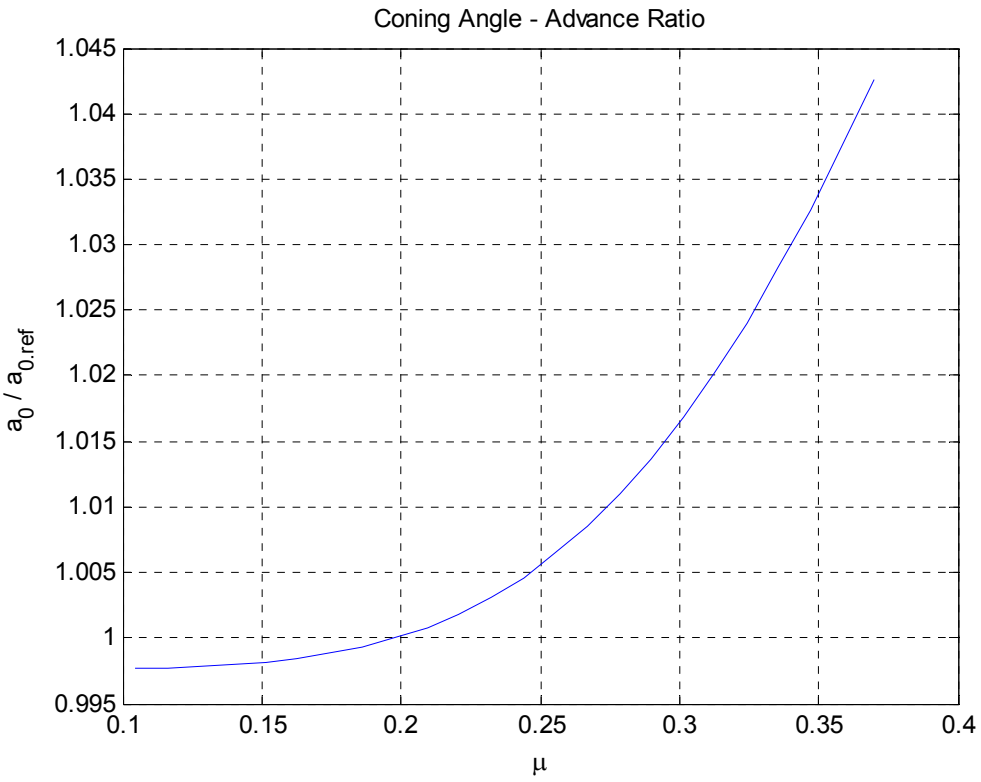

Figure 3-13: Coning angle vs. advance ratio.

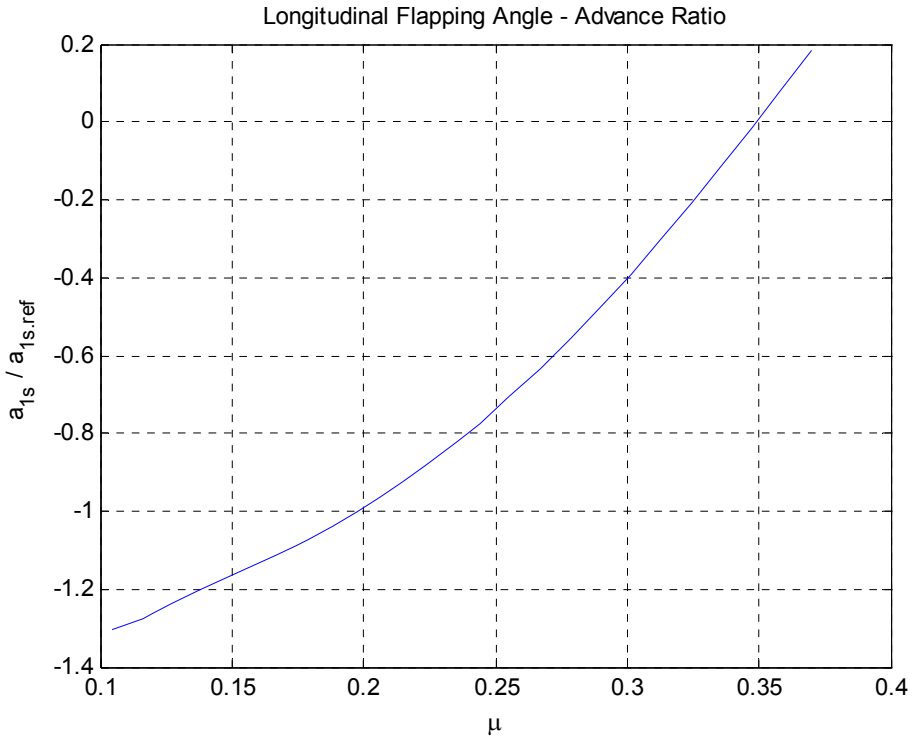

Figure 3-14: Longitudinal flapping angle vs. advance ratio.

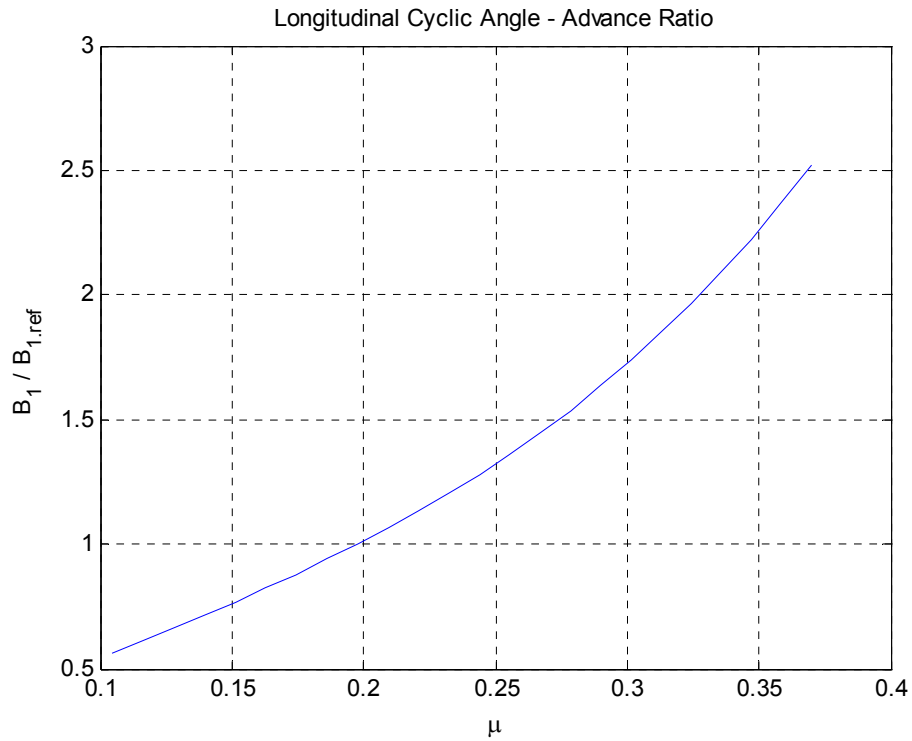

Figure 3-15: Longitudinal cyclic angle vs. advance ratio.

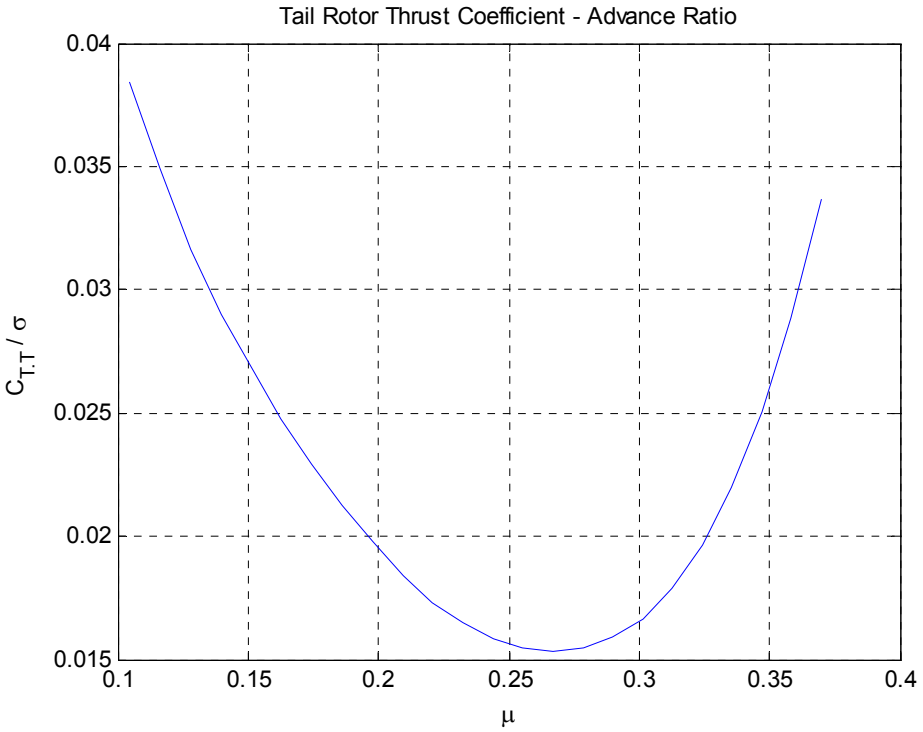

Figure 3-16: Tail rotor thrust coefficient vs. advance ratio.

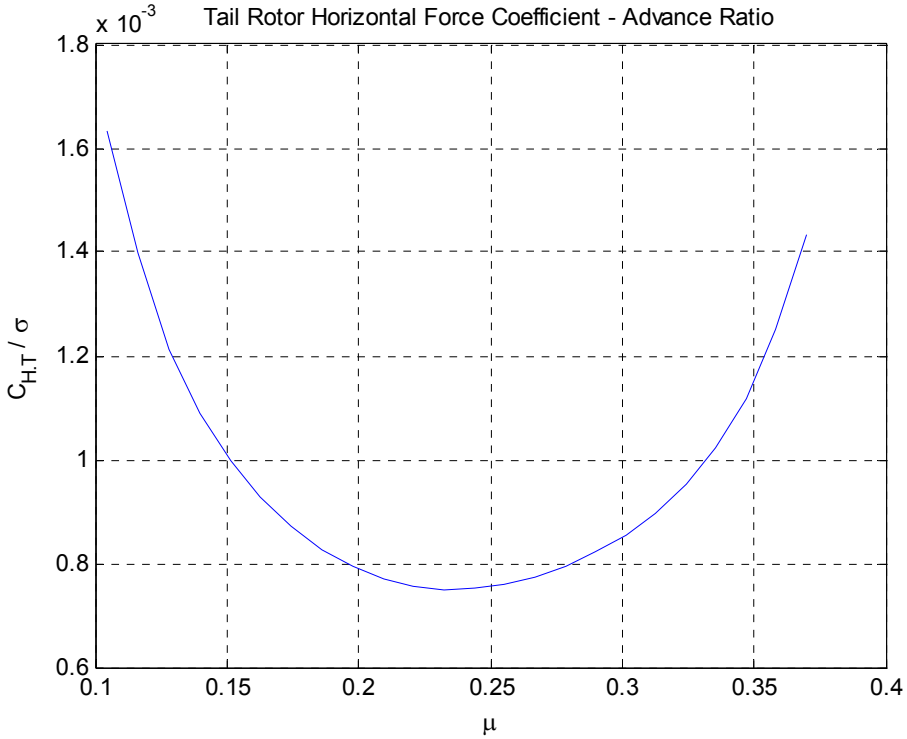

Figure 3-17: Tail rotor H-force coefficient vs. advance ratio.

The tail rotor H force, just as the main rotor H force, takes sign depending on which side is dominant, the advancing side or the retreating side. That force is formed from the drag force. Since the revolution speed is much greater compared to the main rotor, the induced drag force is much greater at the tail rotor. However, the point is the difference between the induced drag obtained at the advancing side and the retreating side (See Figure 3-17).

Tail rotor torque is also a result of the drag force. Since the induced drag decreases, the torque also decreases with increasing velocity, demonstrated in Figure 3-18.

The inflow ratio of the tail rotor is directly related with the tail rotor thrust, and inversely proportional to the forward velocity (Figure 3-19).

The coning angle differs little, shown in Figure 3-20. It is directly proportional to the thrust force.

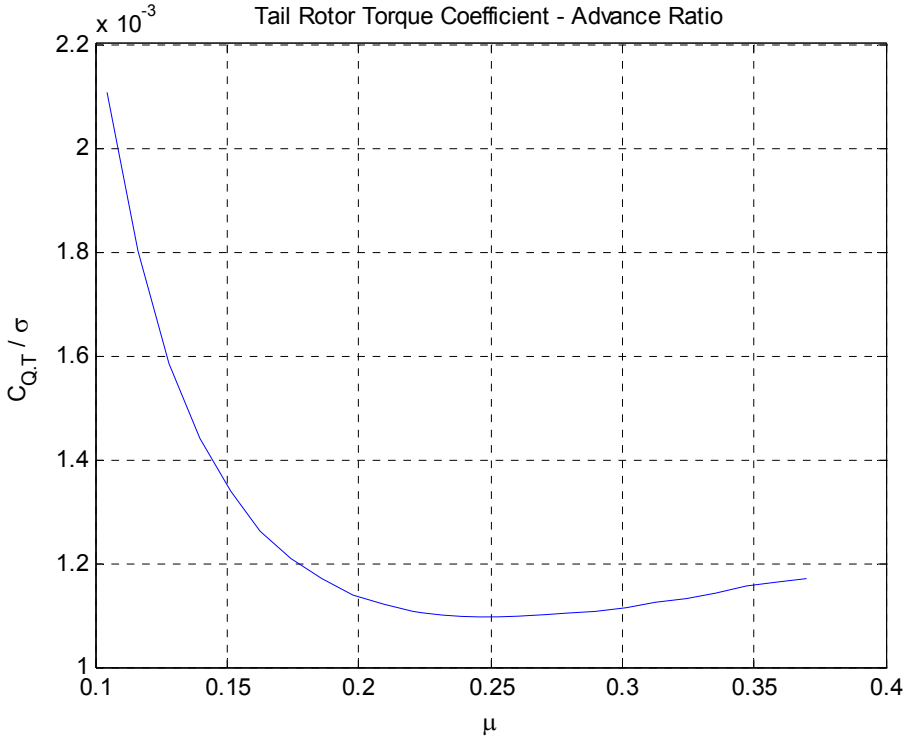

Figure 3-18: Tail rotor torque coefficient vs. advance ratio.

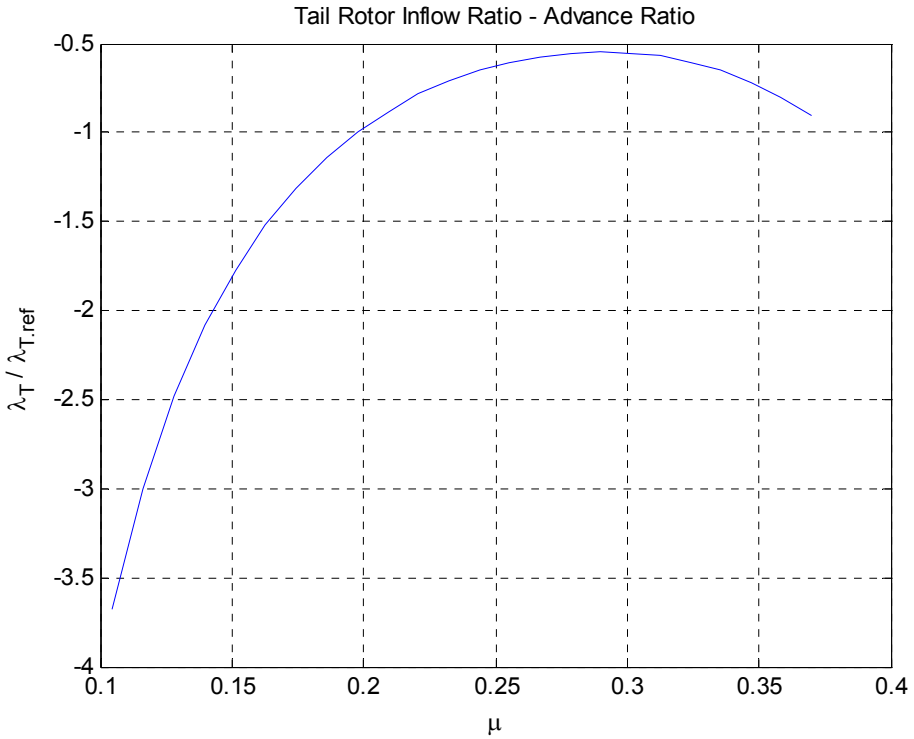

Figure 3-19: Tail rotor inflow ratio vs. advance ratio.

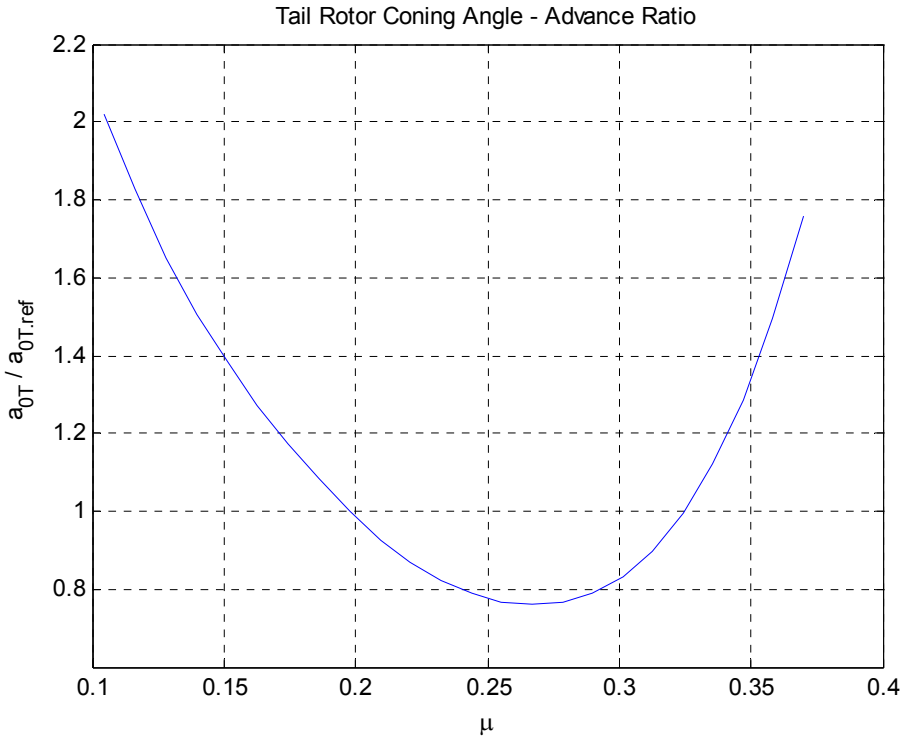

Figure 3-20: Tail rotor coning angle vs. advance ratio.

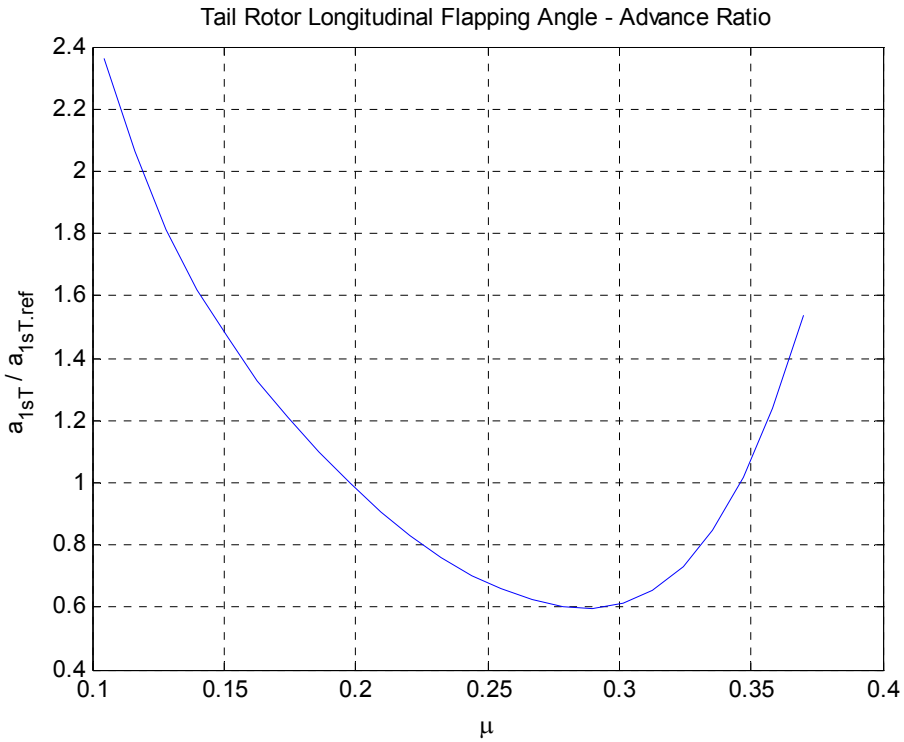

Figure 3-21: Tail rotor longitudinal flapping angle vs. advance ratio.

The longitudinal and lateral flapping angles, shown in Figure 3-21 and Figure 3-22, depend on the δ_3 angle, which is defined as the slant angle of the flapping hinge. If there is no slanted hinge, then δ_3 angle is the angle between the pitch horn and the flapping axis. This angle relates flapping with feathering (pedals angle) motion.

The average value of the pedals angle is directly proportional to the thrust, just as the coning angle (See Figure 3-23).

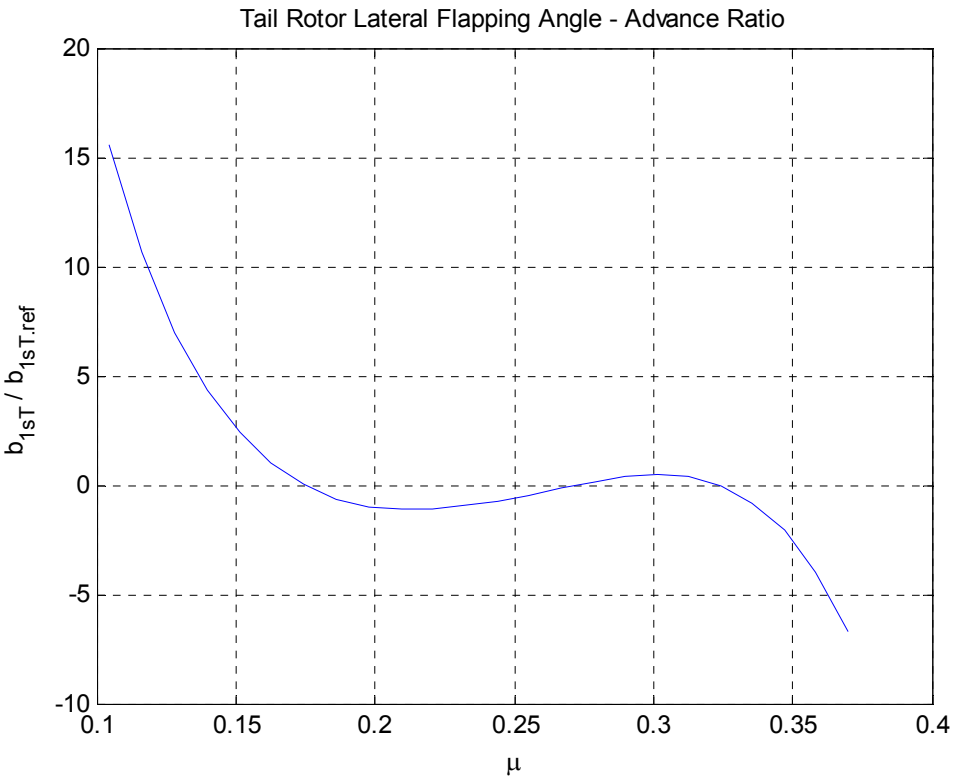

Figure 3-22: Tail rotor lateral flapping angle vs. advance ratio.

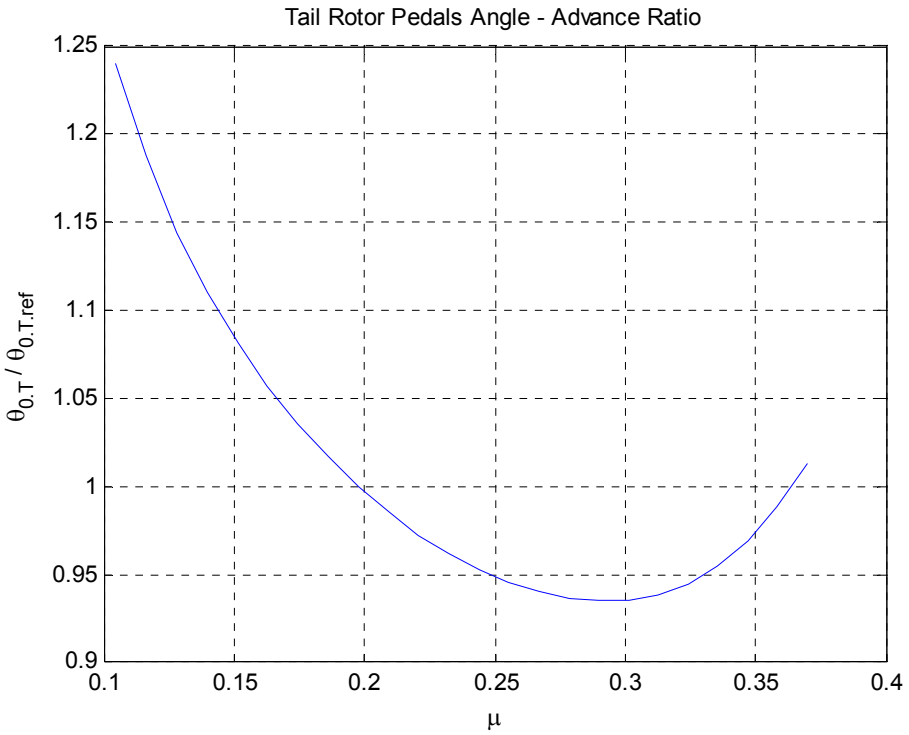

Figure 3-23: Tail rotor pedals angle vs. advance ratio.

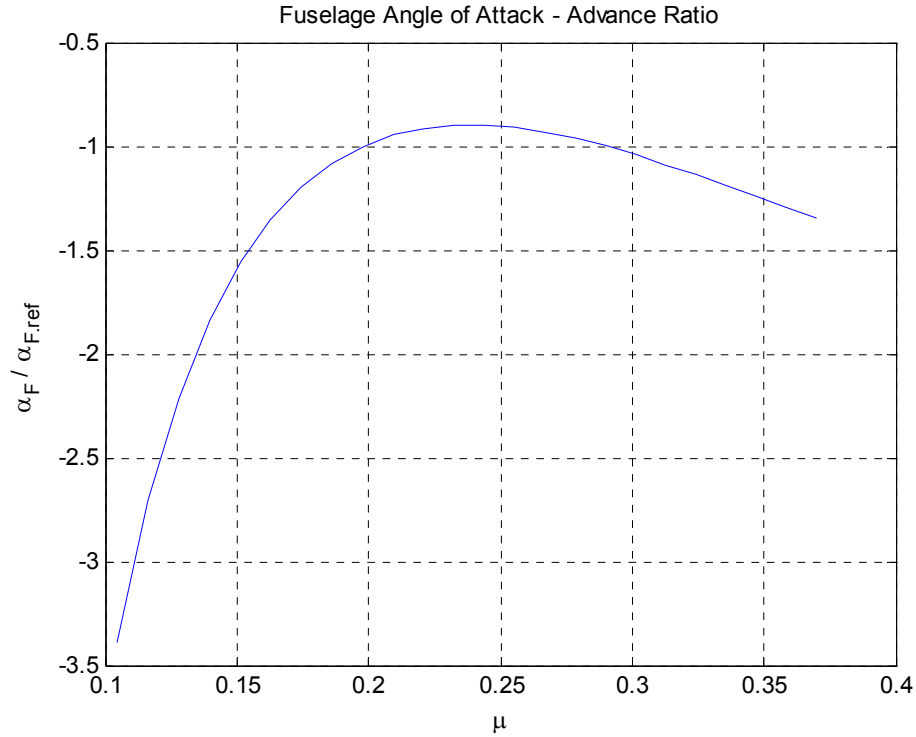

Figure 3-24: Fuselage angle of attack vs. advance ratio.

The fuselage angle of attack is a function of the main rotor tip path plane angle of attack. It directly affects the drag and lift produced on the fuselage. Since in Figure 3-24 the angle is so low at low velocity values, lift is directed downward. With increasing angle of attack, lift is directed upward.

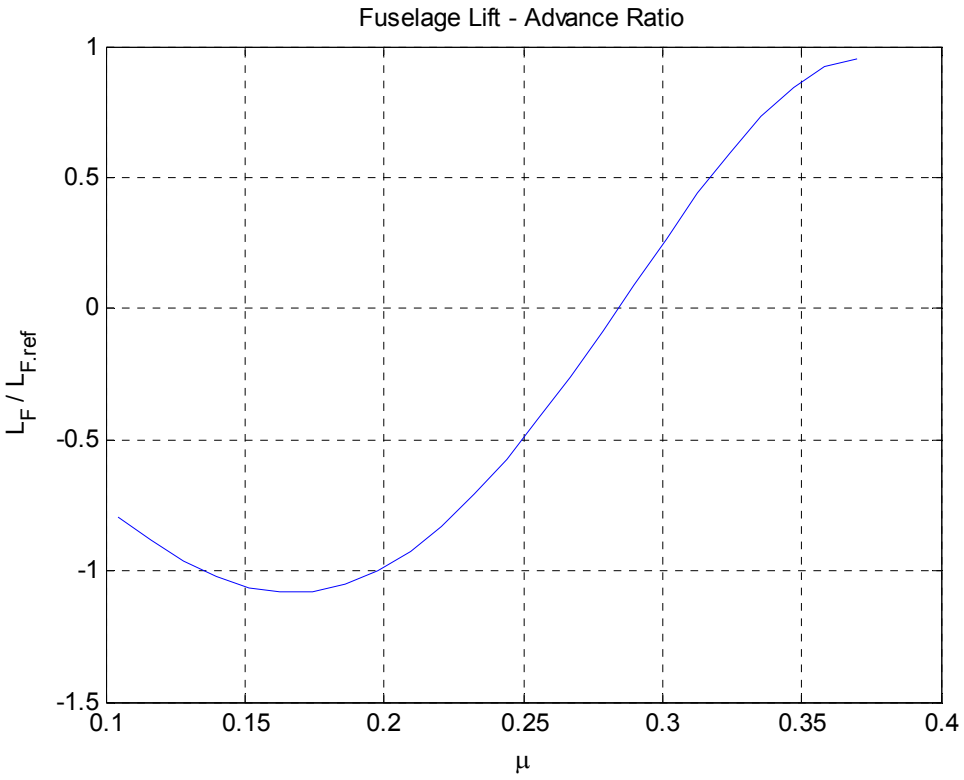

Figure 3-25: Fuselage lift vs. advance ratio.

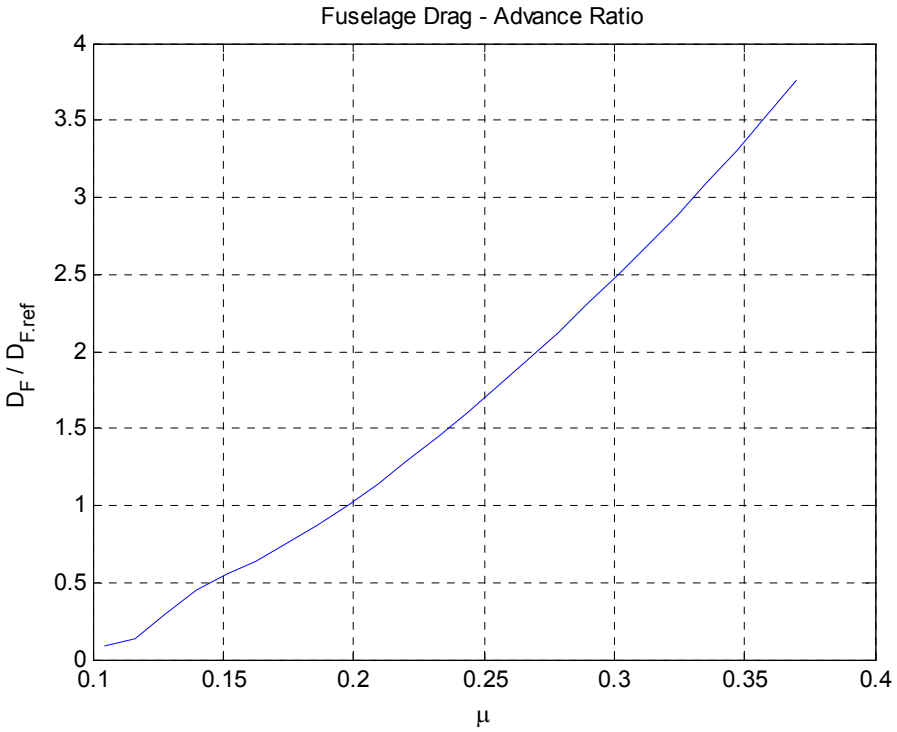

Figure 3-26: Fuselage drag vs. advance ratio.

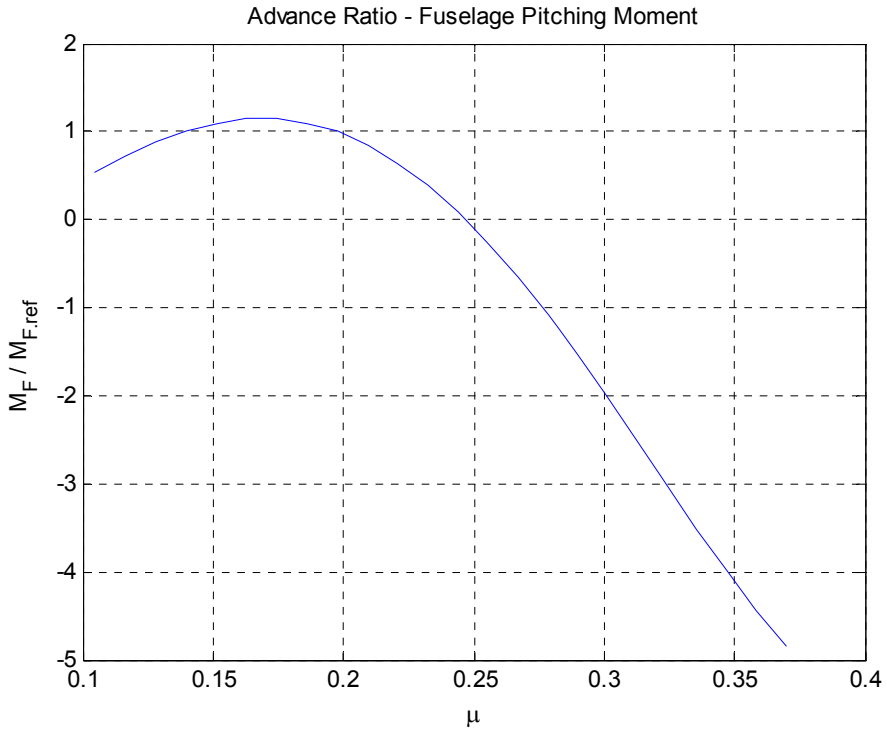

Figure 3-27: Fuselage pitching moment vs. advance ratio.

Similar to the lift force, for low angles of attack at low velocities the pitcing moment is positive, while the sign reverses at high velocities (Figure 3-25 and Figure 3-27).

Horizontal stabilator angle of attack depends on the fuselage angle of attack and the forward speed. As the forward speed increases, the stabilator automatically turns up, decreasing the incidence. Therefore, the angle of attack also decreases. The effect of a decreased angle of attack shows itself with a decrease in lift in Figure 3-28.

The sidewash angles induced by the rotors and the fuselage are calculated and are used to compute the side force created by the vertical stabilizer shown in Figure 3-31.

The drag of the fuselage for the empennage on case (Figure 3-34) are similar to the empennage off case (Figure 3-26), since the effects of the vertical stabilizer and the horizontal stabilator are negligible. However, the fuselage lift (Figure 3-25) and the horizontal stabilizer lift (Figure 3-29) values are comparative.

Compared with the flight test data and explained with theoretical logic, we can say that the forward flight trim results are reasonable and acceptable for the stability analysis.

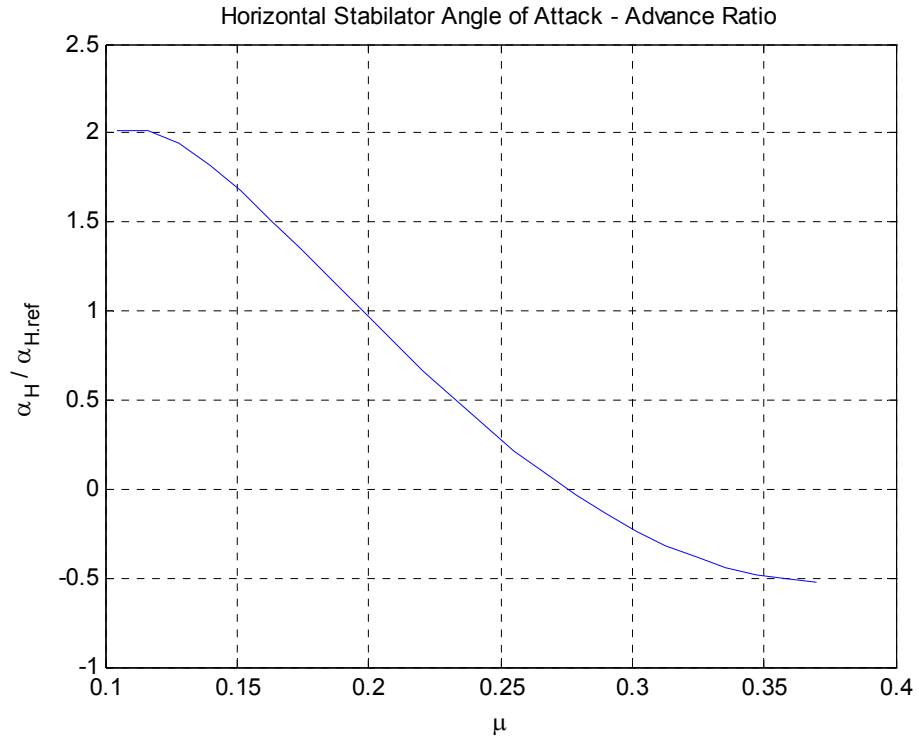

Figure 3-28: Horizontal stabilator angle of attack vs. advance ratio.

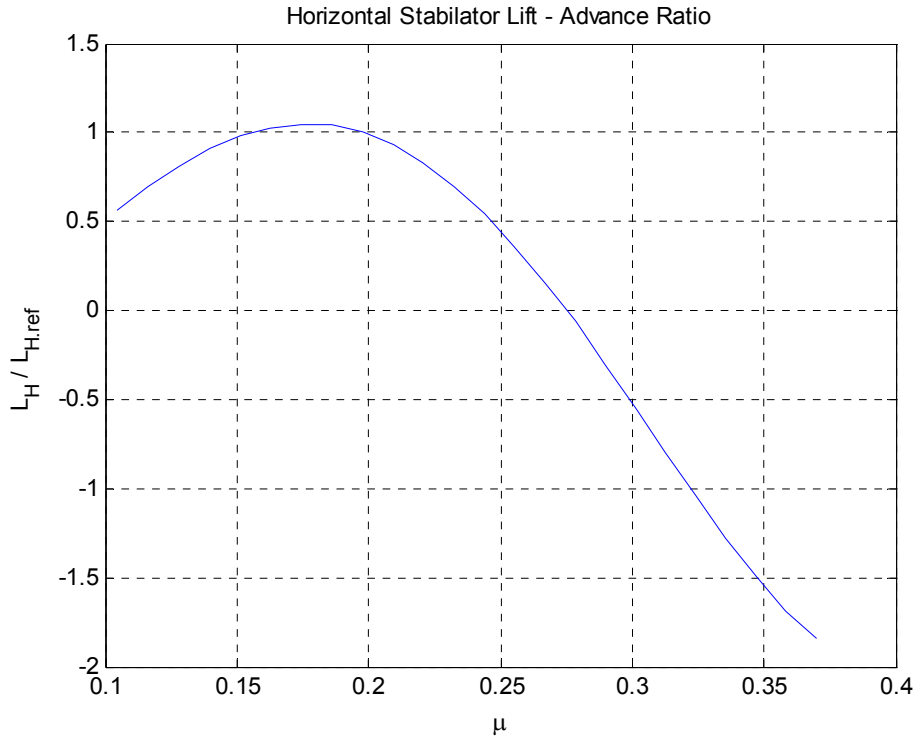

Figure 3-29: Horizontal stabilator lift vs. advance ratio.

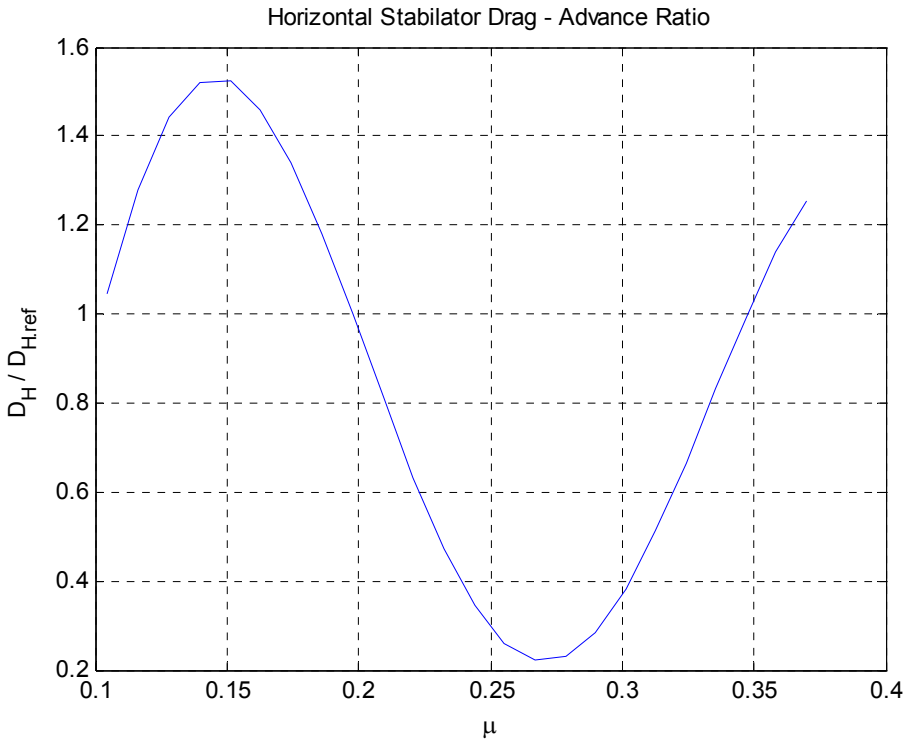

Figure 3-30: Horizontal stabilator drag vs. advance ratio.

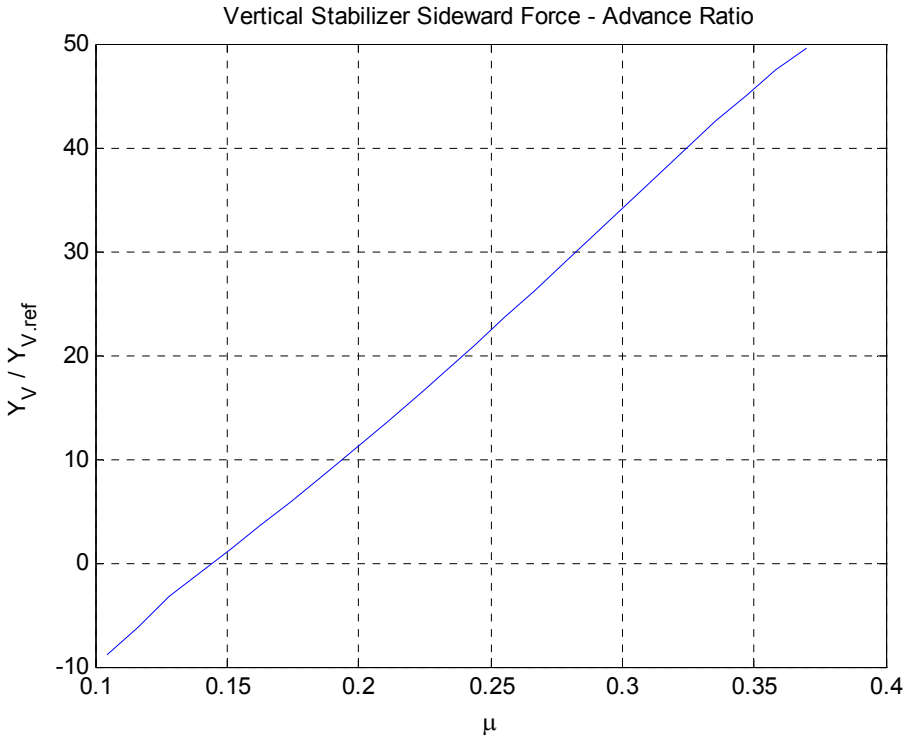

Figure 3-31: Vertical stabilizer sideward force vs. advance ratio.

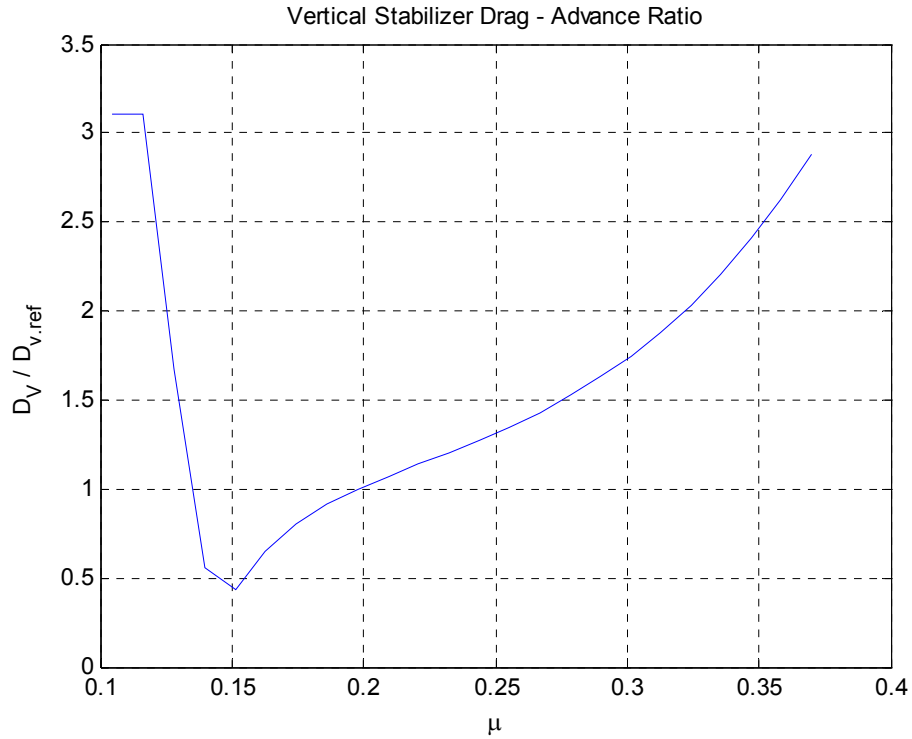

Figure 3-32: Vertical stabilizer drag vs. advance ratio.

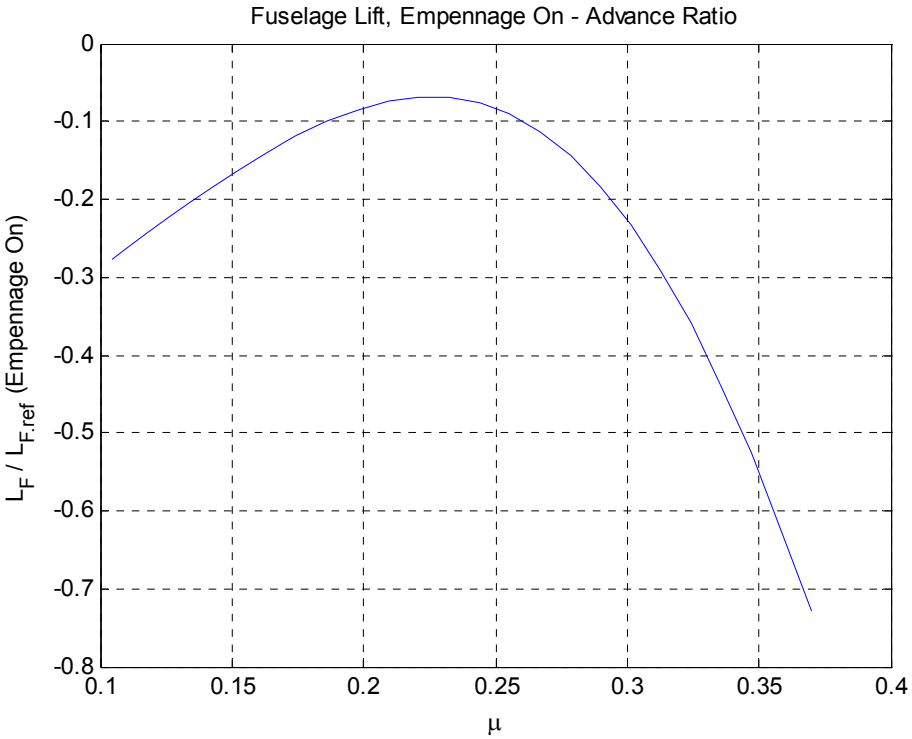

Figure 3-33: Fuselage lift (empennage on) vs. advance ratio.

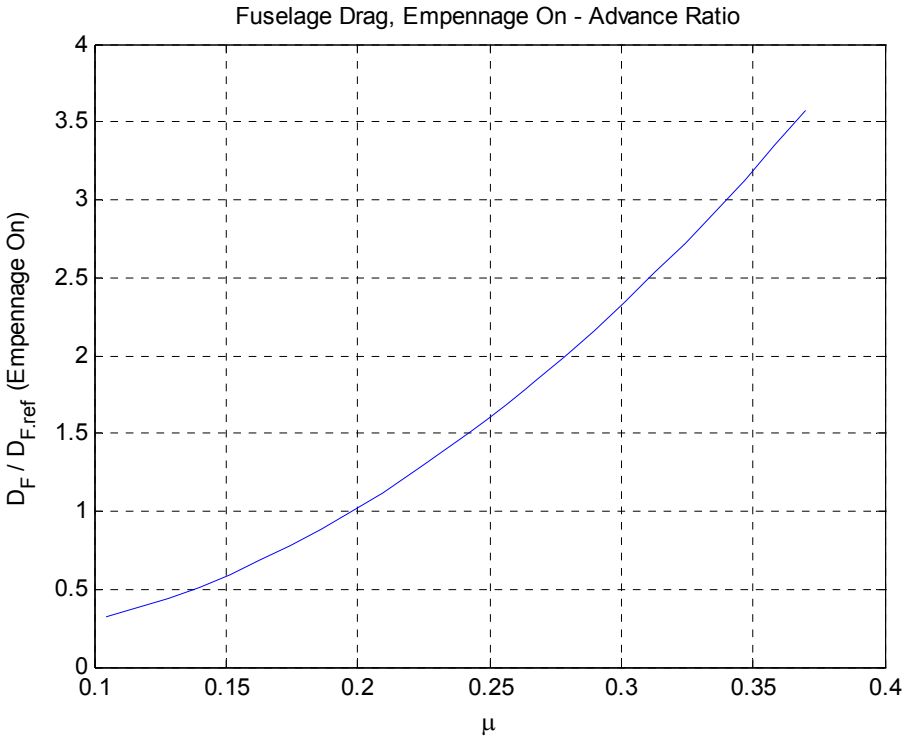

Figure 3-34: Fuselage drag (empennage on) vs. advance ratio.

CHAPTER 4

STABILITY ANALYSIS OF UH-60 HELICOPTER

It is more logical to find out the static stability characteristics before the dynamic stability is analyzed. Partial derivative of pitching moment of the helicopter with respect to the vertical velocity is a good indicator of the static stability: If the sign of the derivative is positive, then the helicopter is statically stable, and vice versa. In Figure 4-1, it is clear that the helicopter is statically unstable up to about 130 knots, and becomes stable after that speed. For the dynamic stability, it can be concluded that the helicopter is unstable up 130 knots. Nothing can be said for the speeds higher than 130.

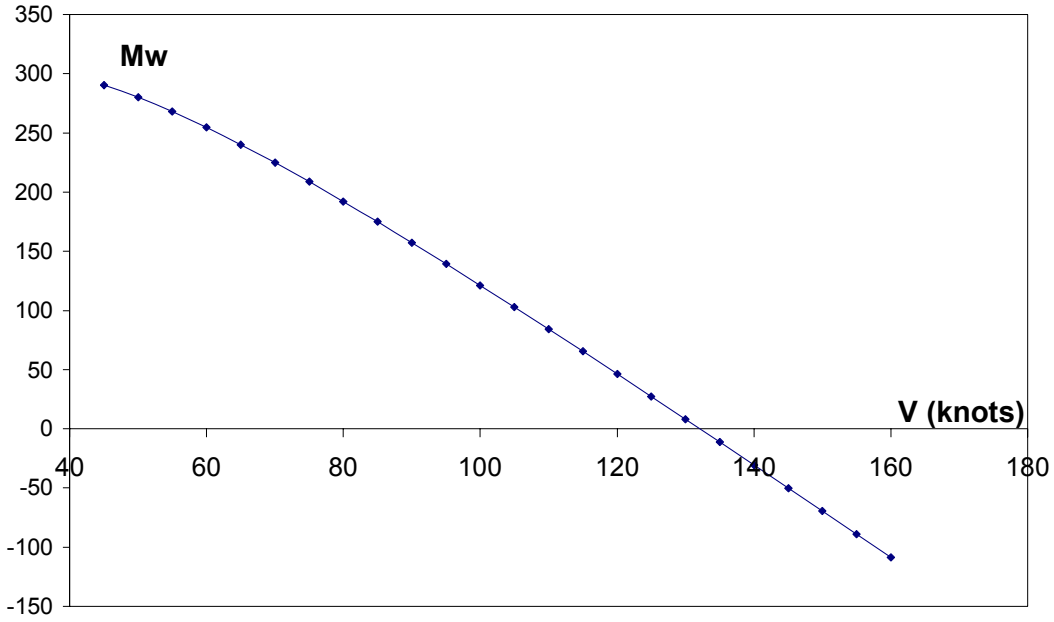

Figure 4-1: Derivative of pitching moment with respect to the vertical velocity.

The coefficients of the characteristic equation and the Routh's Discriminant values for all forward flight cases are shown in Figure 4-2. It is seen that until about 110 knots the helicopter shows tendency to go completely divergent in longitudinal aspect. After that speed until about 150 knots, there should be no unstable oscillations, according to the Routh's test. This means that either there are no oscillations, whether divergent or convergent, or the system is stable, whether oscillatory or not. After 150 knots, the helicopter goes divergent again. Looking to the coefficients, the criterion says that if one of the coefficients is negative, than pure divergence or unstable oscillations occur. This is just the case for UH-60 helicopter, since for all forward flight cases there is only one coefficient which is negative, it is C for speeds below 110 knots and D for speeds after 110 knots. Therefore, it can be concluded that for all forward velocity range the helicopter is purely divergent, even though it is statically stable at speeds higher than 130 knots.

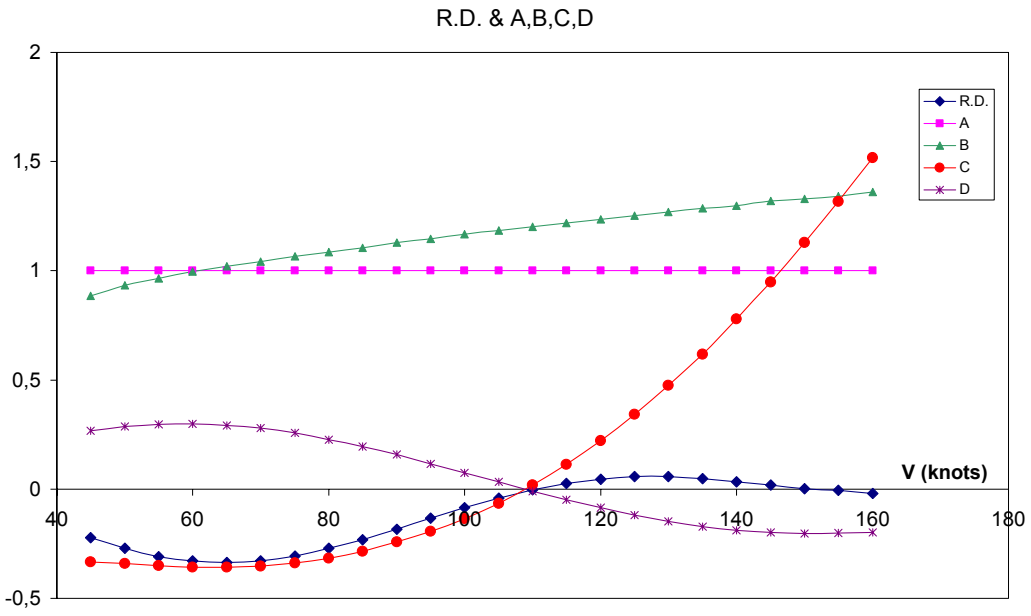

Figure 4-2: Routh's discriminant and the coefficients of characteristic equation.

It can be observed from the root locus shown in Figure 4-3 that the first and the second roots –being complex conjugate– corresponding to each forward velocity case are oscillatory roots, some of which being convergent and some being divergent. The other roots are non-oscillatory. Third root is completely convergent while the forth root is divergent for some cases. Therefore, each case of forward flight contains an oscillatory motion and two non-oscillatory motions. This conclusion is in line with the dynamic stability characteristics results obtained from the Routh's test and the coefficients test, since for all velocity cases there is at least one divergent motion, whether oscillatory or not.

Considering the descriptions of the Phugoid and Short Period motions, it can be concluded that the oscillatory roots are belonging to the Phugoid motion, while the others are belonging to the Short Period motion. That conclusion is open to discussion.

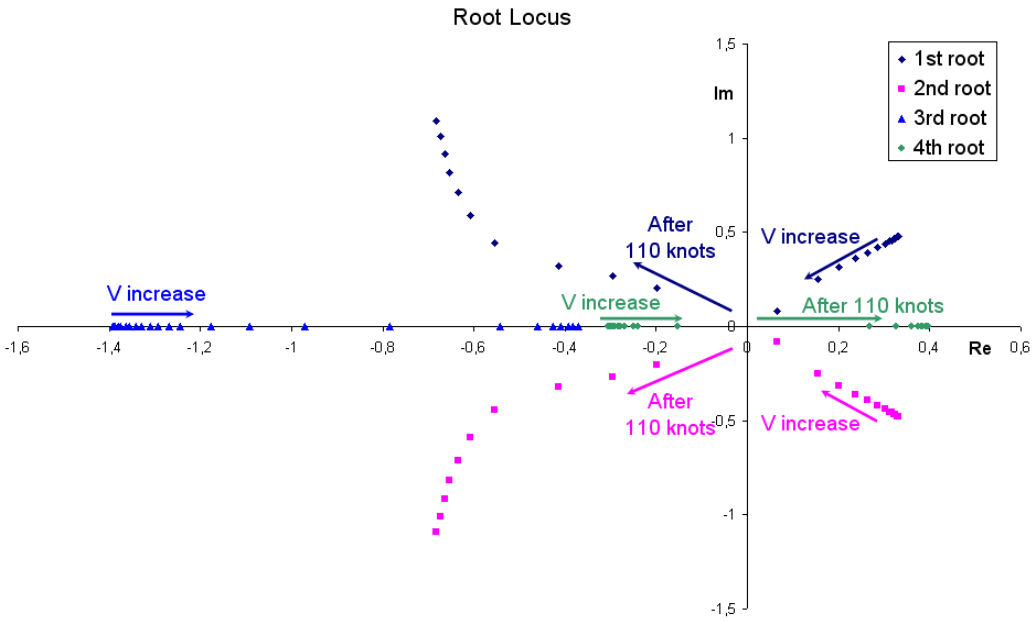

Figure 4-3: Root Locus.

Depending on the strength of the roots, the helicopter shows different characteristics. To give an example; the roots corresponding to 45 knots are -1.27, -0.24, 0.31±0.45i (See Figure 4-3). The smaller the non-oscillatory root (i.e. the greater in absolute value), the faster the motion damps. Therefore, the first root shows greater damping characteristics than the second one. The phugoid roots are divergent and have an oscillation period of about 13 seconds. The period seems reasonable, since generally the phugoid mode has a period between 10 and 30 seconds.

Looking to Figure 4-3, it can be concluded that the change of the attitude from divergent to convergent at about 110 knots is due to the phugoid roots, i.e. the oscillatory roots. In order to analyze the short period roots, it could be more reasonable to give attention to the sum of the two roots which correspond to that mode. The sum of the roots shows a turn to divergent at about 150 knots, which can be the explanation of why the Routh's Discriminant changed sign at that speed. This means that, for very high speeds the short period motion is dominant on the stability characteristics of the helicopter, while for lower speeds the Phugoid motion takes the place.

The Phugoid motion characteristics change with changing speed (See Figure 4-4). The period values are very reasonable up to a point where the period goes to very high values. After that speed the attitude changes from divergent to convergent and the period tends to decrease. 110 knots is very likely to be the maximum range speed. The relation which can be occurring between the maximum range speed and the speed which changes the dynamic stability attitude of the helicopter is a good point of discussion.

The divergency / convergency characteristics of phugoid motion are pretty obvious in Figure 4-5. The time-to-double values change sign at the speed the roots change sign. It is obvious that the motion changes attitude from divergent to convergent at about 110 knots.

The non-oscillatory roots are also describing some of the dynamic stability characteristics. There is a change in mode from convergent to divergent at the same critical speed, 110 knots, as it is seen at Figure 4-6. Those roots belong to the short period mode. It can be concluded that, while the phugoid mode shows divergent characteristics up to that critical speed, the short period mode is convergent, and vice versa. This is an interesting result.

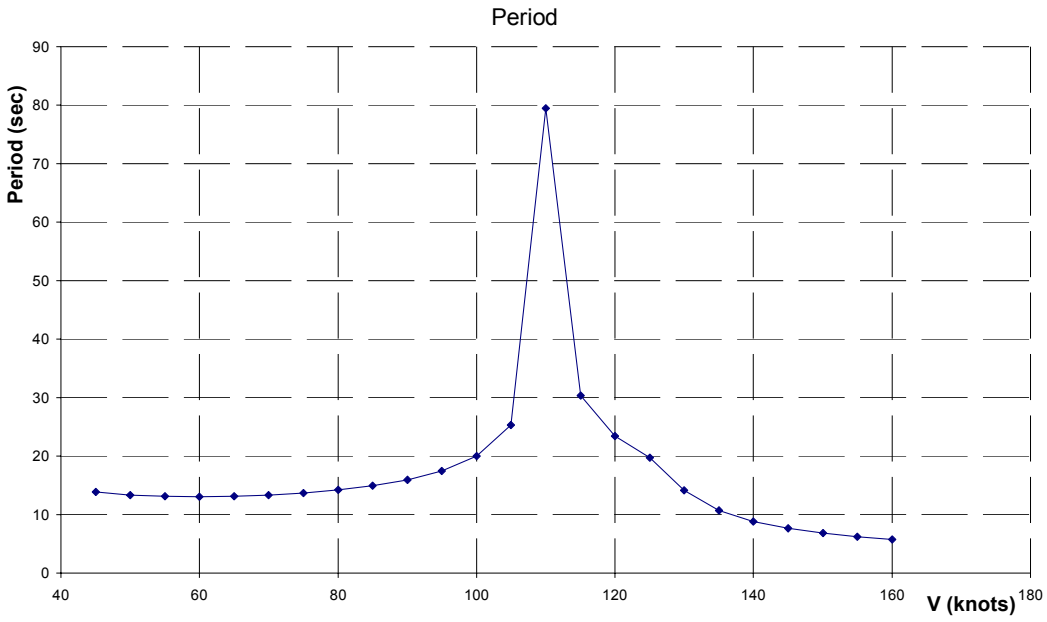

Figure 4-4: Period values belonging to the phugoid mode.

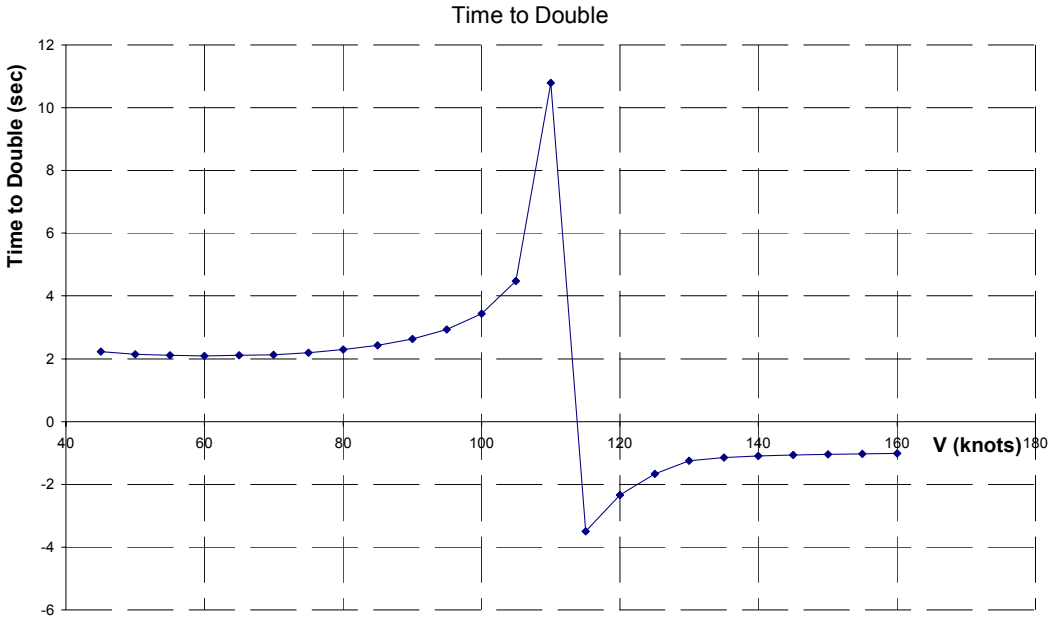

Figure 4-5: Time-to-Double values belonging to the phugoid mode.

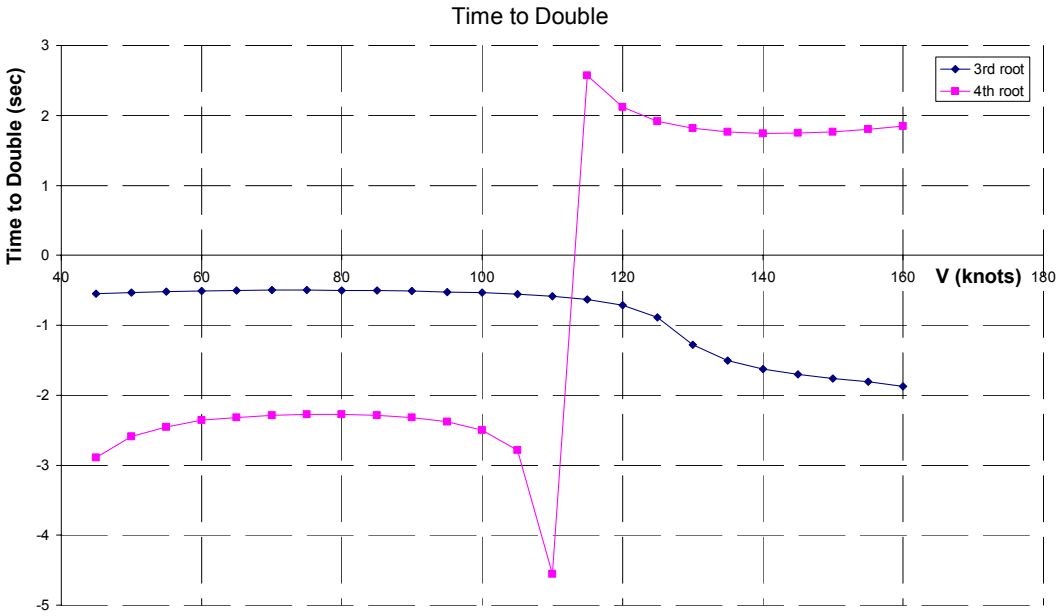

Figure 4-6: Time-to-double values belonging to the non-oscillatory roots.

The change in the X forces per unit change in the forward velocity is called the ‘Drag Damping’, since the dominant effect comes from the drag forces. The graph below shows that the effect of the drag forces increases as the forward flight increases. The same conclusion can be made for the vertical damping and the pitch damping. Those are the greatest parameters which affect the longitudinal stability of the helicopter.

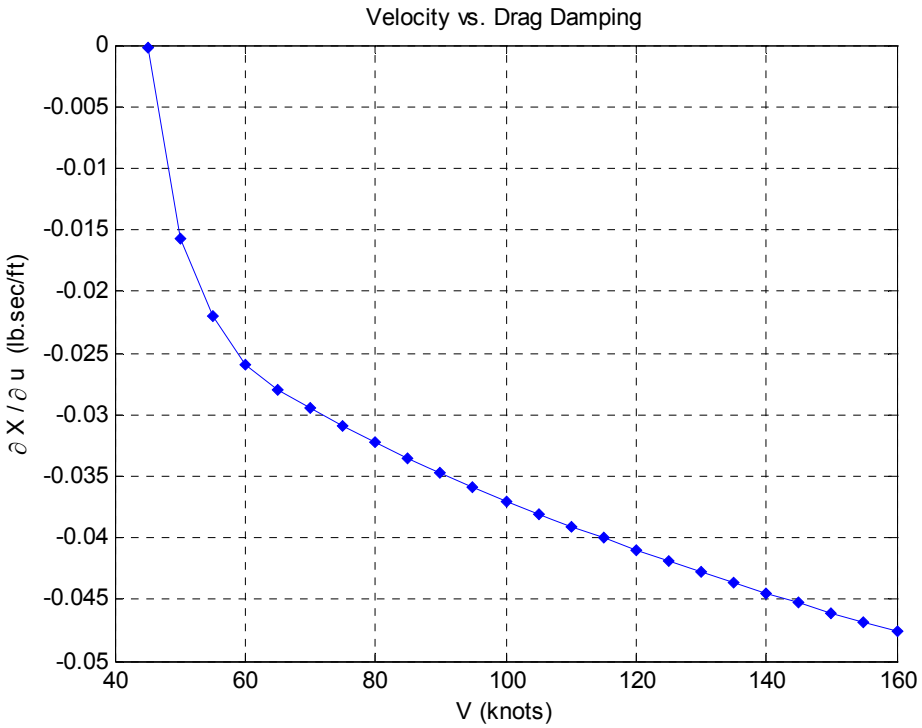

Figure 4-7: Drag Damping.

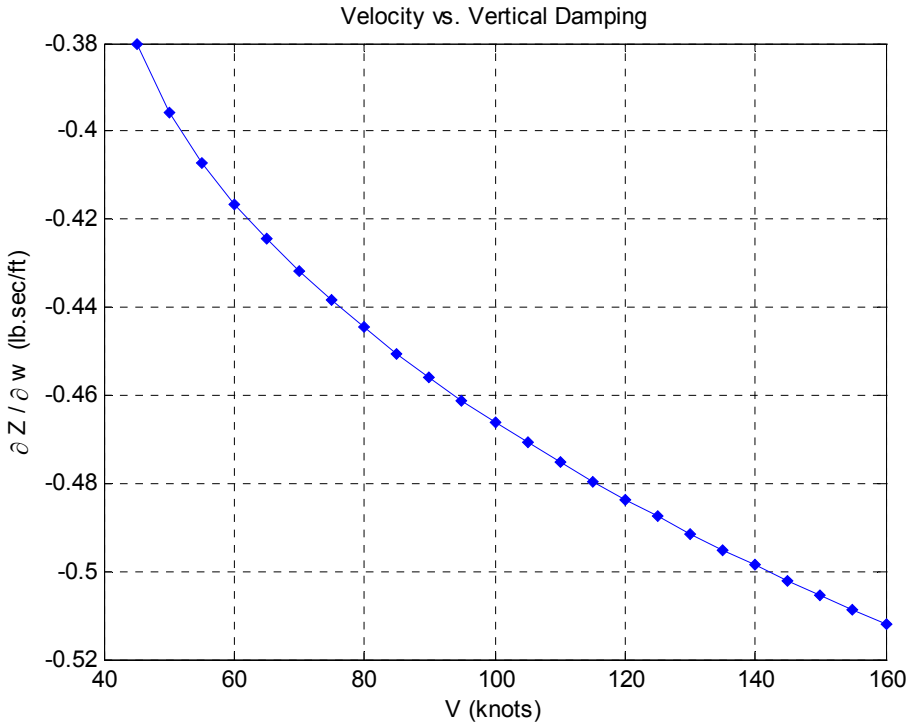

Figure 4-8: Vertical Damping.

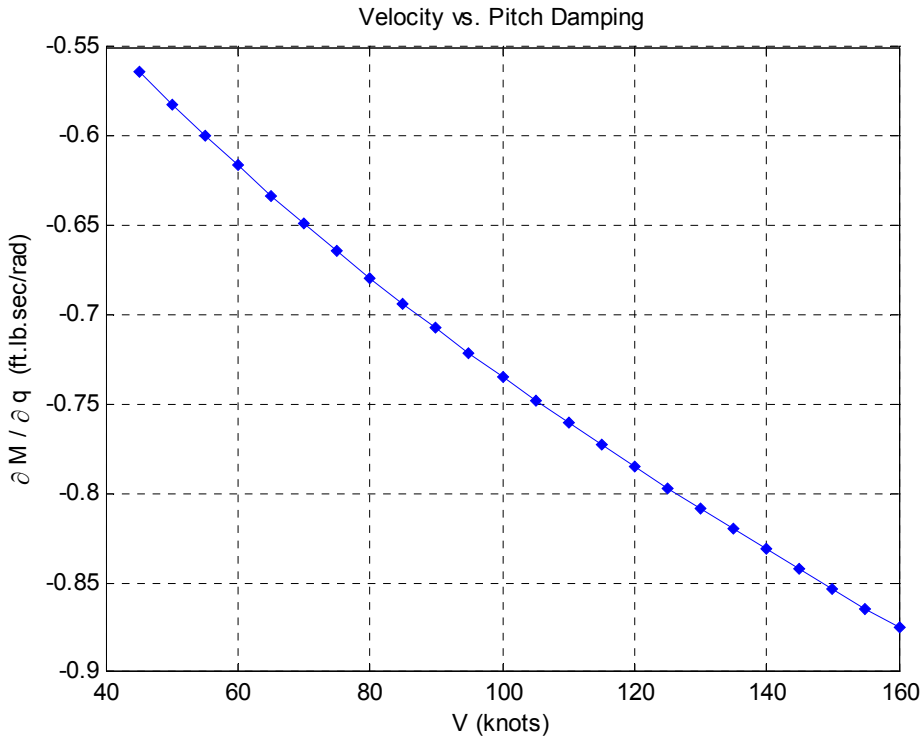

Figure 4-9: Pitch Damping.

CHAPTER 5

CONCLUSIONS AND FUTURE WORK

This thesis describes the development of a series of codes for trim and longitudinal stability analysis of a helicopter in forward flight. The trim analysis results are obtained for a clean UH-60 configuration and the results are compared with flight test data. One of the trim codes is based on momentum theory, while the other one is based on the blade element theory. These codes include many simplifying assumptions such as empirical uniform wake model. Nevertheless, application of these codes to some example helicopters indicated reasonably good agreement with the other available data, particularly for the main rotor performance. The results indicated that, improvements are needed in calculation of the torque, and thereby the parameters related to the tail rotor.

There are several possibilities to improve these codes, which include modifications of the wake models; and extension of the codes to low speed performance, trim and stability calculations. Other future work may include preparation of a graphical user interface and a full Simulink® model.

REFERENCES

1. Seddon, J., Basic Helicopter Aerodynamics, AIAA Education Series, 1990.

2. Padfield, G. D., Helicopter Flight Dynamics: The Theory and Application of Flying Qualities and Simulation Modeling, 1995

3. Prouty, R.W., Helicopter Performance, Stability, and Control, Krieger Publishing Company, 1995.

4. Cooke, A.K., Fitzpatrick, E.W.H., Helicopter Test and Evaluation, AIAA Education Series, 2002.

5. Leishman, J.G., Principles of Helicopter Aerodynamics, Cambridge University Press, 2000.

6. U.S. Army Helicopter Design Datcom, Volume I – Airfoils, Boeing Doc. No. D210-11097-1, 1976.

7. Hoerner, Fluid Dynamic Drag, Published by Author, 1965.

8. MATLAB Getting Started Guide

9. MATLAB help files

10. MATHWORKS Company, www.mathworks.com, last visited on 21.06.2007

11. Method for Studying Helicopter Longitudinal Maneuver Stability, NACA TN 3022, 1953

12. Longitudinal Stability and Control of the Single-Rotor Helicopter, Aeronautical Research Council Reports And Memoranda, A.R.C. Technical Report, R.&M. No:3104, 1959

13. An Analysis of the Longitudinal Stability and Control of a Single-Rotor Helicopter, Aeronautical Research Council Reports And Memoranda, A.R.C. Technical Report, R.&M. No:2958, 1957

14. Stability And Control Of Helicopters, AE397 BTech Seminar Report, Department of Aerospace Engineering, Indian Institute of Technology, Bombay, Khadilkar Harshad Dilip, Dr. Ashok Joshi, 2008

15. Aerodynamic Characteristics of SC1095 and SC1094 R8 Airfoils, William G. BOUSMAN, Aeroflightdynamics Directorate U.S. Army Research, Development, and Engineering Command Ames Research Center, NASA/TP–2003-212265, AFDD/TR-04-003, December 2003

16. A Mathematical Model of the UH-60 Helicopter, NASA Technical Memorandum 85890, USAAVSCOM Technical Memorandum 84-A-2, Kathryn B. Hilbert, Aeromechanics Laboratory, U.S. Army Research and Technology Laboratories - AVSCOM Ames Research Center, Moffett Field, California

17. Power balance method in calculation of helicopter maneuverability taking into account specific operational conditions, Allerton Press, Inc. S. A. Mikhailov Contact Information and A. Yu. Onushkin

18. Analytical Calculation of Helicopter Main Rotor Blade Flight Loads in Hover and Forward Flight, Ki C. Kim, Survivability/Lethality Analysis Directorate, Army Research Laboratory, ARL-TR-3180, April 2004

19. Johnson W., Helicopter Theory, 1980

20. Bramwell A. R. S., Done G., Balmford D., Bramwell's Helicopter Dynamics, Butterworth-Heinemann, ISBN 0 7506 5075 3, 2001

21. Wikipedia, http://en.wikipedia.org/wiki, last visited on 04.10.2008

22. Imperial College London, http://www3.imperial.ac.uk/aeronautics/wingcentre/aerodynamics, last visited on 04.09.2008

23. Aerospaceweb.org, http://www.aerospaceweb.org/aircraft/helicopter-m/uh60/ , last visited on 04.10.2008

24. Demand Media, Inc., http://www.airliners.net/aircraft-data, last visited on 27.09.2008

25. http://www.zap16.com/mil%20fact/Bo105.htm, last visited on 29.09.2008

26. FAS Military Analysis Network, http://www.fas.org/man/dod-101/sys/ac/row/bo105.htm, last visited on 29.09.2008

27. All The World's Rotorcraft, http://www.aviastar.org/helicopters_eng/mbb-105.php, last visited on 29.09.2008

28. Tom Speer, http://www.tspeer.com/NACA23012/N23012wflap.htm, last visited on 29.09.2008

29. Public Domain Aeronautical Software (PDAS), http://www.pdas.com/naca456samples.htm, last visited on 29.09.2008

30. Defence Journal, http://www.defencejournal.com/jan99/s-70a.htm, last visited on 04.10.2008

31. All The World's Rotorcraft, http://www.aviastar.org/helicopters_eng/sik_s-70.php, last visited on 04.10.2008

32. Forecast International, http://www.dfeeler.com/forecastinc/sampledocs/MilitaryAircraft/Sikorsky.doc, last visited on 04.10.2008

33. Wikimedia Foundation, Inc., http://en.wikipedia.org/wiki/Simpson's_rule, last visited on 15.04.2008

34. Metric, http://www.metric.ma.ic.ac.uk/integration/techniques/definite/numerical-methods/simpsons-rule/index.html, last visited on 15.04.2008

35. Wolfram Research, Inc., http://mathworld.wolfram.com/SimpsonsRule.html, last visited on 15.04.2008

36. California State University, Fullerton, http://math.fullerton.edu/mathews/n2003/SimpsonsRuleMod.html, last visited on 15.04.2008

37. University of Maryland, http://terpconnect.umd.edu/~leishman/Aero/tailrotors.html, last visited on 12.10.2008

38. Air Force Technology, http://www.airforce-technology.com/projects/black_hawk/, last visited on 12.10.2008

39. Lycos,http://www.angelfire.com/pa3/cadet985/aviation/blackhawk.html, last visited on 12.10.2008

APPENDIX A

TRIM-BE CODE

A.1 MAIN ROTOR PARAMETERS

The figures below demonstrate the angles, forces and moments over a helicopter.

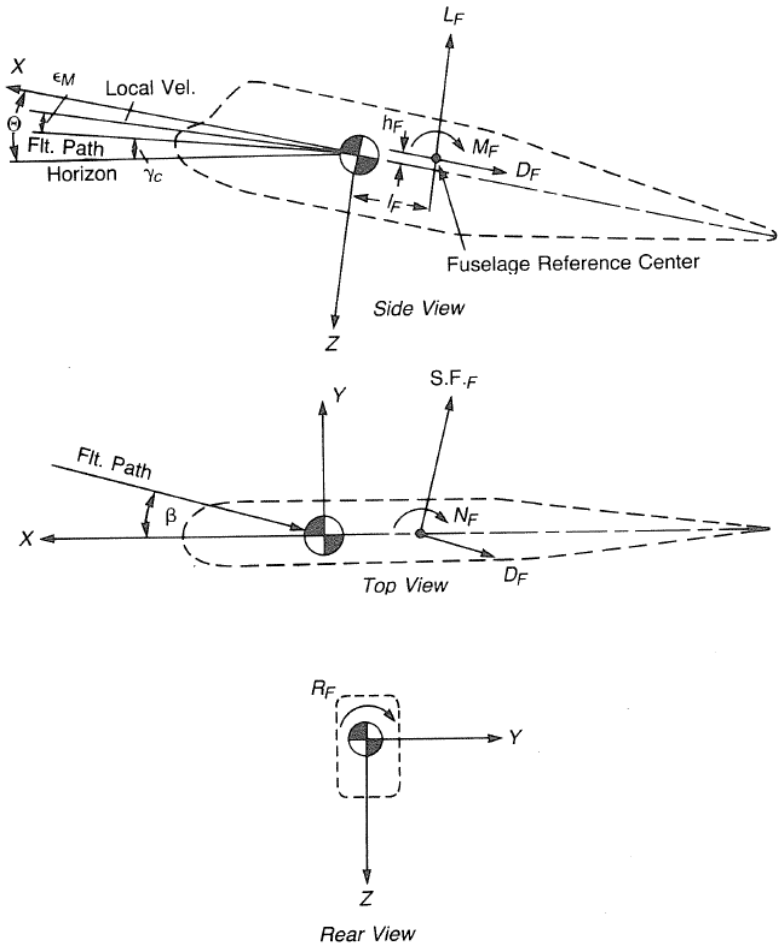

Figure A- 1: Fuselage angles, forces and moments [3].

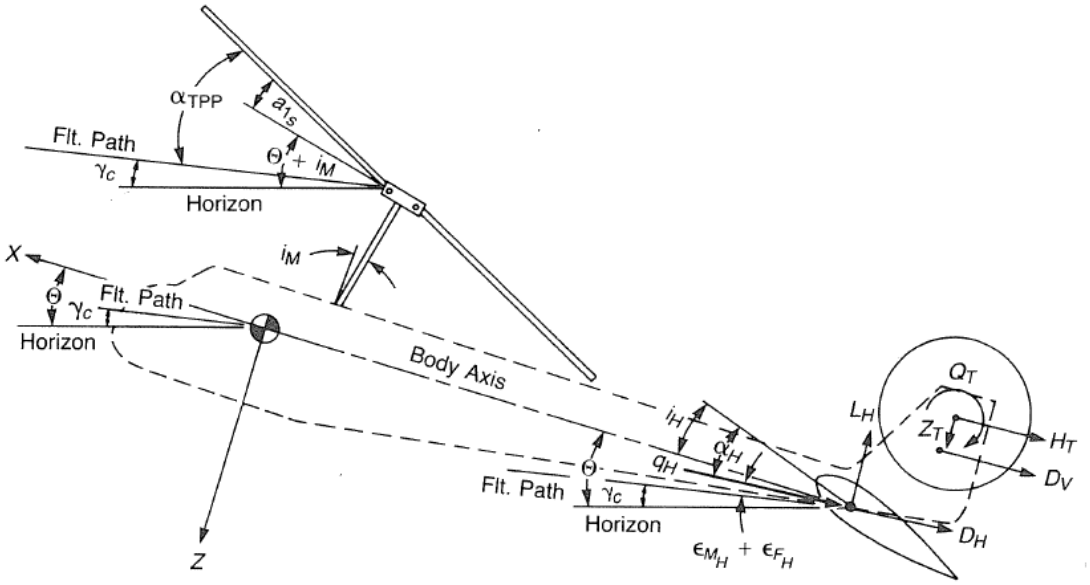

Figure A- 2: Main rotor, empennage and fuselage angles, forces and moments [3].

The advance ratio and the dynamic pressure are defined as:

$$\mu = \frac{V.\cos(\alpha_{TPP})}{\Omega R} \tag{12}$$

$$q = \frac{1}{2}\rho V^2 \tag{13}$$

The lock number and the solidity of the rotors have the following formulas:

$$\gamma = \frac{\rho a c R^4}{I_b} \tag{14}$$

$$\sigma = \frac{bc}{\pi R} \tag{15}$$

A.1.1 CALCULATIONS OF LOCAL FORCES

The following procedures explain the calculations of the local lift and drag coefficients, used in the core of the code.

Total pitching angle of the main rotor blades:

$$\theta = \theta_0 + \theta_1 \frac{r}{R} - A_1 \cos\psi - B_1 \sin\psi \qquad (16)$$

Here θ_0 is named collective angle, the coefficient of the third term A_1 is first harmonic lateral pitching coefficient (lateral cyclic angle), and the forth term coefficient B_1 is first harmonic longitudinal pitching coefficient (longitudinal cyclic angle). The angle in the second term θ_1 is the twist angle of the blade. See Figure A- 3 for the angles.

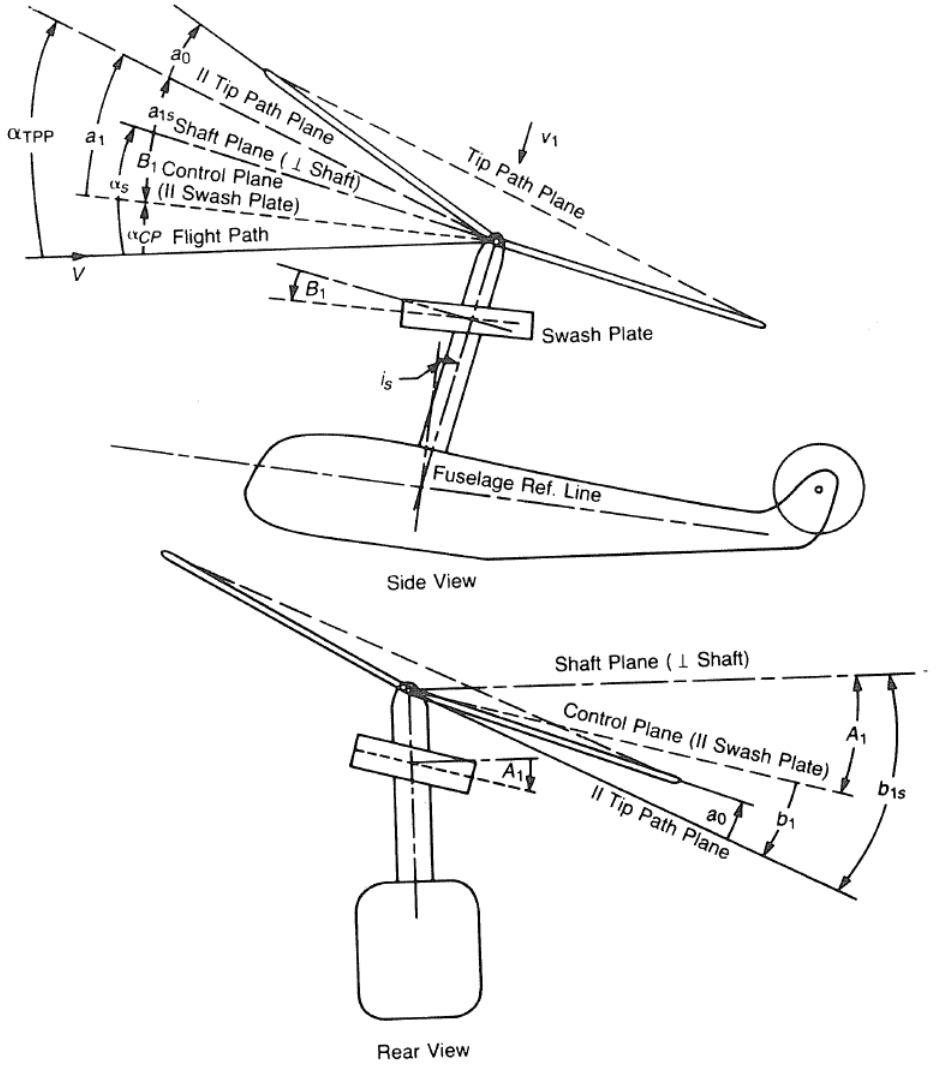

Figure A- 3: Reference planes and angles on the main rotor [3].

The local flapping angle of the blades is represented by the following formula:

$$\beta = a_0 - a_{1S}\cos\psi - b_{1S}\sin\psi \qquad (17)$$

Here the first term a_0 is called the coning angle, the coefficient of the second term a_{1s} is the first harmonic longitudinal flapping angle, and the coefficient of the third term b_{1s} is the first harmonic lateral flapping angle.

The difference between the first harmonic lateral pitching coefficient (lateral cyclic angle) and the first harmonic lateral flapping angle $(b_{1s} - A_1)$ gives the total lateral flapping angle b_1 with respect to the no-feathering plane (or control plane which is parallel to the swash plate). Similarly, the difference between the first harmonic longitudinal pitching coefficient (lateral cyclic angle) and the first harmonic longitudinal flapping angle $(B_1 + a_{1s})$ gives the total longitudinal flapping angle a_1 with respect to the no-feathering plane. See Figure A- 3.

As far as rotor aerodynamics is concerned, one degree of cyclic pitch produces the same effect as one degree of flapping. Therefore, this combination of cyclic pitch and flapping is referred to as flapping with respect to the "Plane of No-Feathering" and is designated as $a_1 = a_{1S} + B_1$.

The longitudinal cyclic angle is half the difference in pitch between the advancing and retreating blades. It is positive when the pitching on the retreating blade is greater than the pitch on the advancing blade.

A.1.1.1. Induced Velocity Calculation Using the Momentum Theory

Using the conservation of mass and energy rule on the actuator disc of a hovering helicopter (See Figure A- 4), it can be obtained that:

$$T = \dot{m}\Delta\upsilon\,,\ \dot{m} = \rho\upsilon_1 A,\ \Delta\upsilon = \upsilon_2 - \upsilon_0 \qquad (18)$$

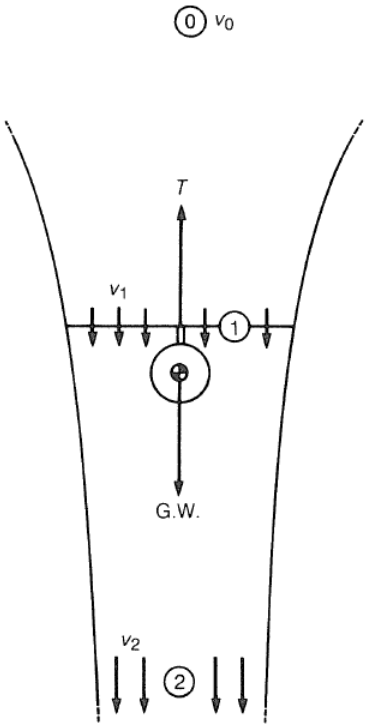

Figure A- 4: Induced velocities in the vicinity of a hovering rotor [3].

Since the total air speed far away from the rotor is zero,

$$\Delta\upsilon = \upsilon_2 \tag{19}$$

Therefore,

$$T = \rho\upsilon_1 A\upsilon_2 \tag{20}$$

The work done becomes;

$$\dot{E} = T\upsilon_1 = \rho A\upsilon_1^2\upsilon_2 \tag{21}$$

If the work done is equated to the change in the kinetic energy;

$$\rho A\upsilon_1^2\upsilon_2 = \frac{1}{2}\dot{m}_2\upsilon_2^2 \tag{22}$$

Using the conservation of mass;

$$\dot{m}_2 = \dot{m}_1 = \rho\upsilon_1 A \tag{23}$$

Therefore;

$$\rho A \upsilon_1^2 \upsilon_2 = \frac{1}{2} \rho \upsilon_1 A \upsilon_2^2 \quad (24)$$

Simplifying:

$$\upsilon_2 = 2\upsilon_1 \quad (25)$$

Therefore the thrust becomes:

$$T = 2\rho \upsilon_1^2 A \quad (26)$$

The induced velocity is calculated using the above thrust equation:

$$\upsilon_{1,hover} = \sqrt{\frac{T_M}{2\rho A_M}} \quad (27)$$

The momentum equations used for the wings of aircraft can also be used for rotor of rotorcraft. For the cases where the forward velocity component exists, with an analogy to the wing aerodynamics, the main rotor thrust equation can be written as (See Figure A- 5):

$T = \dot{m}\Delta\upsilon$ and (28)

$$\dot{m} = \rho A \sqrt{V^2 + \upsilon_1^2} \quad (29)$$

$$\Delta\upsilon = (V + \upsilon_2) - (V) = \upsilon_2 \quad (30)$$

The previously derived equation $\upsilon_2 = 2\upsilon_1$ is applicable here.

If the equation is solved for the induced velocity υ_1,

$$\upsilon_1 = \sqrt{-\frac{V^2}{2} + \sqrt{\frac{V^4}{4} + \upsilon_{1,hover}^4}} \quad (31)$$

This equation is independent of the forward velocity component. It gives best results for low velocities.

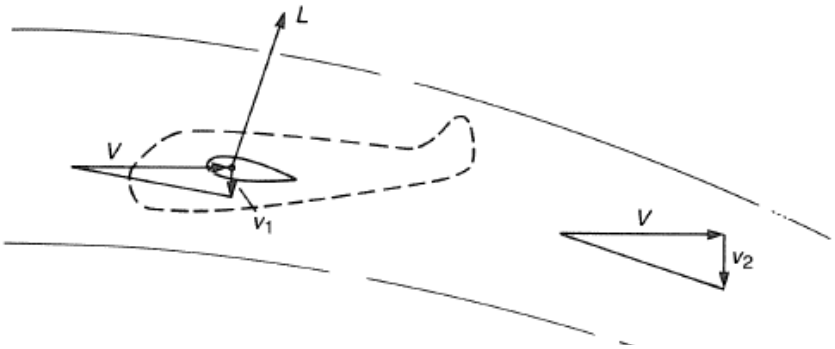

Figure A- 5: The induced velocity on an aircraft [3].

A.1.1.2. Local Induced Velocity

Local induced velocity υ_L distribution on the main rotor is more like a sinusoidal function, rather than a constant value. Then the induced velocity υ_1 becomes the average value of the local induced velocity υ_L along the rotor. If it is assumed that the induced velocity is parallel to the shaft, the relation between the two velocity values becomes (See Figure A- 6):

$$\upsilon_L = \upsilon_1\left(1+\frac{r}{R}\cos\psi\right) \tag{32}$$

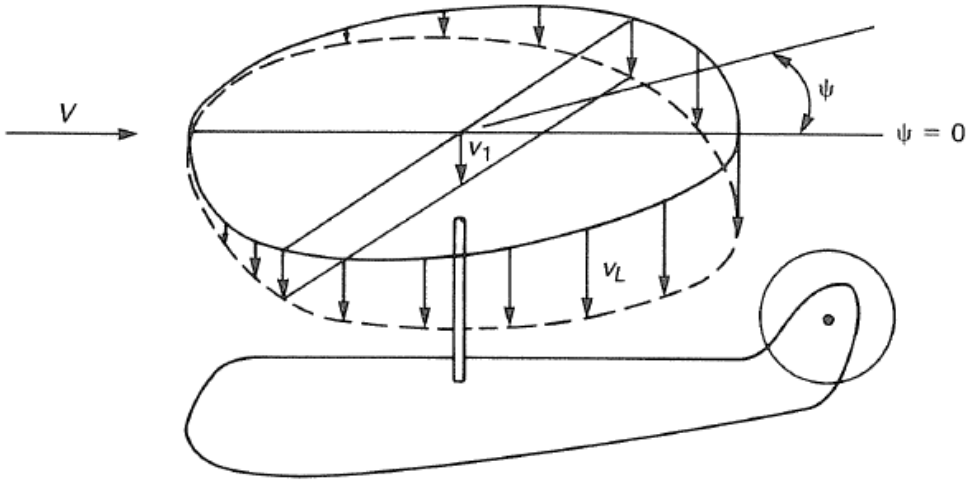

Figure A- 6: Local induced velocity distribution on the main rotor [3].

In the TRIM-BE module, an advanced version of the local induced velocity is used:

$$\upsilon_L = \upsilon_1\left(1 + K_{ind}\,\frac{r}{R}\cos\psi\right) \tag{33}$$

The coefficient K_{ind} of the oscillating term is the induced velocity distortion factor. The formula for the factor, given in Figure A- 7, is:

$$K_{ind} = \begin{cases} 1 & \mu \geq 0.24 \\ 24.35\mu - 55.4\mu^2 - 118\mu^3 & \mu < 0.24 \end{cases} \tag{34}$$

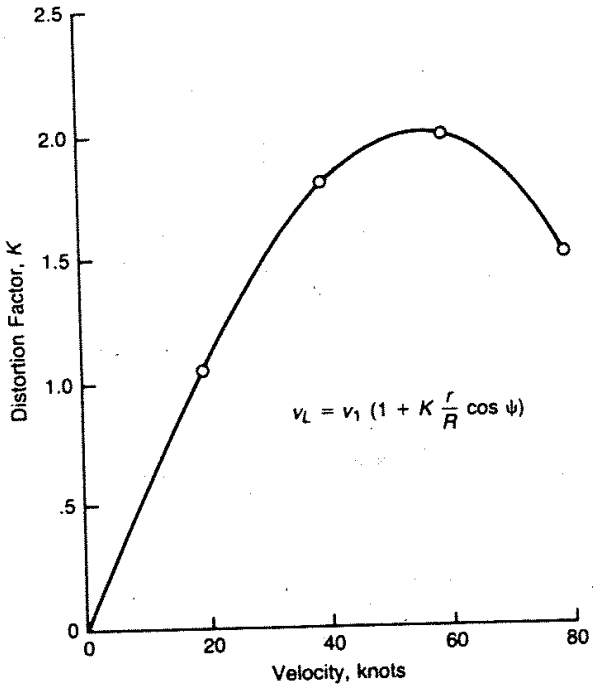

Figure A- 7: Distortion factor of the local induced velocity distribution [3].

A.1.1.3. Non-Dimensional Velocity Components

The local velocity components U_T, U_R and U_P are non-dimensionalized by dividing by ΩR:

$$\overline{U}_T = \frac{U_T}{\Omega R}, \overline{U}_R = \frac{U_R}{\Omega R}, \overline{U}_P = \frac{U_P}{\Omega R} \tag{35}$$

See Figure A- 8 for the local velocity components.

The tangential velocity component:

$$\overline{U}_T = \frac{r}{R} + \mu \sin \psi \tag{36}$$

The radial velocity component:

$$\overline{U}_R = \mu \cos \psi \tag{37}$$

And the perpendicular velocity component:

$$\overline{U}_P = \lambda' - \mu a_0 \cos\psi - \frac{\upsilon_1}{\Omega R} K_{ind} \frac{r}{R} \cos\psi \tag{38}$$

The derivation of the last equation is given below:

The perpendicular velocity in dimensional form is:

$$U_P = V\alpha_S - \upsilon_L - r\dot{\beta} - V\beta\cos\psi \tag{39}$$

It is more convenient to use the TPP angle of attack instead of the shaft angle of attack:

$$\alpha_{TPP} = \alpha_S - a_{1S} \tag{40}$$

If it is assumed that the forward velocity is much bigger than the induced velocity, using equation 3:

$$\upsilon_1 = \frac{\Omega R}{\mu} \frac{C_T}{2} \tag{41}$$

Using the general formula for the flapping angle and taking its derivative:

$$\beta = a_0 - a_{1S}\cos\psi - b_{1S}\sin\psi \tag{42}$$

$$\dot{\beta} = \left(a_{1S}\sin\psi - b_{1S}\cos\psi\right)\frac{d\psi}{dt} \tag{43}$$

$$\dot{\beta} = \left(a_{1S}\sin\psi - b_{1S}\cos\psi\right)\Omega \tag{44}$$

If the 10th-12th equations are gathered:

$$\overline{U}_P = \frac{U_P}{\Omega R} = \begin{pmatrix} \mu\alpha_{TPP} - \frac{\upsilon_1}{\Omega R} - \frac{r}{R} a_{1S}\sin\psi - \mu a_{1S}\sin^2\psi \\ + \left[\left(b_{1S} - \frac{\upsilon_1}{\Omega R}\right)\frac{r}{R} - \mu a_0\right]\cos\psi + \mu b_{1S}\sin\psi\cos\psi \end{pmatrix} \tag{45}$$

If the first harmonic flapping angles a_{1s} and b_{1s} are taken as zero, and the velocity component is non-dimesionalized, the 9th equation is obtained. It is acceptable to assume the flapping angles as zero at that stage of the module.

Some other velocity components can be introduced for the ease of the calculations:

$$\overline{U} = \sqrt{\overline{U}_T^2 + \overline{U}_R^2} \tag{46}$$

$$\overline{U}_B = \sqrt{\overline{U}_T^2 + \overline{U}_P^2} \tag{47}$$

A.1.1.4. Lift and Drag Coefficients

See Figure A- 8 for the angle of attack:

$$\alpha = \theta + \tan^{-1}\frac{\overline{U}_P}{\overline{U}_T} \tag{48}$$

And the local Mach number:

$$M_{local} = \Omega R\frac{\overline{U}_B}{a_{sound}} \tag{49}$$

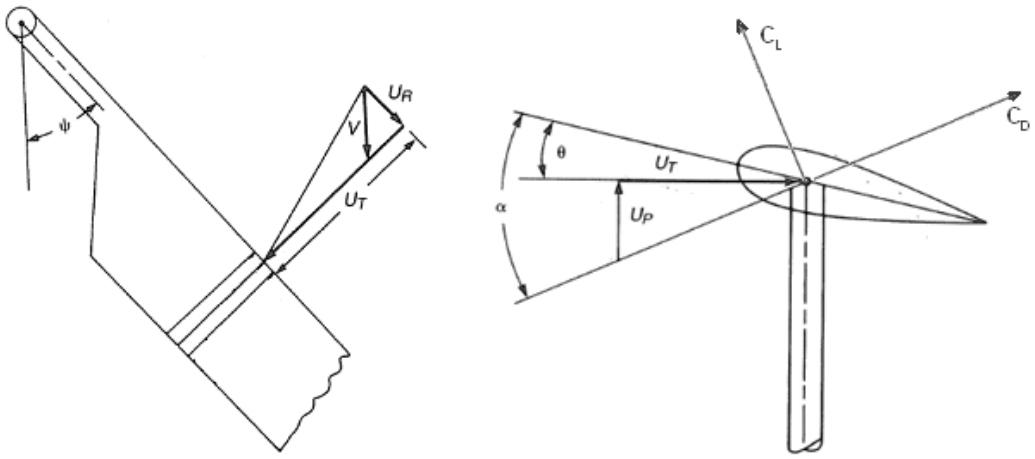

Figure A- 8: Local velocity components acting on the blade section [3].

For the NACA0012 airfoil of the example helicopter [3], the empirical formulas below [3] can be used to calculate the lift and drag coefficients.

$$C_l = a\alpha \tag{50}$$

$$C_d = C_{d_0} + C_{d_1}\alpha + C_{d_2}\alpha^2 \tag{51}$$

Those formulas are for low angles of attack. Some modifications should be used in order to cover higher angles of attack. The modifications are explained below.

The Mach number at which the drag coefficient reaches twice the value of the incompressible drag coefficient is called the drag divergence Mach number, M_{dd}. Depending on M_{dd}, the angle of attack and force coefficients of the blades (having a profile NACA0012) are expressed by the following formulas:

$$a = \begin{cases} \dfrac{0.1}{\sqrt{1-M^2}} - 0.01M, & M < M_{dd} \\ 0.677 - 0.744M, & M > M_{dd} \end{cases} \tag{52}$$

The angle of attack at which the lift coefficient first shows the effect of stall is defined as α_L.

$$\alpha_L = \begin{cases} 15 - 16M, & M < M_{dd} \\ 3.4, & M > M_{dd} \end{cases} \tag{53}$$

The lift coefficient:

$$K_1 = \begin{cases} 0.0233 + 0.342M^{7.15}, & M < M_{dd} \\ 0.0575 - 0.144\left(M - M_{dd}\right)^{0.44}, & M > M_{dd} \end{cases} \tag{54}$$

$$K_2 = 2.05 - 0.95M \tag{55}$$

$$C_l = \begin{cases} a\alpha & \alpha < \alpha_L \\ a\alpha - K_1\left(\alpha - \alpha_L\right)^{K_2} & \alpha > \alpha_L \end{cases} \tag{56}$$

$$C_{d,incomp} = C_{d,0,\min} + \left(65.8\alpha^2 - 0.226\alpha^4 + 0.0046\alpha^6\right).10^{-6} \tag{57}$$

The angle at which the individual drag curves break away from the incompressible curve of drag coefficient is defined as α_D.

$$\alpha_D = \begin{cases} 17 - 23.4M, & M < M_{dd} \\ 0, & M > M_{dd} \end{cases} \tag{58}$$

$$K_3 = \begin{cases} 0.00066, & M < M_{dd} \\ 0.00035, & M > M_{dd} \end{cases} \tag{59}$$

$$K_4 = 2.54 \tag{60}$$

$$K_5 = 21 \tag{61}$$

$$K_6 = 3.2 \tag{62}$$

$$C_d = \begin{cases} C_{d,incomp} & M < M_{dd}, \alpha < \alpha_D \\ C_{d,incomp} + K_3(\alpha - \alpha_D)^{K_4} & M < M_{dd}, \alpha > \alpha_D \\ C_{d,incomp} + K_3(\alpha - \alpha_D)^{K_4} + K_5(M - M_{dd})^{K_6} & M > M_{dd} \end{cases} \tag{63}$$

The lift and drag coefficients expressed above are only applicable to hover. The corrections below are applied to cover forward flight:

$$C_l = \begin{cases} C_l, & \alpha < 20° \\ 1.15\sin(2\alpha) & 20° < \alpha < 161° \\ -0.7 & 161° < \alpha < 173° \\ 0.1(\alpha - 180°) & 173° < \alpha < 199° \\ 0.7 & 199° < \alpha < 201 \\ 1.15\sin(2\alpha) & 201° < \alpha < 340° \\ C_l & 340° < \alpha < 360° \end{cases} \tag{64}$$

$$C_d = \begin{cases} C_d & \alpha < 20° \\ 1.03 - 1.02\cos(2\alpha) & 20° < \alpha < 340° \\ C_d & 340° < \alpha < 360° \end{cases} \tag{65}$$

The drag coefficient above is the steady flow drag coefficient, $C_{L,steady}$. The unsteady flow effect will be discussed in the following pages.

When airfoils rapidly change the angle of attack, a non-linear unsteady phenomenon, called Dynamic Stall, occurs. The rapid change can cause a strong vortex to be shed from the leading edge of the aerofoil, and travel backwards above the wing / blade. The vortex, containing high velocity airflows, briefly increases the lift produced by the wing. As soon as it passes behind the trailing edge, however, the lift reduces dramatically, and the wing is in normal stall. Dynamic stall is an effect most associated with helicopters and flapping wings. During forward flight, some regions of a helicopter blade may incur flow that reverses (compared to the direction of blade movement), and thus includes rapidly changing angles of attack.

Dynamic stall is a process resulting from a series of events, which involve a hysteresis loop in the aerofoil-lift curve and account for a higher maximum lift force than that achieved in the static curve, during a cycle of pitching motion. Helicopter, turbine and windmill blades may all be affected by this phenomenon, which increases forces and moments applied to the blade and its root, and reduces fatigue life.

The increase in angle of attack of the blade due to dynamic stall can be expressed with the following equation:

$$\Delta\alpha_{stall} = \gamma_{ds}\sqrt{\frac{c}{R}\frac{1}{4\pi}\frac{1}{U_B}\frac{|\Delta\alpha|}{\Delta\psi/360}} \tag{66}$$

Here γ_{ds} is a function depending on Mach number:

$$\gamma_{ds} = 1.76.\ln\left(\frac{0.6}{M}\right) \tag{67}$$

$\Delta\psi$ is the angle difference between the previous azimuthal station and the present station. $\Delta\alpha$ is the angle of attack difference between those two azimuthal stations. It is subtracted from α_L:

$$\alpha_L = \alpha_{L,eff} - \Delta\alpha_{stall} \tag{68}$$

The lift of an airfoil is affected by the rate of change of angle of attack and by the rate of plunge, both of which produce shed vorticity lying behind the trailing edge, which induces velocities at the front of the airfoil coming after. This phenomenon is called classical unsteady potential flow. The effect of classical unsteady potential flow is taken into account by the formulas below.

For an airfoil that is pitching about its quarter chord – a good assumption for most rotors – the equation for lift coefficient may be written as:

$$C_l = a\left\{\alpha_{mean} + F\left[\Delta\alpha + k\frac{\dot{\theta}}{\Omega}\right] + G\left[\frac{\dot{\alpha}}{\Omega} + \frac{k\ddot{\theta}}{\Omega^2}\right] + \frac{k}{2}\frac{\dot{\alpha}}{\Omega} + \left(\frac{k}{2}\right)^2\frac{\ddot{\theta}}{\Omega^2}\right\} \quad (69)$$

This theory assumes that the blade flaps about a mean angle of attack with a frequency. The reduced frequency k is the angular displacement during the time the air moves half a cord:

$$k = \frac{1}{2}\frac{c/R}{U} \quad (70)$$

The mean angle of attack:

$$\alpha_{mean} = \theta_0 + \theta_1\frac{r}{R} + \frac{1}{2}\tan^{-1}\left(\frac{\lambda'}{r/R}\right) + \frac{1}{4}\tan^{-1}\left(\frac{\lambda'}{r/R+\mu}\right) + \frac{1}{4}\tan^{-1}\left(\frac{\lambda'}{r/R-\mu}\right) \quad (71)$$

Therefore, the additional lift coefficient due to unsteady potential flow can be expressed as:

$$\Delta C_{l,unsteady} = a\left\{(F-1)(\alpha-\alpha_{mean}) + Fk\frac{\dot{\theta}}{\Omega} + G\left[\frac{\dot{\alpha}}{\Omega} + \frac{k\ddot{\theta}}{\Omega^2}\right] + \frac{k}{2}\frac{\dot{\alpha}}{\Omega} + \left(\frac{k}{2}\right)^2\frac{\ddot{\theta}}{\Omega^2}\right\} \quad (72)$$

The functions G and F and the pitching derivatives are calculated with the following formulas:

$$F = \begin{cases} 0.9 - 0.00178\left(15 - 1/k\right)^2, & \frac{1}{k} < 15 \\ F = 0.864 + \frac{0.0024}{k}, & \frac{1}{k} > 15 \end{cases} \quad (73)$$

$$G = -0.2 + \frac{0.0025}{k} \quad (74)$$

$$\frac{\dot{\theta}}{\Omega} = A_1 \sin\psi - B_1 \cos\psi \quad (75)$$

$$\frac{\ddot{\theta}}{\Omega^2} = A_1 \cos\psi + B_1 \sin\psi \quad (76)$$

The final lift coefficient is obtained by adding the unsteady effect to the steady value:

$$C_l = C_{l,steady} + \Delta C_{l,unsteady} \quad (77)$$

For high forward velocities ($\mu \geq 0.25$), there occurs a reverse flow region at the retreating side of the rotor (see Figure A- 9). Within the reverse flow region, the tangential velocity component changes sign and the lift changes direction. The region can be modeled as:

$$U_T \leq 0 \quad (78)$$

$$\frac{r}{R} + \mu \sin\psi \leq 0 \quad (79)$$

$$\frac{r}{R} \leq -\mu \sin\psi \quad (80)$$

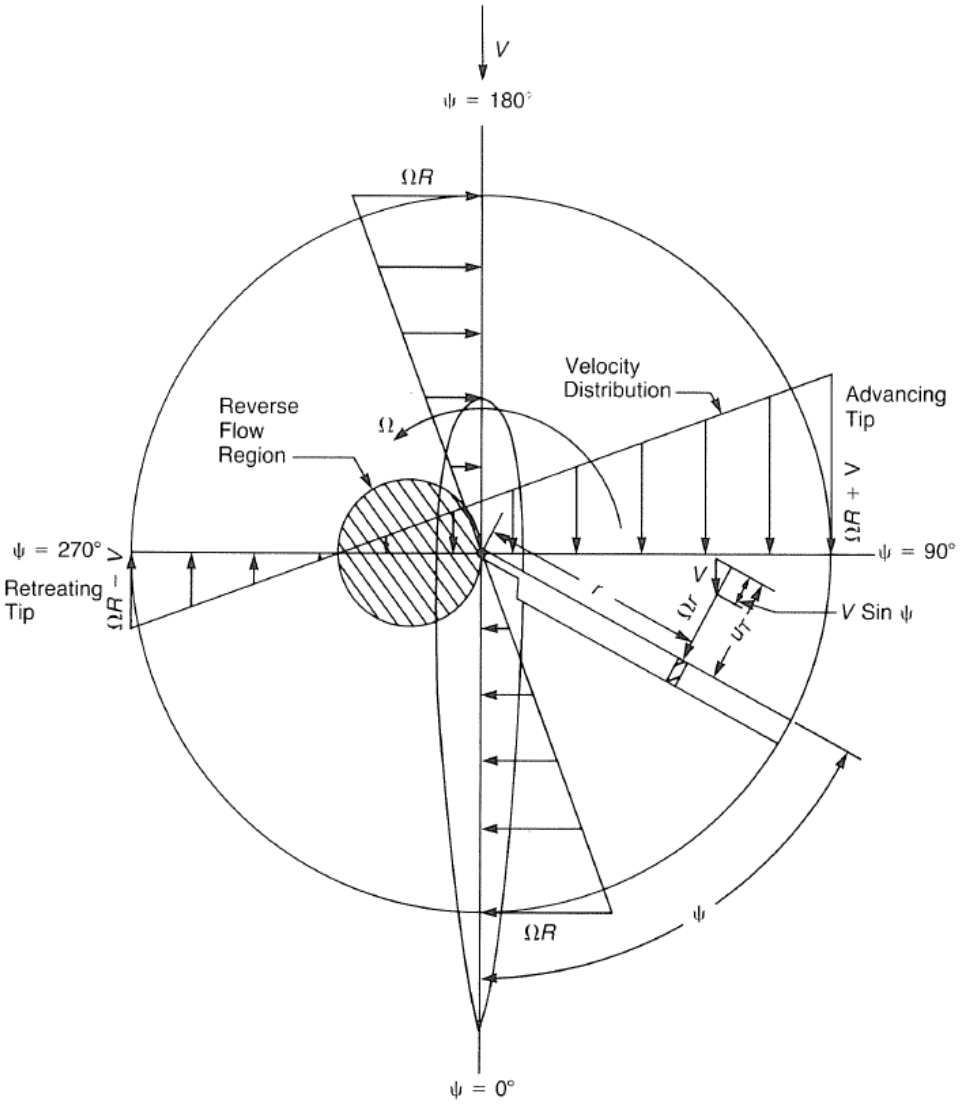

Figure A- 9: Local velocity components and the reverse flow region [3].

A.1.1.5. Force Coefficients

Having introduced the effects of reverse flow, dynamic stall and the unsteady potential flow, the final lift and drag coefficients are calculated. Using those coefficients, the thrust, H-force, torque and moment coefficients are calculated as follows.

Normal force component (see Figure A- 10):

$$C_N = \frac{C_l \overline{U}_T + C_d \overline{U}_P}{\overline{U}_B} \tag{81}$$

The skin friction force coefficient:

$$C_f = 0.006 \tag{82}$$

The pressure drag force coefficient:

$$C_{d_P} = C_d - C_f \tag{83}$$

The chordwise coefficient due to pressure drag and skin friction:

$$C_{C_0} = C_{d_P} \frac{\overline{U}_T}{\overline{U}_B} + c_f \frac{\overline{U}_T \sqrt{\overline{U}_T^2 + \overline{U}_R^2}}{\overline{U}_B^2} \tag{84}$$

Induced chordwise coefficient:

$$C_{C_{ind}} = -C_l \frac{\overline{U}_P}{\overline{U}_B} \tag{85}$$

Total chordwise coefficient (see Figure A- 10)

$$C_C = C_{C_0} + C_{C_{ind}} \tag{86}$$

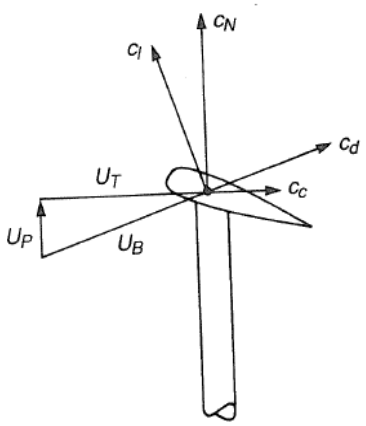

Figure A- 10: Normal and chordwise force coefficients [3].

A.1.2 INTEGRATION

The following procedures explain the integrations.

The thrust coefficient:

$$\frac{\partial}{\partial\psi}\left(\frac{\partial\left(C_T/\sigma\right)}{\partial\left(r/R\right)}\right)=\frac{\overline{U}_B^2}{2}C_N \tag{87}$$

The torque coefficient due to profile drag:

$$\frac{\partial}{\partial\psi}\left(\frac{\partial\left(C_Q/\sigma\right)}{\partial\left(r/R\right)}\right)_{profile}=\frac{\overline{U}_B^2}{2}\frac{r}{R}C_{C_0} \tag{88}$$

The torque coefficient due to induced drag:

$$\frac{\partial}{\partial\psi}\left(\frac{\partial\left(C_Q/\sigma\right)}{\partial\left(r/R\right)}\right)_{induced}=\frac{\overline{U}_B^2}{2}\frac{r}{R}C_{C_{ind}} \tag{89}$$

H-force coefficient due to drag:

$$\frac{\partial}{\partial\psi}\left(\frac{\partial\left(C_H/\sigma\right)}{\partial\left(r/R\right)}\right)_{Drag\_contribution}=\frac{\overline{U}_B^2}{2}C_{C_0}\sin\psi \tag{90}$$

H-force coefficient due to lift:

$$\frac{\partial}{\partial\psi}\left(\frac{\partial\left(C_H/\sigma\right)}{\partial\left(r/R\right)}\right)_{Lift\_contribution}=\frac{\overline{U}_B^2}{2}C_{C_{ind}}\sin\psi \tag{91}$$

Roll moment coefficient:

$$\frac{\partial}{\partial\psi}\left(\frac{\partial\left(C_R/\sigma\right)}{\partial\left(r/R\right)}\right)=-\frac{\partial}{\partial\psi}\left(\frac{\partial\left(C_T/\sigma\right)}{\partial\left(r/R\right)}\right)\frac{r}{R}\sin\psi \tag{92}$$

Pitch moment coefficient:

$$\frac{\partial}{\partial\psi}\left(\frac{\partial\left(C_M/\sigma\right)}{\partial\left(r/R\right)}\right)=-\frac{\partial}{\partial\psi}\left(\frac{\partial\left(C_T/\sigma\right)}{\partial\left(r/R\right)}\right)\frac{r}{R}\cos\psi \tag{93}$$

Those values are all integrated along the blade and along the azimuthal range:

$$I=\int_0^{2\pi}\int_0^1\frac{\partial}{\partial\psi}\left(\frac{\partial\left(C_M/\sigma\right)}{\partial\left(r/R\right)}\right).d\,\frac{r}{R}.d\psi \tag{94}$$

The integration is performed with the Simpson's integration rule. Simpson's rule, being more sophisticated compared to the trapezoidal rule, uses quadratic polynomials to calculate the approximate value of a function (See Figure A- 11). Let's introduce a function f tabulated at points x_0, x_1 and x_2 equally spaced by distance h. The Simpson's rule says that:

$$\int_{x_0}^{x_2} f(x)dx=\int_{x_0}^{x_0+2h} f(x)dx\approx\frac{1}{3}h\left(f_0+4f_1+f_2\right) \tag{95}$$

Since it uses quadratic polynomials to approximate functions, Simpson's rule actually gives exact results when approximating integrals of polynomials up to cubic degree.

The composite Simpson's rule stands for multiple point functions:

$$\begin{aligned}\int_{x_0}^{x_{2n}} f(x)dx&\approx\frac{1}{3}h\left[f_0+4\left(f_1+f_3+\ldots+f_{2n-1}\right)+2\left(f_2+f_4+\ldots+f_{2n-2}\right)+f_{2n}\right]\\ \int_{x_0}^{x_{2n}} f(x)dx&\approx\frac{h}{3}\left(f_0+f_{2n}\right)+\frac{2h}{3}\sum_{k=1}^{n-1}f\left(x_{2k}\right)+\frac{4h}{3}\sum_{k=1}^{n}f\left(x_{2k-1}\right)\end{aligned} \tag{96}$$

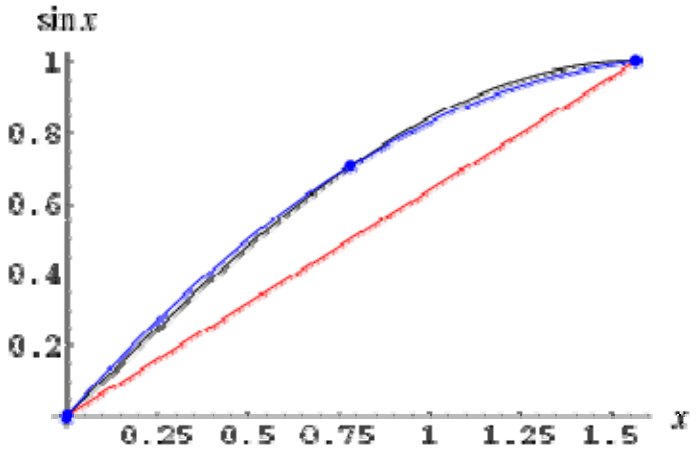

Figure A- 11: Function $f = \sin x$ (black curve) is calculated with Simpson's rule (blue lines) and by trapezoidal rule (red line) [36].

After integrating the parameters over the blade, the root and tip losses are subtracted from the result:

$$\int_0^1 \frac{\partial\left(C_T/\sigma\right)}{\partial\left(r/R\right)} d\left(r/R\right)\Bigg|_{@\psi=c} = I - \frac{x_0\left(y_0 + y_{x_0}\right)}{2} - \left(1-B\right)\frac{\left(y_B + y_{10}\right)}{2} \tag{97}$$

B is the tip loss factor, being typically 0.97, meaning that 3% of the blade at tip is exposed to loss of lift. y_0, y_{x_0}, y_B and y_{10} are the integrand values corresponding to first radial station, the cut-out station, the station where tip loss begins (i.e. B) and the last radial station respectively:

$$y_j = \frac{\partial}{\partial\psi}\left(\frac{\partial\left(C_i/\sigma\right)}{\partial\left(r/R\right)}\right)_{@\frac{r}{R}=0} \tag{98}$$

Where $i = T, H, Q, M, R$, $j = 0, x_0, B, 10$

The inflow ratio is defined as:

$$\lambda' = \mu \sin \alpha_{TPP} - \frac{\upsilon_1}{\Omega R} \cong \mu \alpha_{TPP} - \frac{\upsilon_1}{\Omega R} \tag{99}$$

The TPP angle of attack can be obtained from the inflow ratio as:

$$\alpha_{TPP} = \sin^{-1}\left(\frac{\lambda' + \frac{\upsilon_1}{\Omega R}}{\mu} \right) \cong \frac{\lambda' + \frac{\upsilon_1}{\Omega R}}{\mu} \tag{100}$$

Or an alternative equation can be used:

$$\alpha_{TPP} = \Theta + a_{1s} + i_M \tag{101}$$

A.1.3 WHOLE ROTOR PARAMETERS

Whole rotor parameters obtained after the integration process are defined in this section.

A.1.3.1. Coning Angle

The coning angle a_0 is derived from equating the total moments at the flapping hinge to zero:

$$M_{hinge} = M_{lift} + M_{c.f.} + M_w = 0 \tag{102}$$

Here the moment due to lift:

$$M_{lift} = \int_0^R \frac{dL}{dr} r dr = \int_0^R \frac{\rho}{2} \Omega^2 R a c (\theta_t - \phi_t) r^2 dr = \frac{2}{3} \frac{C_T}{\sigma} \frac{1}{a} \Omega^2 \rho a c R^4 \tag{103}$$

The moment due to centrifugal forces:

$$M_{c.f.} = -\int_0^R (\Omega^2 m r) a_0 r dr = a_0 \Omega^2 I_b \tag{104}$$

And the moment due to the weight only:

$$M_w = -\int_0^R gmrdr = -\frac{3}{2}\frac{g}{R} I_b \tag{105}$$

Where I_b is the flapping inertia of the blade.

$$I_b = \int_0^R mr^2 dr \tag{106}$$

The blade is assumed to have a homogeneous mass distribution.

The coning angle is found from the total moments equation:

$$a_0 = \frac{2}{3}\gamma \frac{C_T \diagup \sigma}{a} - \frac{\frac{3}{2}gR}{(\Omega R)^2} \tag{107}$$

That equation is written for a hovering rotor with ideal twist, but it gives very good results for forward flight and for teetering and rigid rotors.

The Lock Number γ is the ratio of the aerodynamic forces to the inertial forces and is defined as:

$$\gamma = \frac{\rho a c R^4}{I_b} \tag{108}$$

A.1.3.2. Forces, Moments and Power

The thrust, H-force and torque are calculated as:

$$T_M = \frac{C_T}{\sigma}\rho A_b (\Omega R)^2 \tag{109}$$

$$H_M = \frac{C_H}{\sigma}\rho A_b (\Omega R)^2 \tag{110}$$

$$Q_M = \frac{C_Q}{\sigma}\rho A_b (\Omega R)^2 R \tag{111}$$

The total forces on the main rotor longitudinal axis can be expressed as:

$$\sum X = -T_M \tan\alpha_{TPP} - H_M \tag{112}$$

The induced and profile required power of the main rotor can be calculated as:

$$HP_M = \frac{C_Q}{\sigma}\frac{\rho A_b (\Omega R)^3}{550} \tag{113}$$

The total power is calculated using transmission, generator and hydraulic system losses. The transmission losses are calculated using the equation below:

$$HP_{Trans} = \rho\left(HP_{X,const} + C_{HP,M,X} HP_M + C_{HP,T,X} HP_T\right) \tag{114}$$

Here $HP_{X,const}$ stands for the constant transmission losses, $C_{HP,M,X}$ and $C_{HP,T,X}$ are main rotor and tail rotor transmission system power losses respectively. The total power:

$$HP = HP_M + HP_T + HP_{Trans} + HP_{Gen} + HP_{Hyd} \tag{115}$$

Where HP_{Gen} and HP_{Hyd} are generator and hydraulic system power losses.

A.1.3.3. First Harmonic Flapping Angles

Pitch and roll moments are used in order to find the 1st harmonic flapping angles:

$$\frac{dM_M}{da_{1,S}} = \frac{3}{4}\frac{eA_b\rho(\Omega R)^2 a_M}{\gamma} \tag{116}$$

$$a_{1,S} = \frac{T_M l_M - H_M h_M + Q_T - H_T h_T + L_H l_H + L_T l_T + M_F}{\frac{dM_M}{da_{1,S}} + T_M h_M} \tag{117}$$

$$b_{1,S} = -\frac{T_T h_T}{\frac{dM_M}{da_{1,S}} + T_M h_M} \tag{118}$$

The effects of the components of the helicopter on lift and drag are mainly due to the induced velocities. The main rotor induces velocity on fuselage and on empennage, the tail rotor and the fuselage induce velocity on the empennage, a wing -if exists- induces velocity on the empennage. The parameters below are angle of attack components due to the induced velocities. The first subscript indicates the component which induces, and the second indicates the one which is exposed to the induced velocity.

$$\varepsilon_{M_F} = \Delta\alpha_{D.W.} = \frac{\upsilon_1}{V} = \frac{\upsilon_F}{\upsilon_1}\frac{T_M}{4qA_M} \tag{119}$$

$$\varepsilon_{M_H} = \frac{\upsilon_H}{V} = \frac{\upsilon_H}{\upsilon_1}\frac{\upsilon_1}{V} = \frac{\upsilon_H}{\upsilon_1}\frac{D.L.}{4q} = \frac{\upsilon_H}{\upsilon_1}\frac{\upsilon_F}{\upsilon_1}\frac{T_M}{4qA_M} \tag{120}$$

The sidewash term, η_{M_V}, is a component to be added to the sideslip angle.

A.2 FUSELAGE PARAMETERS

The angle of attack of the fuselage can be calculated using different formulas below:

$$\alpha_F = \alpha_{TPP} - \varepsilon_{M_F} - i_M - a_{1s}$$

$$\alpha_F = \Theta - \varepsilon_{M_F} = \Theta - \frac{\upsilon_1}{V} = \Theta - \frac{\upsilon_F}{\upsilon_1}\frac{T_M}{4qA_M} \tag{121}$$

$$\alpha_F = \frac{\lambda'}{\mu} - i_M - a_{1s}$$

The fuselage lift, drag and pitch moments are obtained with the following equations, which are supplied either by the wind tunnel measurements, or CFD programs:

$$L_F = q\left(\left(L_F / q \right)_{\alpha_F = 0} + \frac{\partial \left(L_F / q \right)}{\partial \alpha_F} \alpha_F \right) \tag{122}$$

$$D_F = q\left(f_0 + \frac{\partial f}{\partial \left(\alpha_F^2 \right)} \alpha_F^2 \right) \tag{123}$$

$$M_F = q\left(\left(M_F / q \right)_{\alpha_F = 0} + \frac{\partial \left(M_F / q \right)}{\partial \alpha_F} \alpha_F \right) \tag{124}$$

Here the unknown parameters are found either by wind tunnel tests of the fuselage, or by extensive static aerodynamic analysis on fuselage.

The pitch attitude of the fuselage can be found using:

$$\begin{aligned} \Theta &= \alpha_F + \varepsilon_{M_F} \\ \Theta &= \alpha_{TPP} - a_{1s} - i_M \\ \Theta &= \alpha_H - i_H + \varepsilon_{M_H} + \varepsilon_{F_H} \end{aligned} \tag{125}$$

The sidewash angle induced by the fuselage on the vertical stabilizer is obtained by an empirical formula:

$$\eta_{F_V} = 0.06\beta \tag{126}$$

A.3 EMPENNAGE PARAMETERS

The angle of attack the horizontal stabilator will see can be obtained from different ways:

$$\begin{aligned} \alpha_H &= \Theta + i_H - \varepsilon_{M_H} - \varepsilon_{F_H} \\ \alpha_H &= \alpha_F + \varepsilon_{M_F} + i_H - \varepsilon_{M_H} - \varepsilon_{F_H} \\ \alpha_H &= \alpha_{TPP} - i_M - a_{1s} + i_H - \varepsilon_{M_H} - \varepsilon_{F_H} \end{aligned} \tag{127}$$

The lift produced by the horizontal stabilator:

$$L_H = \frac{q_H}{q} q A_H a_H \left(\alpha_H - \alpha_{L=0_H}\right) \quad (128)$$

The induced and profile drag:

$$D_{H,ind} = L_H \varepsilon_{M_H} \quad (129)$$

$$D_{H,pro} = q A_H C_{D_H} \quad (130)$$

$$D_H = D_{H,ind} + D_{H,pro} \quad (131)$$

The sideslip angle of the vertical stabilizer is:

$$\beta_V = \beta + \alpha_{L=0_V} + \eta_{M_V} + \eta_{T_V} + \eta_{F_V} \quad (132)$$

The lift (i.e. the side force parallel to the β_V sideslip angle) can be obtained (see Figure A- 13):

$$L_V = -q \frac{q_V}{q} A_V a_V \beta_V \quad (133)$$

The side force generated by the vertical stabilizer perpendicular to the longitudinal axis:

$$Y_V = L_V \cos\left(\beta_V\right) - D_V \sin\left(\beta_V\right) \quad (134)$$

If wings exist on the rotorcraft, then the following equations are used to count for their effects:

The angle of attack of the wing:

$$\alpha_W = \alpha_F + i_W \quad (135)$$

Lift:

$$L_W = q A_W a_W \alpha_W \quad (136)$$

The induced velocity on the wings:

$$\upsilon_W = \frac{L_W}{2\rho\pi\left(b_W / 2\right)^2 V} \quad (137)$$

The induced angle of attack by the main rotor on the wings:

$$\alpha_{i,W} = \varepsilon_{M_W} = \frac{\upsilon_W}{V} \tag{138}$$

Therefore, the induced drag is:

$$D_{W,ind} = L_W \frac{\varepsilon_{M_W}}{e_W} \tag{139}$$

Where e_W term is the Oswald efficiency factor for the wings.

The profile drag:

$$D_{W,pro} = qA_W C_{D_W} \tag{140}$$

And the total drag :

$$D_W = D_{W,ind} + D_{W,pro} \tag{141}$$

A.4 CONVERGENCE CRITERIA

Total integration over the rotor is followed by corrections to the 1st harmonic cyclic angles which are the convergence parameters of the innermost loop of the code:

$$\Delta B_1 = -100(1-\mu)C_R/\sigma \tag{142}$$

$$\Delta A_1 = -30(2+\mu^2)C_M/\sigma \tag{143}$$

The coefficients are chosen with trial and error and they give best convergence rate and accuracy. Considering the cyclic angles convergence, therefore, means considering the moment coefficients convergence.

A loop is constructed to analyze the total forces on the vertical axis. The following error is defined on the vertical forces:

$$\Delta Z_{err} = T_M \cos\alpha_{TPP} + L_F + L_H - W \tag{144}$$

This error can be related to the collective angle in order to change a parameter within the loop.

$$\Delta\theta_0 = -k_1 \Delta Z_{err} \tag{145}$$

Similarly, an error is introduced on the longitudinal forces and the error is related to the inflow ratio:

$$\Delta X_{err} = \sum X - D_F - D_H - H_{TR} \tag{146}$$

$$\Delta\lambda' = k_2 \Delta X_{err} \tag{147}$$

The coefficients k_1 and k_2 are chosen by trial and error method which give best convergence.

A.5 TAIL ROTOR PARAMETERS

The advance ratio for the tail rotor is:

$$\mu_T = \frac{V}{(\Omega R)_T} \tag{148}$$

The disc loading of the tail rotor is defined as:

$$D.L_T. = \frac{\frac{Q_M}{l_T} - L_V \frac{l_V}{l_T}}{A_T} \tag{149}$$

Where the nominator is approximately the thrust of tail rotor:

$$T_T = \frac{Q_M}{l_T} - Y_V \frac{l_V}{l_T} \tag{150}$$

The thrust coefficient of the tail rotor:

$$\left.\frac{C_T}{\sigma}\right)_T = \frac{T_T}{\rho A_{b,T} (\Omega R)^2} \tag{151}$$

For the cases except the helicopter does side slip or the shaft angle is not perpendicular to the longitudinal axis, the TPP angle of attack of the tail rotor is zero. Then, the thrust coefficient can be calculated as:

$$\left.\frac{C_T}{\sigma}\right)_T = \frac{4}{a_T}\left\{\begin{array}{l}\left(\frac{2}{3}+\mu_T{}^2\right)\left(\theta_{0,T}+a_{0,T}\tan\delta_3\right)\\ +\left(\frac{1}{2}+\frac{\mu_T{}^2}{2}\right)\theta_{1,T}-\mu_T b_{1s,T}\tan\delta_3+\lambda_T\end{array}\right\} \qquad (152)$$

Where, δ_3 angle is the slant angle of the flapping hinge (See Figure A- 12) and the other parameters are just like the ones corresponding to the main rotor.

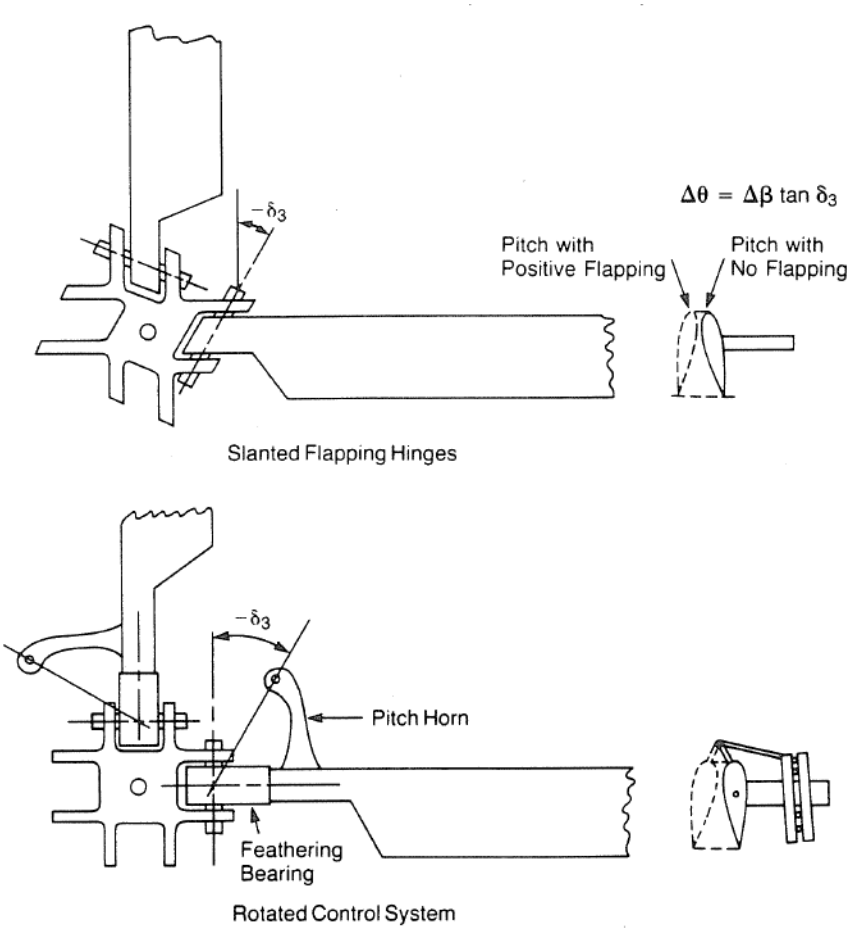

Figure A- 12: Delta-3 angle [3].

The coning angle:

$$a_{0,T} = \frac{2}{3}\gamma_T \frac{\left(C_T/\sigma\right)_T}{a_T} - \frac{\frac{3}{2}gR_T}{(\Omega R)_T^2} \tag{153}$$

The inflow ratio for the case the shaft is perpendicular to the longitudinal axis:

$$\lambda_T = -\left(\frac{C_T}{\sigma}\right)_T \frac{.\sigma_T}{2\mu_T} \tag{154}$$

The pitching angle of the tail rotor is denoted by:

$$\theta_T = \left(\theta_{0,T} + a_{0,T}\tan\delta_3\right) + \theta_{1,T}\frac{r}{R}\Big)_T - a_{1s,T}\tan\delta_3\cos\psi_T - b_{1s,T}\tan\delta_3\sin\psi_T \tag{155}$$

Here it is apparent that the effective fist harmonic pitching angles can be introduced as:

$$\begin{aligned} A_{1,eff} &= a_{1s,T}\tan\delta_3 \\ B_{1,eff} &= b_{1s,T}\tan\delta_3 \end{aligned} \tag{156}$$

The thrust coefficient equation is used to obtain the collective angle of the tail rotor:

$$\theta_{0,T} = \left\{ \frac{\frac{C_T}{\sigma}\frac{4}{a} - \left(\frac{1}{2} + \frac{\mu^2}{2}\right)\theta_1 + \mu b_{1s}\tan\delta_3 - \lambda}{\frac{2}{3} + \mu^2} - a_0\tan\delta_3 \right\}_T \tag{157}$$

Therefore, the flapping angles with respect to the control plane can be expressed as:

$$a_{1s,T} + b_{1s,T}\tan\delta_3 = \frac{\mu_T}{1 + \frac{3}{2}\mu_T^2}\left[\frac{8}{3}\left(\theta_{0,T} + a_{0,T}\tan\delta_3\right) + 2\theta_{1,T} + 2\left(\mu_T a_{1s,T} + \lambda_T\right)\right] \tag{158}$$

$$b_{1s,T} - a_{1s,T}\tan\delta_3 = \frac{\frac{4}{3}\mu_T a_{0,T} + \frac{\upsilon_{1,T}}{(\Omega R)_T}}{1 + \frac{\mu_T^2}{2}} \tag{159}$$

Those two equations with two unknowns are solved and the flapping angles are found as:

$$a_{1s,T} = \frac{\left(\begin{array}{l} \dfrac{4\mu}{2+3\mu^2}\left\{ \dfrac{4}{2+3\mu^2}\left[\left(\dfrac{4}{a}+\dfrac{\sigma}{2\mu} \right)\dfrac{C_T}{\sigma} - \left(1+\mu^2\right)\dfrac{\theta_1}{2} \right] + \theta_1 - \dfrac{C_T}{\sigma}\dfrac{\sigma}{2\mu} \right\} \\ -2\left[\dfrac{\dfrac{4}{3}\mu a_0 + \dfrac{C_T}{\sigma}\dfrac{\sigma}{2\mu}}{2+\mu^2} \right]\left[1-\left(\dfrac{4\mu}{2+3\mu^2} \right)^2 \right]\tan\delta_3 \end{array} \right)_T}{\left\{ \dfrac{2-\mu^2}{2+3\mu^2} + \left[1-\left(\dfrac{4\mu}{2+3\mu^2} \right)^2 \right](\tan\delta_3)^2 \right\}_T} \quad (160)$$

$$b_{1s,T} = 2\left[\frac{\dfrac{4}{3}\mu a_0 + \dfrac{C_T}{\sigma}\dfrac{\sigma}{2\mu}}{2+\mu^2} \right]_T + a_{1s,T}\tan\delta_3 \quad (161)$$

The torque and the H-force coefficients of the tail rotor:

$$\left.\frac{C_H}{\sigma}\right)_T = \left\{ \begin{array}{l} \left[\dfrac{C_D\mu}{4} - \dfrac{a}{4}\left[\dfrac{\mu(\lambda+\mu a_{1s})}{1+\dfrac{3}{2}\mu^2} \right] \right]\left[\begin{array}{l} (\theta_0 + a_0\tan\delta_3)\left(-\dfrac{1}{3}+\dfrac{3}{2}\mu^2 \right) \\ +\dfrac{\theta_1}{2}\left(-1+\dfrac{3}{2}\mu^2 \right) - (\lambda+\mu a_{1s}) \end{array} \right] \\ +\left[\dfrac{\mu}{1+\dfrac{1}{2}\mu^2} \right]\left[\dfrac{a_0^2}{2}\left(\dfrac{1}{9}+\dfrac{\mu^2}{2} \right) + \dfrac{1}{3}\mu a_0\dfrac{\upsilon_1}{\Omega R} + \dfrac{1}{8}\left(\dfrac{\upsilon_1}{\Omega R} \right)^2 \right] + a_{1s}\dfrac{C_T}{\sigma} \end{array} \right\}_T \quad (162)$$

$$\left.\frac{C_Q}{\sigma}\right)_T = \left\{ \frac{C_D}{8}\left(1+3\mu^2\right) - \lambda\frac{C_T}{\sigma} - \mu\frac{C_H}{\sigma} \right\}_T \quad (163)$$

And the torque and H-force values:

$$H_T = \left(\frac{C_H}{\sigma} \right)_T \rho A_{b,T}\left(\Omega R\right)_T^2 \quad (164)$$

$$Q_T = \left(\frac{C_Q}{\sigma} \right)_T \rho A_{b,T}\left(\Omega R\right)_T^2 R_T \quad (165)$$

The sidewash angle induced by the tail rotor on the vertical stabilizer is calculated by:

$$\eta_{T_V} = \frac{D.L._T}{4q\frac{q_V}{q}} \tag{166}$$

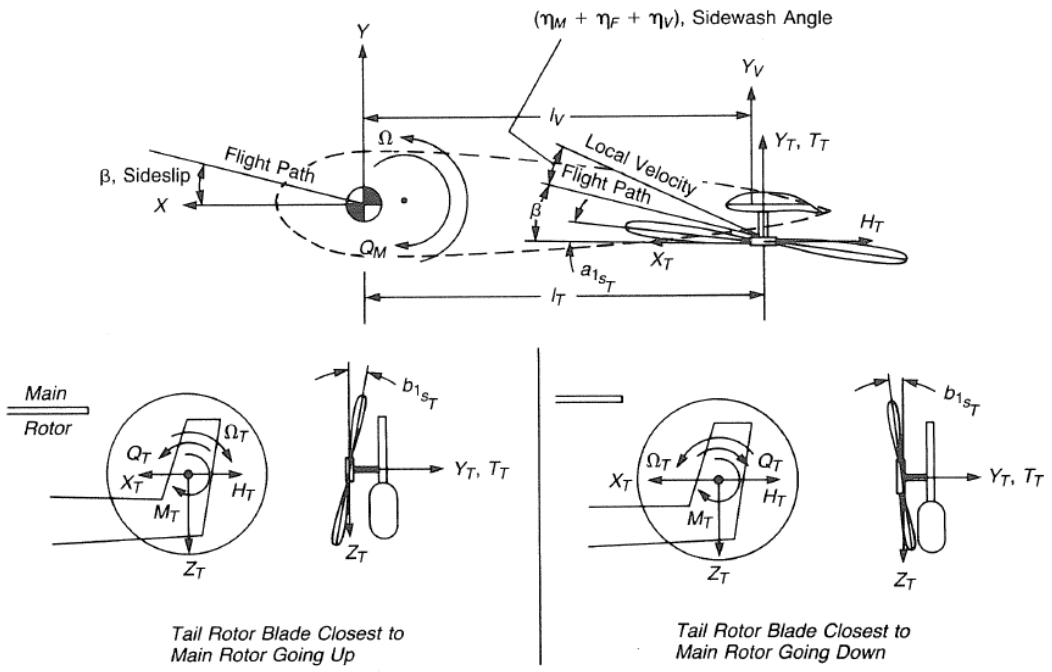

Figure A- 13: Tail rotor and vertical stabilizer angles, forces and moments [3].

APPENDIX B

TRIM-CF CODE

Some of the formulations not stated in this appendix are written in Appendix-A.

B.1 MAIN ROTOR PARAMETERS

The tip path plane angle of attack:

$$\alpha_{TPP} = \tan^{-1}\left(\frac{D_F + H_M + H_T}{W - L_F}\right) \tag{167}$$

The main rotor thrust:

$$T_M = \sqrt{(W - L_F)^2 + (D_F + H_M + H_T)^2} \tag{168}$$

The lift and drag values of fuselage belong to the empennage on case.

First harmonic pitch angles (cyclic angles) are found using the first harmonic flapping angles:

$$A_1 = b_{1s} - \frac{\left[a_0\left(\frac{4}{3}\mu + \frac{16}{45\pi}\mu^4\right) + \frac{\upsilon_1}{\Omega R}\left(1 + \frac{\mu^4}{24}\right)\right]}{\left(1 + \frac{\mu^2}{2} - \frac{\mu^4}{24}\right)} \tag{169}$$

$$B_1 = -a_{1s} + \frac{\mu\left[\left(\frac{8}{3} + \frac{32}{45}\frac{\mu^3}{\pi}\right)\theta_0 + \left(2 + \frac{\mu^4}{12}\right)\theta_1 + \left(2 - \frac{\mu^2}{2}\right)\lambda'\right]}{\left(1 + \frac{3}{2}\mu^2 - \frac{5\mu^4}{24}\right)} \tag{170}$$

B.1.1 COLLECTIVE ANGLE CALCULATIONS

The collective angle is derived by the following integral calculations. The lift force over an azimuthal station and a radial station is defined as:

$$\Delta L = \frac{1}{2}\rho U_T^2 a_M \alpha_M c_M \Delta r$$

$$\frac{\Delta L}{\Delta r} = \frac{1}{2}\rho U_T^2 a_M \alpha_M c_M \quad (171)$$

where U_T is the tangential component of the local velocity vector at that blade section (See Figure A- 8) and Δr is the blade section.

The parameter is integrated over the blade and then over the azimuthal range to find the total lift produced by the main rotor:

$$L_b\big|_\psi = \int_0^R \frac{\Delta L}{\Delta r} dr \quad (172)$$

$$\sum L_b = \int_0^{2\pi} L_b\big|_\psi d\psi \quad (173)$$

The lift produced by one blade at a specific azimuth angle is approximated as:

$$\bar{L}_b = \frac{1}{2\pi}\int_0^{2\pi} L_b\big|_\psi d\psi \quad (174)$$

And the total thrust force is calculated by multiplying the lift by the number of blades:

$$T_M = \frac{bR}{2\pi}\left\{\int_0^{\pi}\int_{x_0}^{B}\frac{\Delta L}{\Delta r} d\frac{r}{R}.d\psi + \int_{\pi}^{2\pi}\int_{-\mu\sin\psi}^{B}\frac{\Delta L}{\Delta r} d\frac{r}{R}.d\psi - \int_{\pi}^{2\pi-\mu\sin\psi}\int_{x_0}^{}\frac{\Delta L}{\Delta r} d\frac{r}{R}.d\psi\right\} \quad (175)$$

Here the integrals are taken from the cut-out (x_o) to the loss factor (B) station, in order to eliminate the root and tip losses. The integration limits are arranged in order to take the reverse flow effect into account. The limits

of the reverse flow region are defined to be $\mu\sin(\psi)$. The reverse flow effect is also introduced as defined in the Figure B- 1 and in section A.1.1.4.

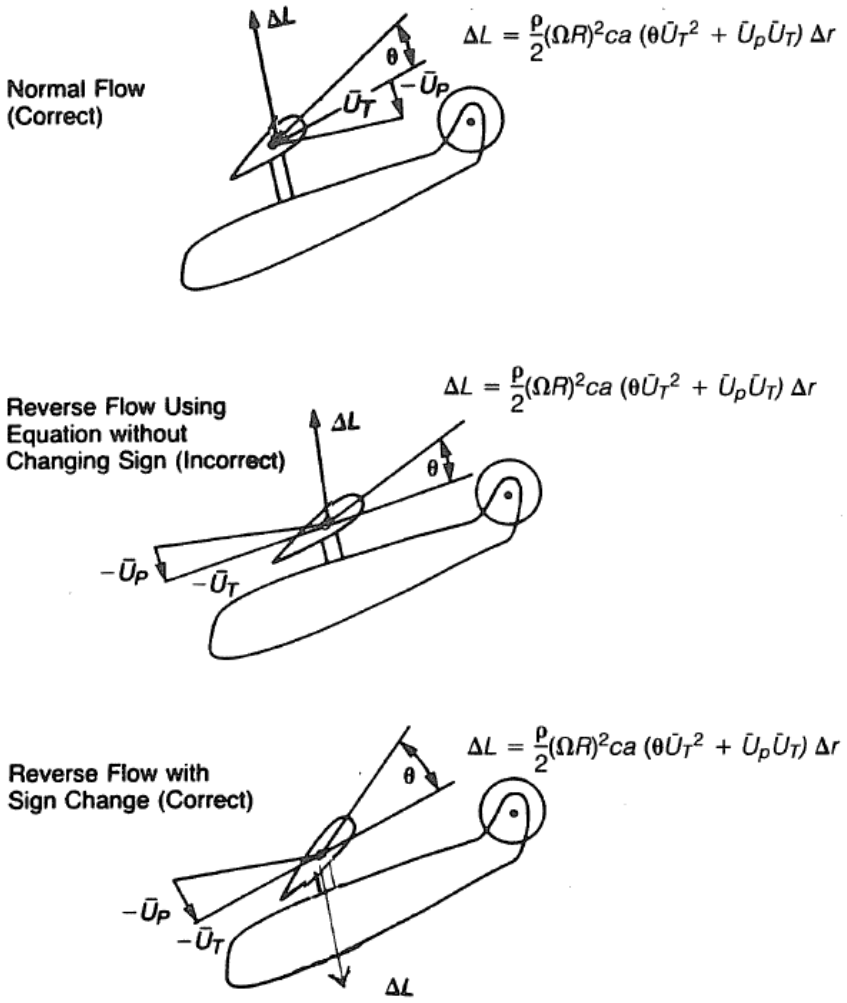

Figure B- 1: The sign change of the lift at the reverse flow region [3].

Therefore;

$$T_M = \frac{bR}{2\pi}\left\{\int_0^{\pi}\int_{x_0}^{B}\frac{1}{2}\rho U_T^2 a_M \alpha_M c_M d\,\frac{r}{R}.d\psi - 2\int_{\pi}^{2\pi-\mu Sin\psi}\int_{x_0}\frac{1}{2}\rho U_T^2 a_M \alpha_M c_M d\,\frac{r}{R}.d\psi\right\} \quad (176)$$

$$T_M = \frac{bR\rho a_M c_M}{4\pi}\left\{\int_0^{\pi}\int_{x_0}^{B} U_T^2\alpha_M d\,\frac{r}{R}.d\psi - 2\int_{\pi}^{2\pi-\mu Sin\psi}\int_{x_0} U_T^2\alpha_M d\,\frac{r}{R}.d\psi\right\} \quad (177)$$

$$\frac{C_T}{\sigma} = \frac{a_M}{4\pi}\left\{\int_0^{\pi}\int_{x_0}^{B} \overline{U}_T^2\alpha_M d\,\frac{r}{R}.d\psi - 2\int_{\pi}^{2\pi-\mu Sin\psi}\int_{x_0} \overline{U}_T^2\alpha_M d\,\frac{r}{R}.d\psi\right\} \quad (178)$$

The local angle of attack is as defined before in Appendix A:

$$\alpha = \theta + \tan^{-1}\left(\frac{U_P}{U_T}\right) \quad (179)$$

The angle can be approximated with small angle assumption:

$$\alpha \cong \theta + \frac{\overline{U}_P}{\overline{U}_T} \quad (180)$$

where the velocity components are non-dimensionalized by the tip speed ΩR.

The thrust coefficient becomes:

$$\frac{C_T}{\sigma} = \frac{a_M}{4\pi}\left\{\int_0^{\pi}\int_{x_0}^{B} \left(\overline{U}_T^2\theta + \overline{U}_T\overline{U}_P\right)d\,\frac{r}{R}.d\psi - 2\int_{\pi}^{2\pi-\mu Sin\psi}\int_{x_0} \left(\overline{U}_T^2\theta + \overline{U}_T\overline{U}_P\right)d\,\frac{r}{R}.d\psi\right\} \quad (181)$$

Introducing the pitch angle:

$$\theta = \theta_0 + \frac{r}{R}\theta_1 - A_1\cos\psi - B_1\sin\psi \quad (182)$$

The tangential velocity is as given before:

$$\overline{U}_T = \frac{r}{R} + \mu\sin\psi \quad (183)$$

The perpendicular velocity component:

$$U_P = V\alpha_S - \upsilon_L - r\dot{\beta} - V\beta c\cos\psi \quad (184)$$

The tipp path plane angle of attack is used instead of the shaft angle of attack:

$$\alpha_{TPP} = \alpha_S - a_{1S} \quad (185)$$

The induced velocity can be approximated with the following formula, assuming that it is much greater than the forward speed:

$$\upsilon_1 = \frac{\Omega R}{\mu}\frac{C_T}{2} \tag{186}$$

The flapping angle can be derived as:

$$\beta = a_0 - a_{1S}\cos\psi - b_{1S}\sin\psi \tag{187}$$

$$\dot{\beta} = \left(a_{1S}\sin\psi - b_{1S}\cos\psi\right)\Omega \tag{188}$$

Taking the last equations, normalized perpendicular velocity component becomes:

$$\overline{U}_P = \frac{U_P}{\Omega R} = \begin{pmatrix} \mu\alpha_{TPP} - \dfrac{\upsilon_1}{\Omega R} - \dfrac{r}{R}a_{1S}\sin\psi - \mu a_{1S}\sin^2\psi \\ + \left[\left(b_{1S} - \dfrac{\upsilon_1}{\Omega R}\right)\dfrac{r}{R} - \mu a_0\right]\cos\psi + \mu b_{1S}\sin\psi\cos\psi \end{pmatrix} \tag{189}$$

Solving the integrals at the 154th equation:

$$\frac{C_T}{\sigma} = \frac{a_M}{4}\left\{\begin{matrix} \left(\dfrac{2}{3}\left(B^2 - x_0^2\right) + \mu^2\left(B - x_0\right) - \dfrac{8\mu^3}{9\pi}\right)\theta_0 + \left(B^4 - x_0^4 + \mu^2\left(B^2 - x_0^2\right) - \dfrac{\mu^4}{8}\right)\dfrac{\theta_1}{2} \\ + \left(B^2 - x_0^2 + \dfrac{\mu^2}{2}\right)\lambda' - \left(\mu\left(B^2 - x_0^2\right) + \dfrac{\mu^3}{4}\right)\left(B_1 + a_{1S}\right) \end{matrix}\right\} \tag{190}$$

Using the above equations, we obtain the collective equation:

$$\theta_0 = \frac{\begin{pmatrix} \dfrac{4}{a}\left(1 + \dfrac{3}{2}\mu^2 - \dfrac{5}{24}\mu^4\right)C_T/\sigma - \left(1 - \dfrac{3}{2}\mu^2 + \dfrac{\mu^4}{6} - \dfrac{9}{16}\mu^6 - \dfrac{3}{192}\mu^8\right)\dfrac{\theta_1}{2} \\ - \left(1 + \dfrac{13}{24}\mu^4 + \dfrac{\mu^6}{48}\right)\lambda' \end{pmatrix}}{\left(\dfrac{2}{3} - \dfrac{2}{3}\mu^2 - \dfrac{8}{9\pi}\mu^3 + \dfrac{25}{36}\mu^4 - \dfrac{92}{45\pi}\mu^5 - \dfrac{5}{24}\mu^6 + \dfrac{\mu^7}{135\pi}\right)} \tag{191}$$

B.1.2 FORCES, MOMENTS AND POWER

Derivations similar to the ones of thrust coefficient are made in order to find the following torque and H-force coefficients:

$$\frac{C_Q}{\sigma} = \frac{c_D}{8}\left(1+3\mu^2+\frac{3}{8}\mu^4\right) - \left(\lambda' - \mu a_{1S}\right)\frac{C_T}{\sigma} - \mu\frac{C_H}{\sigma} \tag{192}$$

$$\frac{C_H}{\sigma} = \left\{ \begin{array}{l} \frac{c_d}{4}\left(\mu+\frac{\mu^3}{4}\right) \\ -\frac{a_M}{4}\left\{ \begin{array}{l} \frac{\mu\lambda'}{\left(1+\frac{3\mu^2}{2}-\frac{5\mu^4}{24}\right)}\left[\begin{array}{l} \frac{\theta_0}{3}\left(-1-\frac{4\mu}{\pi}+\frac{3\mu^2}{2}-\frac{106\mu^3}{15\pi}-\frac{5\mu^4}{8}+\frac{\mu^5}{30\pi}\right) \\ +\frac{\theta_1}{2}\left(-1-\frac{\mu^2}{4}-\frac{2\mu^4}{3}-\frac{\mu^6}{96}\right)+\lambda'\left(\mu^2-\frac{\mu^4}{48}\right) \end{array} \right] \\ -\frac{\mu}{\left(1+\frac{\mu^2}{2}-\frac{\mu^4}{4}\right)}\left\{ \begin{array}{l} \frac{a_0^2}{2}\left[\begin{array}{l} \frac{1}{9}+\frac{\mu^2}{4}-\frac{64\mu^3}{135\pi}-\frac{\mu^4}{6} \\ -\left(\frac{128}{45^2\pi^2}-\frac{1}{96}\right)\mu^6 \end{array} \right] \\ +a_0\frac{\upsilon_1}{\Omega R}\frac{\mu}{3}\left[\begin{array}{l} 1-\frac{8\mu}{5\pi}-\frac{\mu^2}{6} \\ -\frac{8\mu^3}{15\pi}+\frac{\mu^5}{95\pi} \end{array} \right] \\ +\frac{1}{8}\left(\frac{\upsilon_1}{\Omega R}\right)^2\left[1-\frac{\mu^2}{2}-\frac{\mu^4}{8}+\frac{\mu^6}{144}\right] \end{array} \right\} \end{array} \right\} + \frac{C_T}{\sigma}a_{1s} \end{array} \right\} \tag{193}$$

And the forces are calculated:

$$Q_M = \frac{C_Q}{\sigma}\rho A_b(\Omega R)^2 R \tag{194}$$

$$H_M = \frac{C_H}{\sigma}\rho A_b(\Omega R)^2 \tag{195}$$

Power required is calculated with the following formulas:

$$HP_{M,ind} = \frac{T_M^2}{1100\rho A_M Ve} \tag{196}$$

$$HP_{M,para} = \frac{\rho f V^3}{1100} \tag{197}$$

$$HP_{M,pro} = \rho A_b (\Omega R)^3 \frac{c_d}{8} \frac{(1+3\mu^2)}{550} \tag{198}$$

$$HP_{M,comp} = \frac{\Delta \frac{C_Q}{\sigma}\Big)_{comp}}{\frac{C_Q}{\sigma}} \left(HP_{M,ind} + HP_{M,pro} + HP_{M,para}\right) \tag{199}$$

$$HP_M = HP_{M,ind} + HP_{M,pro} + HP_{M,para} + HP_{M,comp} \tag{200}$$

B.2 TOTAL FORCES AND MOMENTS

The forces can be calculated by the following formulas. The parameters with bars overhead are the output parameters supplied by the CF module. This approximation is used in order to linearize the equations.

$$X_M = -\overline{H}_{a_{1S}=0_M} - \overline{T}_M a_{1S} - T_M i_M \tag{201}$$

$$X_T = -\overline{H}_T \tag{202}$$

$$X_H = \overline{L}_H (\alpha_H - \varepsilon_{F_H}) - \overline{L}_H a_H \begin{pmatrix} \alpha_H + i_H \\ -\alpha_{L=0_H} - \varepsilon_{F_H} \end{pmatrix} \frac{(1+\delta_{i_H})}{\pi A R_H} - q \frac{q_H}{q} A_H C_{D_{0,H}} \tag{203}$$

$$X_V = -\overline{D}_V - \overline{L}_V (\eta_{M_V} + \eta_{T_V}) \tag{204}$$

$$X_F = -\overline{D}_F + \overline{L}_F \alpha_F \tag{205}$$

$$Z_M = -T_M \tag{206}$$

$$Z_T = \overline{b}_{1S_T} \overline{T}_T \tag{207}$$

$$Z_H = -q \frac{q_H}{q} A_H a_H (\alpha_H + i_H - \alpha_{L=0_H} - \varepsilon_{F_H}) - \overline{D}_H (\alpha_H - \varepsilon_{F_H}) \tag{208}$$

$$Z_V = -(\overline{D}_V + \overline{L}_V (\eta_{M_V} + \eta_{F_V})) \left(\Theta - \frac{\upsilon_V}{\upsilon_1} \frac{T_M}{4qA_M} - \varepsilon_{F_V}\right) \tag{209}$$

$$Z_F = -q\left(\left(L_F/q\right)_{\alpha_F=0} + \frac{\partial\left(L_F/q\right)}{\partial\alpha_F}\alpha_F\right) - \overline{D}_F\alpha_F \tag{210}$$

$$M_M = \frac{\partial M}{\partial a_{1S}}a_{1S} \tag{211}$$

$$M_T = -\overline{Q}_T \tag{212}$$

$$M_F = q\left(\left(M_F/q\right)_{\alpha_F=0} + \frac{\partial\left(M_F/q\right)}{\partial\alpha_F}\alpha_F\right) \tag{213}$$

Total forces and moments:

$$\sum X = X_M + X_T + X_H + X_V + X_F - W\Theta = 0 \tag{214}$$

$$\sum Z = Z_M + Z_T + Z_H + Z_V + Z_F + W = 0 \tag{215}$$

$$\sum M = \begin{pmatrix} M_M + M_T + M_F - X_M h_M + Z_M l_M - X_T h_T \\ + Z_T l_T - X_H h_H + Z_H l_H - X_V h_V + Z_F l_F - X_F h_F \end{pmatrix} = 0 \tag{216}$$

APPENDIX C

DYNA-STAB CODE

The parameters with bars overhead are the output parameters supplied by a trim analysis code.

C.1 MAIN ROTOR STABILITY DERIVATIVES

$$\frac{\partial \mu}{\partial \dot{x}} = \frac{1}{\Omega R} \tag{217}$$

$$\frac{\partial \lambda'}{\partial \dot{x}} = \frac{1}{\Omega R}\left[\overline{\alpha}_{TPP} - \frac{\sigma}{2\mu}\left(\frac{\partial C_T/\sigma}{\partial \mu} - \frac{C_T/\sigma}{\mu}\right)\right] \tag{218}$$

$$\frac{\partial \lambda'}{\partial \dot{z}} = \frac{1}{\Omega R\left(1 + \dfrac{\partial C_T/\sigma}{\partial \lambda'}\dfrac{\sigma}{2\mu}\right)} \tag{219}$$

$$\frac{\partial C_H/\sigma}{\partial a_{1S}} = \frac{\overline{C}_T}{\sigma} + \frac{a}{8}\lambda' \tag{220}$$

$$\frac{\partial a_{1S}}{\partial q} = -\frac{16}{\gamma\Omega\left(1 - e/R\right)^2\left(1 - \mu^2/2\right)} - \frac{12\, e/R}{\gamma\Omega\left(1 - e/R\right)^3\left(1 - \mu^4/4\right)} \tag{221}$$

$$\frac{\partial a_{1S}}{\partial B_1} = -\frac{\left(1 + \dfrac{3\mu^2}{2}\right)}{\left(1 - \dfrac{\mu^2}{2}\right)} \tag{222}$$

$$\frac{\partial M}{\partial a_{1S}} = \frac{3}{4}\frac{e}{R}A_b\rho\left(\Omega R\right)^2\frac{a}{\gamma} \tag{223}$$

$$\left(\frac{\partial X}{\partial \dot{x}}\right)_M = -A_b \rho (\Omega R)^2 \left\{ \begin{array}{l} \left[\frac{\partial C_H/\sigma}{\partial \mu} + \frac{\partial C_H/\sigma}{\partial a_{1S}} \frac{\partial a_{1S}}{\partial \mu} + (\bar{a}_{1S} + i_M) \frac{\partial C_T/\sigma}{\partial \mu} \right] \frac{\partial \mu}{\partial \dot{x}} \\ + \left[\frac{\partial C_H/\sigma}{\partial \lambda'} + \frac{\partial C_H/\sigma}{\partial a_{1S}} \frac{\partial a_{1S}}{\partial \lambda'} + (\bar{a}_{1S} + i_M) \frac{\partial C_T/\sigma}{\partial \lambda'} \right] \frac{\partial \lambda'}{\partial \dot{x}} \end{array} \right\} \quad (224)$$

$$\left(\frac{\partial X}{\partial \dot{z}}\right)_M = -A_b \rho (\Omega R)^2 \left[\frac{\partial C_H/\sigma}{\partial \lambda'} + \frac{\overline{C}_T}{\sigma} \frac{\partial a_{1S}}{\partial \lambda'} + (\bar{a}_{1S} + i_M) \frac{\partial C_T/\sigma}{\partial \lambda'} \right] \frac{\partial \lambda'}{\partial \dot{z}} \quad (225)$$

$$\left(\frac{\partial X}{\partial q}\right)_M = -A_b \rho (\Omega R)^2 \frac{\partial C_H/\sigma}{\partial a_{1S}} \frac{\partial a_{1S}}{\partial q} - \left(\frac{\partial X}{\partial \dot{x}}\right)_M h_M \quad (226)$$

$$\left(\frac{\partial X}{\partial \theta_o}\right)_M = -A_b \rho (\Omega R)^2 \left[\frac{\partial C_H/\sigma}{\partial \theta_o} + \frac{\partial C_H/\sigma}{\partial a_{1S}} \frac{\partial a_{1S}}{\partial \theta_o} + (\bar{a}_{1S} + i_M) \frac{\partial C_T/\sigma}{\partial \theta_o} \right] \quad (227)$$

$$\left(\frac{\partial X}{\partial B_1}\right)_M = -A_b \rho (\Omega R)^2 \frac{\partial C_H/\sigma}{\partial a_{1S}} \frac{\partial a_{1S}}{\partial B_1} \quad (228)$$

$$\left(\frac{\partial Z}{\partial \dot{x}}\right)_M = -A_b \rho (\Omega R)^2 \left[\frac{\partial C_T/\sigma}{\partial \mu} \frac{\partial \mu}{\partial \dot{x}} + \frac{\partial C_T/\sigma}{\partial \lambda'} \frac{\partial \lambda'}{\partial \dot{x}} \right] \quad (229)$$

$$\left(\frac{\partial Z}{\partial \dot{z}}\right)_M = -A_b \rho (\Omega R)^2 \frac{\partial C_T/\sigma}{\partial \lambda'} \frac{\partial \lambda'}{\partial \dot{z}} \quad (230)$$

$$\left(\frac{\partial Z}{\partial \theta_o}\right)_M = -A_b \rho (\Omega R)^2 \frac{\partial C_T/\sigma}{\partial \theta_o} \quad (231)$$

$$\left(\frac{\partial Z}{\partial B_1}\right)_M = -A_b \rho (\Omega R)^2 \frac{\partial C_T/\sigma}{\partial \lambda'} \frac{\partial \lambda'}{\partial a_{1S}} \frac{\partial a_{1S}}{\partial B_1} \quad (232)$$

$$\left(\frac{\partial M}{\partial \dot{x}}\right)_M = \left(\frac{dM}{da_{1S}}\right)_M \left[\frac{\partial a_{1S}}{\partial \mu} \frac{\partial \mu}{\partial \dot{x}} + \frac{\partial a_{1S}}{\partial \lambda'} \frac{\partial \lambda'}{\partial \dot{x}} \right] - \left(\frac{\partial X}{\partial \dot{x}}\right)_M h_M + \left(\frac{\partial Z}{\partial \dot{x}}\right)_M l_M \quad (233)$$

$$\left(\frac{\partial M}{\partial \dot{z}}\right)_M = \left(\frac{dM}{da_{1S}}\right)_M \frac{\partial a_{1S}}{\partial \lambda'} \frac{\partial \lambda'}{\partial \dot{z}} - \left(\frac{\partial X}{\partial \dot{z}}\right)_M h_M + \left(\frac{\partial Z}{\partial \dot{z}}\right)_M l_M \tag{234}$$

$$\left(\frac{\partial M}{\partial q}\right)_M = \left(\frac{dM}{da_{1S}}\right)_M \frac{\partial a_{1S}}{\partial q} - \left(\frac{\partial X}{\partial q}\right)_M h_M \tag{235}$$

$$\left(\frac{\partial M}{\partial \theta_o}\right)_M = \left(\frac{dM}{da_{1S}}\right)_M \frac{\partial a_{1S}}{\partial \theta_o} - \left(\frac{\partial X}{\partial \theta_o}\right)_M h_M + \left(\frac{\partial Z}{\partial \theta_o}\right)_M l_M \tag{236}$$

$$\left(\frac{\partial M}{\partial B_1}\right)_M = \left(\frac{dM}{da_{1S}}\right)_M \frac{\partial a_{1S}}{\partial B_1} - \left(\frac{\partial X}{\partial B_1}\right)_M h_M \tag{237}$$

C.2 HORIZONTAL STABILIZER STABILITY DERIVATIVES

$$\frac{\partial \gamma_c}{\partial \dot{z}} = -\frac{1}{V} \tag{238}$$

$$\frac{\partial \varepsilon_{M_H}}{\partial \dot{x}} = \frac{\upsilon_H}{\upsilon_1} \frac{1}{4qA_M} \left[-\left(\frac{\partial Z}{\partial \dot{x}}\right)_M + \frac{2\overline{Z}_M}{V} \right] \tag{239}$$

$$\frac{\partial \varepsilon_{M_H}}{\partial \dot{z}} = -\frac{\upsilon_H}{\upsilon_1} \frac{1}{4qA_M} \left(\frac{\partial Z}{\partial \dot{z}}\right)_M \tag{240}$$

$$\frac{\partial \varepsilon_{F_H}}{\partial \dot{z}} = \frac{d\varepsilon_{F_H}}{d\alpha_F} \left[\frac{1}{4qA_M} \left(\frac{\partial Z}{\partial \dot{z}}\right)_M - \frac{\partial \gamma_c}{\partial \dot{z}} \right] \tag{241}$$

$$\frac{\partial \alpha_H}{\partial \dot{x}} = -\frac{\partial \varepsilon_{M_H}}{\partial \dot{x}} \tag{242}$$

$$\frac{\partial \alpha_H}{\partial \dot{z}} = -\left[\frac{\partial \varepsilon_{M_H}}{\partial \dot{z}} + \frac{\partial \varepsilon_{F_H}}{\partial \dot{z}} + \frac{\partial \gamma_c}{\partial \dot{z}} \right] \tag{243}$$

$$\frac{\partial \alpha_H}{\partial \ddot{z}} = -\left[\frac{\partial \varepsilon_{M_H}}{\partial \dot{z}} \right] \frac{l_H}{V} \tag{244}$$

$$\left(\frac{\partial X}{\partial \dot{x}}\right)_H = \left\{ \frac{2}{V} X_H + \frac{q_H}{q} qA_H a_H \left\{ \begin{matrix} \left(\overline{\alpha}_H - \alpha_{L=0_H}\right) \left[1 - \dfrac{2a_H \left(1 + \delta_{i_H}\right)}{\pi A.R._H} \right] \\ + \left(\overline{\alpha}_H - i_H\right) \end{matrix} \right\} \right\} \frac{\partial \alpha_H}{\partial \dot{x}} \tag{245}$$

$$\left(\frac{\partial X}{\partial \dot{z}}\right)_H = \frac{q_H}{q} q A_H a_H \left\{\left(\overline{\alpha}_H - \alpha_{L=0_H}\right)\left[1 - \frac{2a_H\left(1+\delta_{i_H}\right)}{\pi A.R._H}\right] + \left(\overline{\alpha}_H - i_H\right)\right\}\frac{\partial \alpha_H}{\partial \dot{z}} \quad (246)$$

$$\left(\frac{\partial X}{\partial \dot{z}}\right)_H = \left(\frac{\partial X}{\partial \dot{z}}\right)_H \frac{\frac{\partial \alpha_H}{\partial \dot{z}}}{\frac{\partial \alpha_H}{\partial \dot{z}}} \quad (247)$$

$$\left(\frac{\partial Z}{\partial \dot{x}}\right)_H = \left\{\begin{array}{l} \frac{2}{V}\overline{Z}_H \\ + \frac{q_H}{q} q A_H a_H \left\{\begin{array}{l} 1 + \frac{a_H\left(1+\delta_{i_H}\right)}{\pi A.R._H}\left[\begin{array}{l} 2\left(\overline{\alpha}_H - \alpha_{L=0_H}\right)\left(\overline{\alpha}_H - i_H\right) \\ + \left(\overline{\alpha}_H - \alpha_{L=0_H}\right)^2 \end{array}\right] \\ + c_{D_{o,H}} \end{array}\right\}\frac{\partial \alpha_H}{\partial \dot{x}} \end{array}\right\} \quad (248)$$

$$\left(\frac{\partial Z}{\partial \dot{z}}\right)_H = -\frac{q_H}{q} q A_H a_H \left\{1 + \frac{a_H\left(1+\delta_{i_H}\right)}{\pi A.R._H}\left[\begin{array}{l} 2\left(\overline{\alpha}_H - \alpha_{L=0_H}\right)\left(\overline{\alpha}_H - i_H\right) \\ + \left(\overline{\alpha}_H - \alpha_{L=0_H}\right)^2 \end{array}\right] + c_{D_{o,H}}\right\}\frac{\partial \alpha_H}{\partial \dot{z}} \quad (249)$$

$$\left(\frac{\partial Z}{\partial \ddot{z}}\right)_H = \left(\frac{\partial Z}{\partial \dot{z}}\right)_H \frac{\frac{\partial \alpha_H}{\partial \ddot{z}}}{\frac{\partial \alpha_H}{\partial \dot{z}}} \quad (250)$$

$$\left(\frac{\partial Z}{\partial q}\right)_H = \left(\frac{\partial Z}{\partial \dot{z}}\right)_H l_H \quad (251)$$

$$\left(\frac{\partial M}{\partial \dot{x}}\right)_H = -\left(\frac{\partial X}{\partial \dot{x}}\right)_H h_H + \left(\frac{\partial Z}{\partial \dot{x}}\right)_H l_H \quad (252)$$

$$\left(\frac{\partial M}{\partial \dot{z}}\right)_H = -\left(\frac{\partial X}{\partial \dot{z}}\right)_H h_H + \left(\frac{\partial Z}{\partial \dot{z}}\right)_H l_H \quad (253)$$

$$\left(\frac{\partial M}{\partial \ddot{z}}\right)_H = -\left(\frac{\partial X}{\partial \ddot{z}}\right)_H h_H + \left(\frac{\partial Z}{\partial \ddot{z}}\right)_H l_H \quad (254)$$

$$\left(\frac{\partial M}{\partial q}\right)_H = \left(\frac{\partial Z}{\partial q}\right)_H l_H \quad (255)$$

C.3 VERTICAL STABILIZER STABILITY DERIVATIVES

$$\left(\frac{\partial X}{\partial \dot{x}}\right)_V = \frac{2}{V}\left[\overline{X}_V + 2\Delta\overline{D}_{V_{\text{int}}}\right] \tag{256}$$

Where $\Delta\overline{D}_{V_{\text{int}}}$ is the additional drag coming from the interference effect between the vertical stabilizer and the tail rotor:

$$\Delta\overline{D}_{V_{\text{int}}} = \frac{8}{\pi q}\left|\frac{T_T}{2R_T}\frac{Y_V}{b_V}\right|K_{\text{int}} \tag{257}$$

C.4 FUSELAGE STABILITY DERIVATIVES

$$\frac{\partial \gamma_c}{\partial \dot{z}} = -\frac{1}{V} \tag{258}$$

$$\frac{\partial \varepsilon_{M_F}}{\partial \dot{x}} = \frac{\upsilon_F}{\upsilon_1}\frac{1}{4qA_M}\left[-\left(\frac{\partial Z}{\partial \dot{x}}\right)_M + \frac{2\overline{Z}_M}{V}\right] \tag{259}$$

$$\frac{\partial \varepsilon_{M_F}}{\partial \dot{z}} = -\frac{\upsilon_F}{\upsilon_1}\frac{1}{4qA_M}\left(\frac{\partial Z}{\partial \dot{z}}\right)_M \tag{260}$$

$$\frac{\partial \alpha_F}{\partial \dot{x}} = -\frac{\partial \varepsilon_{M_F}}{\partial \dot{x}} \tag{261}$$

$$\frac{\partial \alpha_F}{\partial \dot{z}} = -\left[\frac{\partial \varepsilon_{M_F}}{\partial \dot{z}} + \frac{\partial \gamma_c}{\partial \dot{z}}\right] \tag{262}$$

$$\left(\frac{\partial X}{\partial \dot{x}}\right)_F = \frac{2}{V}\overline{X}_F \tag{263}$$

$$\left(\frac{\partial X}{\partial \dot{z}}\right)_F = \left(\overline{L}_F - q\frac{\partial f}{\partial \alpha_F}\right)\frac{\partial \alpha_F}{\partial \dot{z}} \tag{264}$$

$$\left(\frac{\partial Z}{\partial \dot{x}}\right)_F = \frac{2}{V}\overline{Z}_F \tag{265}$$

$$\left(\frac{\partial Z}{\partial \dot{z}}\right)_F = -\left(\overline{D}_F + q\frac{\partial L/q}{\partial \alpha_F}\right)\frac{\partial \alpha_F}{\partial \dot{z}} \tag{266}$$

$$\left(\frac{\partial M}{\partial \dot{x}}\right)_F = \frac{2}{V}\overline{M}_F + q\frac{\partial M/q}{\partial \alpha_F}\frac{\partial \alpha_F}{\partial \dot{x}} \tag{267}$$

$$\left(\frac{\partial M}{\partial \dot{z}}\right)_F = q\frac{\partial M/q}{\partial \alpha_F}\frac{\partial \alpha_F}{\partial \dot{z}} \tag{268}$$

C.5 TOTAL STABILITY DERIVATIVES

The total derivatives are found by adding the corresponding terms of main rotor, tail rotor, empennage and the fuselage:

$$\frac{\partial X_i}{\partial x_i} = \left(\frac{\partial X_i}{\partial x_i}\right)_M + \left(\frac{\partial X_i}{\partial x_i}\right)_T + \left(\frac{\partial X_i}{\partial x_i}\right)_{HS} + \left(\frac{\partial X_i}{\partial x_i}\right)_{VS} + \left(\frac{\partial X_i}{\partial x_i}\right)_F \tag{269}$$

Where $X_i = X, Z, M$ and $x_i = \dot{x}, \dot{z}, \ddot{z}, q, \theta_o, B_1$